AD-A097 724 TENNESSEE UNIV KNOXVILLE ULTRASONICS LAB F/G 20/11
A DETAILED STUDY OF ULTRASONIC NONLINEARITY IN RELATION TO OTHE--ETC(U)
MAR 81 J PHILIP N00014-76-C-0177
UNCLASSIFIED TR-19 NL

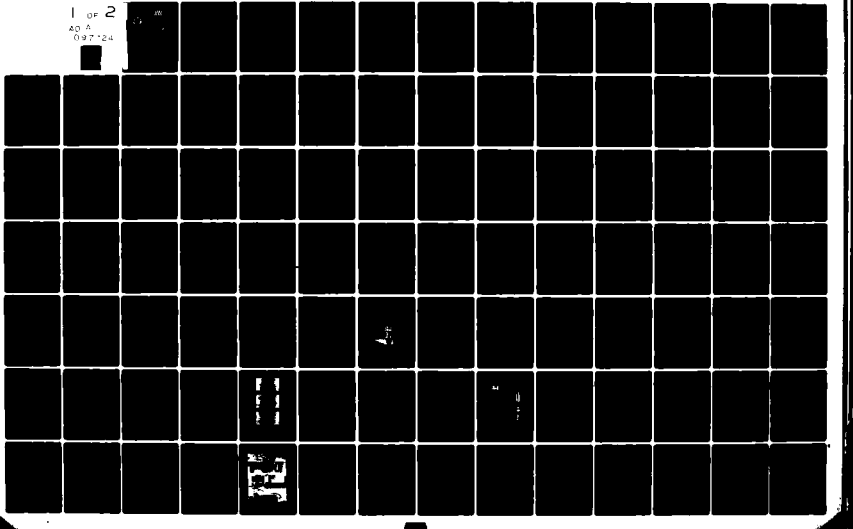

LEVEL II

OFFICE OF NAVAL RESEARCH
CONTRACT NO. N00014-71-A-0121-0001
PROJECT NO. 384-306

TECHNICAL REPORT NO. 19

A DETAILED STUDY OF ULTRASONIC NONLINEARITY IN RELATION TO OTHER THERMODYNAMIC PROPERTIES OF SOLIDS: RESULTS FOR SILICON AND GERMANIUM BETWEEN 3 AND 300 K

JACOB PHILIP

M. A. BREAZEALE
PRINCIPAL INVESTIGATOR
ULTRASONICS LABORATORY
DEPARTMENT OF PHYSICS

THE UNIVERSITY OF TENNESSEE
Knoxville, Tennessee

MARCH, 1981

Unclassified

SECURITY CLASSIFICATION OF THIS PAGE (When Data Entered)

REPORT DOCUMENTATION PAGE		READ INSTRUCTIONS BEFORE COMPLETING FORM
1. REPORT NUMBER 19	2. GOVT ACCESSION NO. AD-A097 724	3. RECIPIENT'S CATALOG NUMBER
4. TITLE (and Subtitle) A DETAILED STUDY OF ULTRASONIC NONLINEARITY IN RELATION TO OTHER THERMODYNAMIC PROPERTIES OF SOLIDS: RESULTS FOR SILICON AND GERMANIUM BETWEEN 3 AND 300 K		5. TYPE OF REPORT & PERIOD COVERED Interim 6. PERFORMING ORG. REPORT NUMBER
7. AUTHOR(s) Jacob Philip		8. CONTRACT OR GRANT NUMBER(s) N00014-76-C-0177
9. PERFORMING ORGANIZATION NAME AND ADDRESS Department of Physics The University of Tennessee Knoxville, TN 37916		10. PROGRAM ELEMENT, PROJECT, TASK AREA & WORK UNIT NUMBERS
11. CONTROLLING OFFICE NAME AND ADDRESS Office of Naval Research, Code 421 Department of the Navy Arlington, VA 22217		12. REPORT DATE March 1981 13. NUMBER OF PAGES 166
14. MONITORING AGENCY NAME & ADDRESS(if different from Controlling Office)		15. SECURITY CLASS. (of this report) Unclassified 15a. DECLASSIFICATION/DOWNGRADING SCHEDULE

16. DISTRIBUTION STATEMENT (of this Report)

Approved for public release; distribution unlimited.

17. DISTRIBUTION STATEMENT (of the abstract entered in Block 20, if different from Report)

18. SUPPLEMENTARY NOTES

19. KEY WORDS (Continue on reverse side if necessary and identify by block number)

Ultrasonic nonlinearity parameters;
Harmonic generation;
Capacitive detector;
Third-order elastic constants;
Grüneisen parameter;
The Keating model
Anharmonic force constants
Thermal expansion

20. ABSTRACT (Continue on reverse side if necessary and identify by block number)

It is shown that measurement of the ultrasonic nonlinearity parameters of solids throws light on their thermodynamic properties. Establishment of the relation between ultrasonic nonlinearity ~~(an elastic property)~~ and thermal properties has been achieved for the diamond-like solids by determining the third-order elastic (TOE) constants and their variation with temperature. Study has been done on silicon and germanium.

DD FORM 1 JAN 73 1473 EDITION OF 1 NOV 65 IS OBSOLETE
S/N 0102-LF-014-6601

Unclassified

SECURITY CLASSIFICATION OF THIS PAGE (When Data Entered)

20 ABSTRACT (continued)

The nonlinear equation for the propagation of acoustic waves is derived and solved for longitudinal wave propagation along the pure mode directions of a cubic crystal. Because of the nonlinearity of the medium, an initially sinusoidal 30 MHz wave undergoes waveform distortion and harmonics are generated. The ultrasonic nonlinearity parameters of the medium can conveniently be determined by measuring the amplitudes of the fundamental and generated second harmonic. Such measurements are done ~~on silicon~~ and germanium as a function of temperature between liquid helium and room temperature using a capacitive receiver. The measurements lead to the K_3 parameters which are combinations of TOE constants. Temperature variation of these parameters are studied.

Combining our results with an established lattice dynamical model for diamond-like solids (the Keating model) has enabled us to determine the anharmonic force constants involved in the model as a function of temperature, and subsequently to determine all the six TOE constants. The temperature variations of all the TOE constants of silicon and germanium are plotted between 3 and 300°K, ~~first of its kind in literature.~~ Using temperature dependent TOE constants, we have evaluated and plotted the thermal properties: thermal expansion Grüneisen parameter, pressure derivatives of the second-order elastic constants, and the Anderson-Grüneisen parameters. Wherever possible, the results are compared with previous data.

OFFICE OF NAVAL RESEARCH
CONTRACT NO. N00014-76-C-0177
PROJECT NO. 384-306

A DETAILED STUDY OF ULTRASONIC NONLINEARITY IN RELATION TO OTHER THERMODYNAMIC PROPERTIES OF SOLIDS: RESULTS FOR SILICON AND GERMANIUM BETWEEN 3 AND 300 K

by

Jacob Philip

Ultrasonics Laboratory
Department of Physics
The University of Tennessee
Knoxville, TN 37916

TECHNICAL REPORT, NO. 19

March 1981

TABLE OF CONTENTS

PAGE

LIST OF TABLES

LIST OF FIGURES

FIGURE PAGE

PREFACE

The ultrasonic harmonic generation technique has been extended to the study of the nonlinear elastic behavior and thermal properties of the diamond-like solids silicon and germanium. A complete study of the temperature variation of the third-order elastic constants of silicon and germanium has been done. In order to make the technical report intelligible, it has been divided into four chapters as follows.

The importance of the study of the nonlinear properties of solids is emphasized in the Introduction which forms the first section of Chapter I. A brief review of the theoretical and experimental work done in higher-order elasticity is given. The remainder of Chapter I concentrates on the theoretical basis of the work. The nonlinear wave equation in a cubic solid is derived and its solutions along the symmetry directions are given. The ultrasonic nonlinearity parameter for longitudinal wave propagation along pure mode directions in cubic crystals is defined. The relationship between the nonlinearity parameters and elastic constants is derived.

Chapter II describes the experimental setup. A brief description of the capacitive detector which is used for wave amplitude measurements is given. Both room temperature and cryogenic apparatus are described with diagrams wherever necessary. The measurement procedure is also outlined in this chapter. The block diagrams of the room temperature as well as cryogenic apparatus are given. Details about the individual parts are given wherever necessary. Ultrasonic nonlinearity parameters of silicon have been measured at room temperature and as a function of

temperature down to liquid helium temperature. The numerical results are tabulated and the temperature variation of the nonlinearity parameters and some combinations of third-order elastic constants have been plotted. Chapter III is made up of these results. Comparison of the results with previous experimental and theoretical values are made as far as possible. The strain generalized Grüneisen parameters along the principal directions are evaluated and reported.

Keating's central force model is one of the most successful and established models for diamond-like solids. We have developed a method to isolate all the six individual third-order elastic constants from nonlinearity parameters of diamond-like solids by combining our measured values with this lattice dynamical model. Expressions for the Keating force constants are given in terms of the nonlinearity parameters. The method is applied to silicon and germanium and the temperature variation of all the six independent third-order elastic constants have been studied between room temperature and 3°K. The method and results are given in Chapter IV. Numerical knowledge of the temperature dependent third-order elastic constants can be related to the temperature dependence of the anharmonic parameters such as thermal expansion, Grüneisen parameter, etc. of solids. Such a study made for silicon and germanium also is incorporated in this chapter. Low temperature thermal expansion measurements of diamond-like solids by various workers have shown that they possess a negative thermal expansion at low temperatures. Grüneisen parameters follow the same anomaly. Theoretical calculations of low temperature thermal expansion and Grüneisen parameters from room

temperature third-order elastic constants by earlier workers do not account for the negative thermal expansion in certain temperature ranges. We have tried to bridge this gap by evaluating the thermal expansion and Grüneisen parameters of silicon and germanium as a function of temperature from temperature dependent third-order elastic constants in the quasi-harmonic approximation. Temperature variation of other anharmonic parameters of silicon and germanium have been studied and the results are presented.

CHAPTER I

INTRODUCTION AND THEORY

A. INTRODUCTION

A solid medium, in general, is nonlinear. Hooke's law is not obeyed by solids because of this nonlinearity. Nonlinearity arises from the higher order terms in the energy density expansion of the solid. A finite amplitude ultrasonic wave propagating through a nonlinear medium distorts as it progresses and generates higher harmonics. Superposed waves generate sum and difference frequency waves. The nonlinear effects are mainly due to the asymmetry of the interatomic potential well; i.e., *due to a nonparabolic interatomic interaction* potential which leads to anharmonic behavior of the crystal lattice. The distortion of a finite amplitude ultrasonic wave in a solid is a measure of the nonlinearity of the medium and measurement of the generated harmonics offers a unique method for the study of anharmonicity of solids. Distortion of a finite-amplitude ultrasonic wave in solids was first observed by Breazeale and Thompson[1] and by Gedroits and Krasilnikov.[2] The fact that such measurements lead to the determination of third-order elastic constants has given impetus for the work to be described in the succeeding chapters.

In describing the physical properties of solids, the elastic constants play a central role. In the macroscopic theory of elasticity the solid is treated as a continuum which has, in the unstrained

equilibrium state, a constant mass density. The elastic energy density is written as a power series in the elements of the strain tensor. The zero-order term represents the energy of the solid in equilibrium. It is independent of the strain and may be set equal to zero. The first-order term is also zero in the absence of external body forces. The coefficients of the second-, third-, and higher-order terms are designated as elastic constants of order corresponding to the power of the strain in the respective terms. In the microscopic theory of crystal lattices, the potential energy of a crystal is expanded as a Taylor series in terms of the displacements of the atoms in the lattice from their equilibrium positions.[3] The coefficients in the series are the derivatives of the potential energy referred to the equilibrium positions and are called the coupling parameters. The zero-order term may be set equal to zero; the first-order term vanishes because the expansion is about the equilibrium positions. As in the macroscopic theory, the higher terms stand for the corresponding coupling parameters. The symmetry properties of the lattice can be used to obtain the relations among the coupling parameters and the corresponding elastic constants. Measurement of the elastic constants yields information about the lattice forces.

If only the second-order terms are retained in the elastic energy density and linear elasticity theory is used, a linear relationship between stress and strain results (Hooke's law). This approximation can be used for infinitesimal deformations; i.e., when the space derivatives of the displacement vectors of a point in the body are small enough that their products and squares may be neglected in comparison

to the terms themselves. Similarly, neglecting terms beyond second order in the lattice potential energy leads to lattice dynamics in the harmonic approximation[4] with which one can account for much of the behavior of solids.

A number of properties of solids are related to the anharmonicity of the lattice potential which involves elastic constants higher than second order. Crystals exhibit lattice thermal expansion. The adiabatic and isothermal elastic constants are, in general, different from each other and the elastic constants do vary with temperature and pressure. At high temperatures the specific heat exhibits a temperature dependence. All these anharmonic properties indicate that harmonic theory is not sufficient for a quantitative description of the properties of a crystal.

Even at low temperatures the harmonic theory is not correct. Because of zero-point vibrations the influence of anharmonicity does appear even at absolute zero. This is particularly large for small atoms or molecules which have correspondingly large zero-point oscillations. The equilibrium positions therefore do not coincide with the minimum of the potential energy. The methods of harmonic theory are no longer applicable in the dynamic theory of elasticity because the anharmonic terms cause a coupling between the different modes of oscillations. In the harmonic theory the oscillator or eigenfrequencies ω_j of the lattice are independent of interatomic distance a. With the correct potential energy, the coupling parameters of second order and therefore ω_j are functions of a. Even if the terms higher than the quadratic ones in the energy expansion are omitted, part of the anharmonic effects

are already described by the dependence ω_j (a). This approximation is called the quasiharmonic approximation which is conveniently used for the evaluation of many physical parameters. Excellent reviews on the anharmonic effects in solids are available in literature.[5]

The conduction of heat in solids depends on the transfer of vibrational energy through the lattice, which is not predicted by harmonic theory. Anharmonic terms represent the interaction between mechanical sound waves and thermal vibrations, which leads to the damping of high frequency (> 10^9 Hz) sound waves and to the damping of moving dislocations by phonon viscosity.[6] Volume increase of an elastic body associated with a change of temperature or the introduction of dislocations, an exact description of stress and strain fields near dislocations, the electrical resistance of screw and edge dislocations, scattering of phonons from defects, etc. demand a treatment by nonlinear elasticity theory.[7,8]

The elastic constants play a dual role of importance in the theory of solids. Only a knowledge of the elastic constants enables one to determine such important physical properties as compressibility, the Debye temperature and its pressure dependence, the Grüneisen parameters and various thermodynamic properties of defects in solids. These properties can be found without having any information about the interatomic forces or potentials. The second important role of elastic constants is a result of their being among the most accurately measurable physical quantities. Ultrasonic techniques have generally enabled one to experimentally determine elastic constants to a greater degree of accuracy than can be obtained from theoretical calculations. Thus, the

elastic constants can serve as a useful guide in developing any related theory. Since elastic constants describe how the energy density of a solid changes with respect to various volume and shear deformations, they are useful in determining the nature of binding forces and interatomic potentials. The macroscopic nonlinear behavior of solids is determined by the intermolecular potential functions of solids. The relations between the force constants and elastic constants of a cubic solid has been given by Coldwell-Horsfall.[9] Ghate[10] uses the Born model of ionic solids to compute the third-order elastic constants and their temperature variation. Hiki and Granato[11] investigate short range repulsive interactions in noble metals and their relationships to the nonlinearity of the solid.

Basically there are two methods for calculating the elastic constants of a crystalline medium: the method of homogeneous deformation[12] and the method of long waves.[13] The results obtained from the two methods should be in agreement when the same model of a solid is used in both cases. In the method of homogeneous deformation the calculation proceeds by determining how the energy density changes with respect to various homogeneous deformations; i.e., deformations for which the resulting structure remains a perfect lattice. The two most widely used types of deformations are those described by the Lagrangian strain parameters and by the Fuchs strain parameters. In the first case, derivatives of the energy density are taken with respect to the Lagrangian strains η_{ij}. The resulting derivatives when evaluated in the undeformed state, are the Brugger elastic constants

$$C_{ijk\ell\ldots} = (\partial^n E/\partial\eta_{ij}\partial\eta_{k\ell}\ldots)_{\eta=0} \tag{1.1}$$

where E is the energy of the crystal per unit undeformed volume. This thermodynamic definition of elastic constants of any order introduced by Brugger[14] is most widely used nowadays. In the other case, one calculates the derivatives of the energy density with respect to Fuch-type strain parameters[15] which consist of a volume deformation and of various volume conserving shear deformations. When evaluated in the undeformed state, these derivatives are referred to as Fuchs elastic constants. The Fuchs constants are linear combinations of the Brugger constants. The relationships between the Fuchs and Brugger elastic constants for cubic crystals are[16]

$$\begin{aligned}
&\partial^2 E/\partial\gamma_1^2 = C_{44} \\
&\partial^2 E/\partial V^2 = \tfrac{1}{3}(C_{11} + 2C_{12}) \\
&\partial^2 E/\partial\varepsilon_1^2 = 2(C_{11} - C_{12}) \\
&\partial^3 E/\partial V^3 = \tfrac{1}{9}(C_{111} + 2C_{123} + 6C_{112}) - \tfrac{1}{3}(C_{11} + 2C_{12}) \\
&\partial^3 E/\partial V\partial\varepsilon_1^2 = \tfrac{2}{3}(C_{111} - C_{123}) + \tfrac{8}{3}(C_{11} - C_{12}) + \tfrac{4}{3}(C_{11} + 2C_{12}) \\
&\partial^3 E/\partial V\partial\gamma_1^2 = \tfrac{1}{3}(C_{144} + 2C_{166}) + \tfrac{1}{3}(C_{11} + 2C_{12}) + \tfrac{4}{3}C_{44} \\
&\partial^3 E/\partial\varepsilon_2\partial\gamma_1^2 = C_{166} - C_{144} + C_{11} - C_{12} + 2C_{144} \\
&\partial^3 E/\partial\varepsilon_1^2\partial\varepsilon_2 = C_{111} + 2C_{123} - 3C_{112} + 7(C_{11} - C_{12}) \\
&\partial^3 E/\partial\gamma_3\partial\gamma_2\partial\gamma_1 = C_{456}\,.
\end{aligned} \tag{1.2}$$

γ_i, γ_i and V are the Fuchs strain parameters. For most symmetric cubic crystals there are three independent second-order elastic constants and six third-order elastic constants. The Voigt notation for elastic constants is used throughout the text of this report. The relationship between Fuchs and Brugger elastic constants for hexagonal crystals have been given elsewhere.[17]

The Fuchs constants are generally more convenient to calculate when dealing with noncentral potentials, whereas the Brugger constants are the preferred type for central potentials. In either case, the final results are usually expressed in terms of the Brugger constants to facilitate comparison with experimental data.

The elastic strain energy for most symmetrical class of cubic crystals, including third-order terms, but omitting terms independent of strain was first given by Birch[18a] as

$$\begin{aligned}\phi = {} & \tfrac{1}{2} C_{11}(\eta_{11}^2 + \eta_{22}^2 + \eta_{33}^2) + C_{12}(\eta_{11}\eta_{22} + \eta_{22}\eta_{33} + \eta_{33}\eta_{11}) \\ & + C_{44}(\eta_{12}^2 + \eta_{21}^2 + \eta_{23}^2 + \eta_{32}^2 + \eta_{31}^2 + \eta_{13}^2) + C_{111}(\eta_{11}^3 + \eta_{22}^3 + \eta_{33}^3) \\ & + C_{112}[\eta_{11}^2(\eta_{22} + \eta_{33}) + \eta_{22}^2(\eta_{33} + \eta_{11}) + \eta_{33}^2(\eta_{11} + \eta_{22})] \\ & + \tfrac{1}{2} C_{144}[\eta_{11}(\eta_{23}^2 + \eta_{32}^2) + \eta_{22}(\eta_{31}^2 + \eta_{13}^2) + \eta_{33}(\eta_{12}^2 + \eta_{21}^2)] \\ & + \tfrac{1}{2} C_{166}[(\eta_{12}^2 + \eta_{21}^2)(\eta_{11} + \eta_{22}) + (\eta_{23}^2 + \eta_{32}^2)(\eta_{22} + \eta_{33}) \\ & + (\eta_{31}^2 + \eta_{13}^2)(\eta_{33} + \eta_{11})] + C_{123}\,\eta_{11}\eta_{22}\eta_{33} \\ & + C_{456}[\eta_{12}\eta_{23}\eta_{31} + \eta_{21}\eta_{32}\eta_{13}] \end{aligned} \tag{1.3}$$

where η_{ij} are the Lagrangian strain components used by Birch and we have corrected the numerical errors pointed out by Bhagavantam and

Suryanarayana.[18b] The relationships between Brugger and Birch third-order elastic (TOE) constants can easily be worked out and are given by

$$
\begin{aligned}
C_{111}\ (\text{Birch}) &= \tfrac{1}{6}\, C_{111}\ (\text{Brugger}) \\
C_{112}\ (\text{Birch}) &= \tfrac{1}{2}\, C_{112}\ (\text{Brugger}) \\
C_{144}\ (\text{Birch}) &= 2C_{144}\ (\text{Brugger}) \\
C_{166}\ (\text{Birch}) &= 2C_{166}\ (\text{Brugger}) \\
C_{123}\ (\text{Birch}) &= C_{123}\ (\text{Brugger}) \\
C_{456}\ (\text{Birch}) &= 4C_{456}\ (\text{Brugger})\ .
\end{aligned}
\tag{1.4}
$$

The role of second-order elastic (SOE) constants in the description of the elastic properties of solids is well established and appears in every work in the field and so is not repeated here. The pulse echo technique of determining the velocity of ultrasonic waves in crystals, first employed by McSkimin,[19] is one of the most accurate and widely prevalent methods of measuring the SOE constants of a cystal. It involves the application of a series of RF pulses of about 15 to 25 MHz to a transducer bonded to the specimen by a suitable bond. The pulse repetition rate is adjusted so that the pulse echoes superimpose exactly on the signal. This pulse renetition frequency ($\simeq$ 100 to 500 kHz) is directly proportional to the square of the natural wave velocity and can be measured with an accuracy of 1 in 10^5. Measurement of the velocities of longitudinal and shear waves along the symmetry directions leads directly to the SOE constants. The pulse interference method[11] is also often used for velocity measurements.

In explaining the anharmonic properties of solids, the TOE constants play an important role. They are necessary to evaluate the

third-order terms of the lattice potential energy and are needed to evaluate the generalized Grüneisen parameters which describe the strain dependence of the lattice vibrational frequencies. The TOE constants can provide quantitative descriptions of acoustic amplification at microwave frequencies besides enabling the evaluation of the Akhieser phonon-phonon interaction mechanism which describes the attenuation of ultrasonic waves in solids. The TOE constant data are needed to determine the changes in the lattice parameters of the solid due to application of hydrastatic pressure.

The most common method of determining the TOE constants is to measure the changes in velocities of ultrasonic waves propagating along different symmetry directions with applied stress. Hughes and Kelley[20] derived expressions for the velocities of elastic waves in stressed solids using third-order terms in the elastic energy and finite strain theory of Birch.[18] Einspruch and Manning[21] applied finite strain elasticity theory to evaluate the TOE constants of anisotropic crystalline solids and has presented results for cubic and uniaxial crystals. The first measurement of TOE constants of isotropic materials polystyrene, iron and pyrex glass has been done by Hughes and Kelly[20] and those of the anisotropic crystal germanium by Bateman et al.[22] The evaluation of all the independent TOE constants involves measurement of wave velocities when uniaxial static stress is applied to the crystal, besides measurements under hydrostatic pressure. Thurston and Brugger[23] have derived the expressions for the sound velocity and for a natural velocity and their stress derivatives evaluated at zero stress in terms of SOE and TOE

constants of the crystal applicable to arbitrary crystal symmetry and arbitrary stress systems depending on a single scalar variable.

In the pulse echo method[19] for measuring the changes in wave velocity due to application of hydrostatic pressure, the specimen is subjected to high pressure in a cylindrical bomb, using compressed gases or liquids. Measurements under uniaxial stress are performed by applying the stress through a 20×10^3 kg hydraulic jack operated by a screw. The ratio of the pulse repetition frequency when the crystal is stressed to the repetition frequency of the unstressed crystal is plotted against the stress. From the slope of the linear portion of the graph for different propagation directions, wave polarizations and stress systems, an adequate number of combinations of TOE constants can be obtained. A set of simultaneous equations are solved to obtain the individual TOE constants. The expressions connecting TOE constants and stress derivatives of sound velocities in solids have been given by a number of authors[22,24,25] and are not reproduced here. The pressure technique has been employed by a number of later workers to determine the TOE constants of silicon,[26] alkali halides,[27] fused silica,[28] noble metals,[11] etc. Salama and Alers[29] used the technique to measure TOE constants of copper at low temperatures.

Graham[30] has described a method of obtaining longitudinal TOE and FOE (fourth-order elastic) constants of solids which sustain elastic compressions under shock wave loading. The shock compression data on sapphire and fused quartz have been analyzed to determine C_{111}, C_{333}, C_{1111} and C_{3333}. The determination of the TOE constants under these

large compressions allows one to test the applicability of the finite strain formulation of constitutive relations. This technique can be applied to materials whose elastic limits are a few percent of their longitudinal elastic constants.

An optical technique for determining the TOE constants of transparent crystals has been proposed[31] and measurements have been carried out[32] on NaCl and C_{111} has been reported. This technique makes use of the fact that when an initially sinusoidal ultrasonic wave of finite amplitude is propagating in a crystal, it gets distorted due to the generation of harmonics. The difference in intensity between the first positive and first negative orders of the diffraction pattern obtained when monochromatic light is transmitted through the crystal perpendicular to the direction of propagation of the ultrasonic wave is a function of the strain amplitude of the wave. A measurement of the asymmetry in the intensity leads to some of the TOE constants. Not much work has been done in this regard.

Measurements of phonon-phonon scattering have been used to determine various combinations of TOE constants. Classical calculations based on the interaction of two intersecting ultrasonic beams within an isotropic solid have been carried out by Jones and Kobett.[33] Quantum mechanical calculations of the same experimental situation have been treated by Taylor and Rollins[34] and experimental results for isotropic materials have been given by Rollins[35] and Rollins et al.[36] Dunham and Huntington[37] used this technique for fused silica and single crystals of NaCl. A treatment of the nonlinear interaction of ultrasonic waves

in the framework of quantum theory has been given by Bajak and Breazeale.[38]

The method of determining the TOE constants presented in this technical report, viz. the ultrasonic harmonic generation technique, involves a measurement of the waveform distortion of an ultrasonic wave as it propagates through a solid. Due to the anharmonic behavior of the solid, higher harmonics are generated during the passage of an initially sinusoidal ultrasonic wave through the solid.[1,2] Breazeale and Ford[39] studied these properties, and correlated them with the solution of the nonlinear equation for a longitudinal wave propagating through a solid. Gauster and Breazeale[40] developed a capacitive detector which is capable of absolute measurement of the amplitudes of the fundamental and harmonics of the waveform impinging on the end of the sample. Three linear combinations of the TOE constants of copper measured at room temperature are reported by them.[41] The harmonic generation technique has the advantage that it can be applied to soft metals as well as to solids which undergo lattice slips and cracks on application of pressure.

Probably the greatest advantage of the harmonic generation method is that it can be used to determine the TOE constants as a function of temperature. The temperature dependence of the TOE constants is very important in the study of anharmonicity of solids. Hydrostatic and uniaxial pressure techniques seem to have practical problems at low temperatures. Harmonic generation technique has been used by Mackey and Arnold[42] to measure TOE constants of strontium titanate and by Meeks and Arnold[43] to measure the temperature dependence of combinations of

TOE constants down to ~ 100 K. Peters et al.[44] developed a variable gap capacitive detector capable of making measurements at low temperatures. These authors[45] measured combinations of TOE constants of copper down to liquid nitrogen temperatures. Subsequently the apparatus has been refined and measurements have been made on germanium,[46] fused silica,[47] and copper[48] down to liquid helium temperatures.

The work presented in this report is the result of the measurement of the ultrasonic nonlinearity parameters and some combinations of TOE constants of silicon as a function of temperature between room temperature and liquid helium temperature. The apparatus, experimental procedure and results are given in the following chapters. Our measured nonlinearity parameters combined with a well-established lattice dynamical model for diamond-like solids has enabled us to isolate all the six independent TOE constants of silicon and germanium and plot them as a function of temperature. This is the first report of the temperature variation of all the individual TOE constants of any material as a function of temperature. This work is explained in detail in the last chapter. Also we have computed some anharmonic parameters as a function of temperature.

B. THEORY

In this section we give the theory on which the ultrasonic wave distortion measurements are based. The general equation of motion for plane elastic waves propagating through a medium is derived. It is then specialized to wave propagation along the symmetry directions in cubic crystals. Pure mode longitudinal wave propagation is possible along

the [100], [110] and [111] symmetry directions of a cubic crystal.[49] Including the nonlinear terms, one finds that pure transverse modes do not exist. The transverse wave is always accompanied by a longitudinal wave.[50] However, pure longitudinal modes continue to exist for all three directions [100], [110], and [111] even when the nonlinear terms are included.

The wavelength of the sound waves in the materials used in this investigation are quite large compared to the interatomic spacing. Typically the wavelength of the ultrasonic wave is about six orders of magnitude greater than the interatomic spacing. The number of atoms affected by one period of vibration is of the order of 10^6. So the solid can be regarded as an elastic continuum and the theory of finite deformations[12] in the Lagrangian formulation can readily be applied. The equations of motion governing finite deformation in cubic crystal have been given by Seeger and Buck,[8] Bateman et al.[22] and by Holt and Ford.[51] The equations of motion are derived here from Lagrange's equations, the approach used by Holt and Ford, and then they are applied to pure mode longitudinal wave propagation in cubic crystals. From the solution to the resulting nonlinear wave equations we derive expressions for the ultrasonic nonlinearity parameters.

1. The Equations of Motion for Plane Elastic Waves Propagating through a Medium

In arriving at the equations of motion of an elastic wave propagating through a solid crystalline medium, the solid is considered to be a lossless, homogeneous and perfectly elastic medium.[51] The elastic continuum is described with the formalism given by Murnaghan[12]

for finite deformations of an elastic solid. The equations of motion for long wavelength finite amplitude sound waves in a solid are derived using Lagrange's equations for continuous media. Let a_i, $i = 1,2,3$ be the cartesian coordinates of a point in the unstrained solid and let x_i, $i = 1,2,3$ be the coordinates at time t of the same point in the deformed solid. x_i depends on the initial coordinates a_i and time t. As has been given by Murnaghan, let the Lagrangian strain matrix η be given by

$$\eta = \frac{1}{2} (J^* J - I) \tag{1.5}$$

where J is the Jacobian matrix with matrix elements

$$J_{k\ell} = \partial x_k / \partial a_\ell \ . \tag{1.6}$$

J* is the transpose of J and I is the unit matrix. If ρ is the unstrained mass density and $\phi(\eta)$ is the elastic potential energy per unit unstrained volume, then the Lagrangian of the system is

$$L = \frac{1}{2} \sum_{i=1}^{3} \rho \dot{x}_i^2 - \phi(\eta) \ . \tag{1.7}$$

Lagrange's equations take the form

$$\frac{d}{dt} \left(\frac{\partial L}{\partial \dot{x}_i}\right) + \sum_{k=1}^{3} \frac{d}{da_k} \left(\frac{\partial L}{\partial (\partial x_i / \partial a_k)}\right) = 0 \ . \tag{1.8}$$

Combining Eqs. (1.7) and (1.8) we have

$$\rho \ddot{x}_i - \sum_{k=1}^{3} \frac{d}{da_k} \left(\sum_{j,\ell=1}^{3} \frac{\partial \phi}{\partial \eta_{j\ell}} \frac{\partial \eta_{j\ell}}{\partial (\partial x_i / \partial a_k)} \right) = 0 \ . \tag{1.9}$$

From Eq. (1.5) we have

$$\frac{\partial \eta_{j\ell}}{\partial(\partial x_i/\partial a_k)} = \frac{1}{2}\,\delta_{jk}\,\frac{\partial x_i}{\partial a_\ell} + \frac{1}{2}\,\delta_{\ell k}\,\frac{\partial x_i}{\partial a_j}\,, \tag{1.10}$$

δ_{jk} being the kronecker delta. Substituting (1.10) in (1.9) we have the equations of motion given by

$$\rho\,\ddot{x}_i = \sum_{k=1}^{3} \frac{d}{da_k}\left(\sum_{\ell=1}^{3} J_{i\ell}\,\frac{\partial \phi}{\partial \eta_{k\ell}}\right) \tag{1.11}$$

where

$$\frac{\partial \phi}{\partial \eta_{k\ell}} = \frac{\partial \phi}{\partial \eta_{\ell k}}\,. \tag{1.12}$$

This way of deriving the equation of motion given by (1.11) requires only the definition of strain and the assumption that the elastic energy is a function of strain alone. This equation of motion is derived for a lossless elastic continuum and is valid for a real solid under the conditions of negligible attenuation and dispersion.

The equation of motion given by Eq. (1.11) is to be simplified to make experimental measurements and hence determine the elastic constants. Let us consider plane waves propagating along a single direction and orient the a_1 axis along the propagation direction. Then Eq. (1.11) simplifies to

$$\rho\,\ddot{x}_1 = \frac{d}{da_1}\sum_{k=1}^{3} J_{ik}\,\frac{\partial \phi(n)}{\partial \eta_{1k}}\,. \tag{1.13}$$

The elastic constants are defined as coefficients in an expansion of the elastic energy in powers of the strain when the strain is calculated with the a_k axes parallel to the symmetry axes of the crystal. Thus, in order

that $\phi(\eta)$ in Eq. (1.13) may contain the usual elastic constants, we must determine the change in ϕ and η under a rotation of the a_k axes. Let a bar superscript denote a quantity calculated with the a_k axes parallel to the crystal symmetry axes. Quantities without a bar superscript are calculated with the a_1 axis parallel to the propagation direction.

If R is the matrix which rotates the $\bar{a}_1$ axis into the a_1 axis and R* the transpose of R, Murnaghan[12] has shown that

$$\bar{\eta} = R^* \, \eta \, R \ . \tag{1.14}$$

The elastic potential energy is a scalar under rotation, and so

$$\phi(\eta) = \bar{\phi}(\bar{\eta}) = \bar{\phi}(R^* \, \eta \, R) \ , \tag{1.15}$$

i.e., if

$$\bar{\phi}(\bar{\eta}) = \frac{C_{11}}{2} \eta_{11}^2 + \frac{C_{111}}{6} \eta_{11}^3 + \ldots \tag{1.16}$$

then

$$\phi(\eta) = \frac{1}{2} C_{11} \left(\sum_{jk} R_{ij}^* \eta_{jk} R_{k1} \right)^2 + \frac{1}{6} C_{111} \left(\sum_{jk} R_{1j}^* \eta_{jk} R_{k1} \right)^3 + \ldots \tag{1.17}$$

Thus Eq. (1.13) will contain the usual elastic constants if we write it in the form

$$\rho \ddot{x}_i = \frac{d}{da_1} \left\{ \sum_{k=1}^{3} J_{ik} \frac{\partial \bar{\phi}(R^* \, \eta \, R)}{\partial \eta_{1k}} \right\} \ , \tag{1.18}$$

η being the strain calculated taking the a_1 axis along the propagation direction.

If U_k are the components of the particle displacement,

$$U_k = x_k - a_k \ , \tag{1.19}$$

the x_k axes and a_k axes being parallel. Substituting for $\phi(n)$ from (1.17) for the elastic energy appropriate to the crystal symmetry in (1.18) and performing the operations indicated, we obtain

$$U_{i,tt} = \sum_{j=1}^{3} A_{ij} U_{j,aa} + \sum_{j,\ell=1}^{3} B_{ij\ell} U_{j,a} U_{\ell,aa} \tag{1.20}$$

where

$$U_{j,a} = \partial U_j / \partial a_1$$

$$U_{i,tt} = \partial^2 U_i / \partial t^2$$

and

$$U_{\ell,aa} = \partial^2 U_\ell / \partial a_1^{\,2} \ . \tag{1.21}$$

In the above equation, A_{ij} are linear combinations of SOE constants and B_{ijk} are linear combinations of SOE and TOE constants. Since we are interested only in the lowest order of nonlinearity, the terms involving fourth- and higher-order elastic constants are neglected in (1.20).

Let us introduce new dependent variables P_k in order to remove the linear coupling of the three compounds U_k through the terms $\sum A_{ij} U_{j,aa}$. The coefficients A_{ij} in (1.20) form a symmetric matrix so that an orthogonal matrix S exists such that S*A S is diagonal. Hence if we introduce the transformation

$$U_j = \sum_{k=1}^{3} S_{ij} P_k \tag{1.22}$$

into Eq. (1.20), we obtain

$$\rho P_{j,tt} = \mu_j P_{j,aa} + \sum_{\ell,m=1}^{3} \nu_{j\ell m} P_{\ell,a} P_{m,aa} \tag{1.23}$$

where μ_j are the eigenvalues of the A_{ij} matrix. The $\nu_{j\ell m}$ form linear combinations of SOE and TOE constants. Equations (1.23) can be simplified further using perturbation theory. A straightforward perturbation calculation shows that only those terms in Eq. (1.23) for which $j = \ell = m$ or for which $\ell = m$ and $\mu_j = \mu_\ell$ yield a second harmonic which increases linearly with propagation distance. Such terms are said to be resonant. Then the experimentally relevant equations of motion for a plane wave take the form

$$\rho P_{j,tt} = \mu_j P_{j,aa} + \nu_{jjj} P_{j,a} P_{j,aa} \tag{1.24}$$

where $j = 1,2,3$. A perturbation solution to (1.24) will be of the form

$$P_j = B_j \sin(\omega t - k_j a) - (\nu_{jjj}/8\mu_j) B_j^2 k_j^2 a \times \cos(2\omega t - 2k_j a) \tag{1.25}$$

where ω is the angular frequency and k_j are the wave numbers which are related by

$$\omega^2 = (\mu_j/\rho) k_j^2 \, . \tag{1.26}$$

a is the propagation distance and B_j is the amplitude of P_j at $a = 0$. The second harmonic amplitude H_{2j} of P_j is given by

$$H_{2j} = -(\nu_{jjj}/8\mu_j) B_j^2 k_j^2 a \, . \tag{1.27}$$

Holt and Ford[51] have tabulated the coefficients μ_j and ν_{jjj} for different propagation and polarization directions for a number of crystals belonging to cubic symmetry.

2. Ultrasonic Nonlinearity Parameters

The ultrasonic nonlinearity parameter is defined as the negative of the ratio of the coefficients of the nonlinear term to the linear term in the nonlinear wave equation. As can be seen from Eq. (1.24), the nonlinearity parameter can be written as

$$\beta = -(\nu_{jjj}/\mu_j) \ . \tag{1.28}$$

The magnitude of the parameter β is a measure of the extent to which the waveform becomes distorted in a specific propagation distance, and so is a direct measure of the nonlinearity of the medium. It is proportional to the ratio of the second harmonic amplitude to the square of the fundamental amplitude. The parameter varies for different directions of propagation. The expressions for these parameters for longitudinal wave propagation along symmetry directions in cubic crystals result from considering the wave propagation along those directions as shown in the following sections.

3. Wave Propagation in Cubic Crystals

The description of the finite deformation of an elastic solid differs in two major respects from that of infinitesimal deformation. Due to the large deformations involved, the initial coordinates of a particle in the undeformed state are not interchangeable with the final coordinates in the deformed state. Moreover, the expression for the

strain energy in terms of the strains must be changed. Finite elastic strain can be treated in two different formulations. In the Lagrangian formulation, the strain is described in the undeformed state and the initial coordinates of a material particle $a_i(a,b,c)$ are taken as independent variables. In the Eulerian formulation the strain is described in the deformed state and the instantaneous coordinates of a material particle $x_i(x,y,z)$ are taken as independent variables. In the following we consider plane wave propagation along the symmetry axes of a cubic crystal in the Lagrangian formulation.

a. Plane wave propagation along [100] direction. Let us consider first the case of plane finite amplitude waves propagating along the [100] direction of a cubic crystal. The displacement components in this case become

$$u = u(a,t) \quad , \quad v = v(a,t) \quad \text{and} \quad w = w(a,t) \; . \tag{1.29}$$

The Jacobian matrix given by (1.6), namely

$$J = \begin{bmatrix} J_{11} & J_{12} & J_{13} \\ J_{21} & J_{22} & J_{23} \\ J_{31} & J_{32} & J_{33} \end{bmatrix} = \begin{bmatrix} \frac{\partial x}{\partial a} & \frac{\partial x}{\partial b} & \frac{\partial x}{\partial c} \\ \frac{\partial y}{\partial a} & \frac{\partial y}{\partial b} & \frac{\partial y}{\partial c} \\ \frac{\partial z}{\partial a} & \frac{\partial z}{\partial b} & \frac{\partial z}{\partial c} \end{bmatrix}$$

$$= \begin{bmatrix} 1 + u_a & u_b & u_c \\ v_a & 1 + v_b & v_c \\ w_a & w_b & 1 + w_c \end{bmatrix} \tag{1.30}$$

where $u_a = \partial u/\partial a$, etc., takes the form[52]

$$J = \begin{bmatrix} 1 + u_a & 0 & 0 \\ v_a & 1 & 0 \\ w_a & 0 & 1 \end{bmatrix} . \tag{1.31}$$

x, y, z in (1.30) are the same as x_1, x_2, x_3, respectively, in (1.6) and similarly a, b, c in (1.30) are the same as a_1, a_2, a_3, respectively, in (1.6). The transpose of the Jacobian is

$$J^* = \begin{bmatrix} 1 + u_a & v_a & w_a \\ 0 & 1 & 0 \\ 0 & 0 & 1 \end{bmatrix} . \tag{1.32}$$

Substituting (1.31) and (1.32) into (1.5) we find that the only nonvanishing strain components are

$$\left.\begin{aligned} \eta_{11} &= u_a + \tfrac{1}{2}\,(u_a^2 + v_a^2 + w_a^2) \\ \eta_{12} &= \eta_{21} = \tfrac{1}{2}\, v_a \\ \eta_{13} &= \eta_{31} = \tfrac{1}{2}\, w_a \end{aligned}\right\} . \tag{1.34}$$

Substituting (1.34) in the expression for elastic strain energy (1.3) and using Birch's values for the TOE constants, we have

$$\begin{aligned} \phi = \tfrac{1}{2}\, C_{11}\eta_{11}^2 + C_{44}(\eta_{12}^2 + \eta_{21}^2 + \eta_{31}^2 + \eta_{13}^2) + C_{111}\eta_{11}^3 \\ + \tfrac{1}{2}\, C_{166}[\eta_{11}(\eta_{12}^2 + \eta_{21}^2 + \eta_{31}^2 + \eta_{13}^2)] . \end{aligned} \tag{1.35}$$

Differentiating (1.35) with respect to the strains,

$$\left.\begin{aligned}
\frac{\partial\phi}{\partial\eta_{11}} &= C_{11}\eta_{11} + 3C_{111}\eta_{11}^2 + \frac{1}{2}C_{166}(\eta_{12}^2 + \eta_{21}^2 + \eta_{31}^2 + \eta_{13}^2) \\
\frac{\partial\phi}{\partial\eta_{21}} &= 2C_{44}\eta_{21} + C_{166}\eta_{11}\eta_{21} \\
\frac{\partial\phi}{\partial\eta_{31}} &= 2C_{44}\eta_{31} + C_{166}\eta_{11}\eta_{31}
\end{aligned}\right\} . \tag{1.36}$$

Let us introduce the engineering stress tensor which is not symmetric as

$$T = J\left(\frac{\partial\phi}{\partial\eta}\right) \tag{1.37}$$

where

$$\frac{\partial\phi}{\partial\eta} = \begin{bmatrix} \frac{\partial\phi}{\partial\eta_{11}} & \frac{\partial\phi}{\partial\eta_{12}} & \frac{\partial\phi}{\partial\eta_{13}} \\ \frac{\partial\phi}{\partial\eta_{21}} & \frac{\partial\phi}{\partial\eta_{22}} & \frac{\partial\phi}{\partial\eta_{23}} \\ \frac{\partial\phi}{\partial\eta_{31}} & \frac{\partial\phi}{\partial\eta_{32}} & \frac{\partial\phi}{\partial\eta_{33}} \end{bmatrix} . \tag{1.38}$$

Then the equations of motion in the Lagrangian coordinate system can be written as

$$\partial T_{ij}/\partial a_j = \rho_0 \ddot{u}_i \tag{1.39}$$

where T_{ij} is the stress matrix, a_j are the Lagrangian coordinates, ρ_0 is the density in the unstrained state and $u_i = x_i - a_i$ is the displacement. The stress matrix can be written in the component form as

$$\begin{bmatrix} T_{11} & T_{12} & T_{13} \\ T_{21} & T_{22} & T_{23} \\ T_{31} & T_{32} & T_{33} \end{bmatrix} = \begin{bmatrix} J_{11} & J_{12} & J_{13} \\ J_{21} & J_{22} & J_{23} \\ J_{31} & J_{32} & J_{33} \end{bmatrix} \begin{bmatrix} \frac{\partial \phi}{\partial n_{11}} & \frac{\partial \phi}{\partial n_{12}} & \frac{\partial \phi}{\partial n_{13}} \\ \frac{\partial \phi}{\partial n_{21}} & \frac{\partial \phi}{\partial n_{22}} & \frac{\partial \phi}{\partial n_{23}} \\ \frac{\partial \phi}{\partial n_{31}} & \frac{\partial \phi}{\partial n_{32}} & \frac{\partial \phi}{\partial n_{33}} \end{bmatrix} \tag{1.38}$$

from which we can write the stress components as

$$\left.\begin{aligned} T_{11} &= J_{11} \frac{\partial \phi}{\partial n_{11}} + J_{12} \frac{\partial \phi}{\partial n_{21}} + J_{13} \frac{\partial \phi}{\partial n_{31}} \\ T_{12} &= J_{11} \frac{\partial \phi}{\partial n_{12}} + J_{12} \frac{\partial \phi}{\partial n_{22}} + J_{13} \frac{\partial \phi}{\partial n_{32}} \\ T_{13} &= J_{11} \frac{\partial \phi}{\partial n_{13}} + J_{12} \frac{\partial \phi}{\partial n_{23}} + J_{13} \frac{\partial \phi}{\partial n_{33}} \\ T_{21} &= J_{21} \frac{\partial \phi}{\partial n_{11}} + J_{22} \frac{\partial \phi}{\partial n_{21}} + J_{23} \frac{\partial \phi}{\partial n_{31}} \\ T_{22} &= J_{21} \frac{\partial \phi}{\partial n_{12}} + J_{22} \frac{\partial \phi}{\partial n_{22}} + J_{23} \frac{\partial \phi}{\partial n_{32}} \\ T_{23} &= J_{21} \frac{\partial \phi}{\partial n_{13}} + J_{22} \frac{\partial \phi}{\partial n_{23}} + J_{23} \frac{\partial \phi}{\partial n_{33}} \\ T_{31} &= J_{31} \frac{\partial \phi}{\partial n_{11}} + J_{32} \frac{\partial \phi}{\partial n_{21}} + J_{33} \frac{\partial \phi}{\partial n_{31}} \\ T_{32} &= J_{31} \frac{\partial \phi}{\partial n_{12}} + J_{32} \frac{\partial \phi}{\partial n_{22}} + J_{33} \frac{\partial \phi}{\partial n_{32}} \\ T_{33} &= J_{31} \frac{\partial \phi}{\partial n_{13}} + J_{32} \frac{\partial \phi}{\partial n_{23}} + J_{33} \frac{\partial \phi}{\partial n_{33}} \end{aligned}\right\} . \tag{1.39}$$

Substituting from (1.31) and (1.36) in Eqs. (1.39), we obtain the following expressions for T_{11}, T_{21} and T_{31}.

$$
\begin{aligned}
T_{11} &= C_{11}[u_a + \tfrac{3}{2} u_a^2 + \tfrac{1}{2} (v_a^2 + w_a^2)] + 3C_{111}u_a^2 + \tfrac{1}{4} C_{166}(v_a^2 + w_a^2) \\
T_{21} &= C_{44}v_a + C_{11}u_a v_a + \tfrac{1}{2} C_{166}u_a v_a \\
T_{31} &= C_{44}w_a + C_{11}u_a w_a + \tfrac{1}{2} C_{166}u_a w_a
\end{aligned}
\tag{1.40}
$$

where we have neglected terms higher than quadratic in the displacement gradients.

Since we are considering the special case of wave propagation in the [100] or $a = a_1$ direction, we require only the three stress components T_{11}, T_{21} and T_{31}. In this case the three component equations of motion according to Eq. (1.39) are

$$
\begin{aligned}
\partial T_{11}/\partial a &= \rho_0 \ddot{u} \\
\partial T_{21}/\partial a &= \rho_0 \ddot{v} \\
\partial T_{31}/\partial a &= \rho_0 \ddot{w}
\end{aligned}
\tag{1.41}
$$

because the stress components are functions of $a_1 = a$ only and not $a_2 = b$ or $a_3 = c$. Differentiating (1.40) and substituting into (1.41) and rearranging the terms we obtain the equations of motion using Birch's TOE constants as

$$
\begin{aligned}
\rho_0 \ddot{u} - C_{11}u_{aa} &= (3C_{11} + 6C_{111})u_a u_{aa} + (C_{11} + \tfrac{1}{2} C_{166})(v_a v_{aa} + w_a w_{aa}) \\
\rho_0 \ddot{v} - C_{44}v_{aa} &= (C_{11} + \tfrac{1}{2} C_{166})(u_a v_{aa} + v_a u_{aa}) \\
\rho_0 \ddot{w} - C_{44}w_{aa} &= (C_{11} + \tfrac{1}{2} C_{166})(u_a w_{aa} + w_a u_{aa})
\end{aligned}
\tag{1.42}
$$

Using the relations between Birch and Brugger elastic constants (Eqs. 1.4) we can write these equations in terms of Brugger elastic constants as

$$\rho_0\ddot{u} - C_{11}u_{aa} = (3C_{11} + C_{111})u_a u_{aa} + (C_{11} + C_{166})(v_a v_{aa} + w_a w_{aa})$$
$$\rho_0\ddot{v} - C_{44}v_{aa} = (C_{11} + C_{166})(u_a v_{aa} + v_a u_{aa}) \qquad (1.43)$$
$$\rho_0\ddot{w} - C_{44}w_{aa} = (C_{11} + C_{166})(u_a w_{aa} + w_a u_{aa})$$

If we write

$$\left.\begin{aligned} \alpha &= C_{11} \\ \mu &= C_{44} \\ \delta &= 3C_{11} + C_{111} \end{aligned}\right\} \qquad (1.44)$$

and

$$\gamma = C_{11} + C_{166}$$

Eqs. (1.43) become

$$\left.\begin{aligned} \rho_0\ddot{u} - \alpha u_{aa} &= \delta u_a u_{aa} + \gamma(v_a v_{aa} + w_a w_{aa}) \\ \rho_0\ddot{v} - \mu v_{aa} &= \gamma(u_a v_{aa} + v_a u_{aa}) \\ \rho_0\ddot{w} - \mu w_{aa} &= \gamma(u_a w_{aa} + w_a u_{aa}) \end{aligned}\right\} \qquad (1.45)$$

Since we attempt to propagate a pure mode longitudinal wave only, we have

$$u = u(a,t), \quad v = w = 0 . \qquad (1.46)$$

Then the three equations of motion in (1.45) reduce to

$$\rho_0\ddot{u} - \alpha u_{aa} = \delta u_a u_{aa} . \qquad (1.47)$$

Hence we see that a pure mode longitudinal wave may propagate in a nonlinear medium along the [100] direction. However, such a wave cannot

propagate without distortion and the generation of higher harmonics.

Let us assume that $\delta << \alpha$ and apply a perturbation solution to (1.47) of the form

$$u = u^{\circ} + u' \tag{1.48}$$

where $u' << u_0$ and use trial solutions

$$u^{\circ} = A \sin(ka - \omega t) \text{ for } \delta = 0 \tag{1.49}$$

$$u' = B\, a \sin 2(ka - \omega t) + C\, a \cos 2(ka - \omega t) \ . \tag{1.50}$$

Substituting (1.48) in (1.47), we have

$$\rho_0 \ddot{u}^{\circ} + \rho_0 \ddot{u}' - \alpha u_{aa}{}^{\circ} - \alpha u_{aa}{}' = \delta(u^{\circ} + u')_a (u^{\circ} + u')_{aa} \tag{1.51}$$

From the linear elastic equation of motion, we know that

$$\rho_0 \ddot{u}^{\circ} - \alpha u_{aa}{}^{\circ} = 0 \ , \tag{1.52}$$

where the phase velocity $C_0 = (\alpha/\rho_0)^{1/2}$. Therefore Eq. (1.51) reduces to

$$\rho_0 \ddot{u}' - \alpha u_{aa}{}' = \delta[u_a{}^{\circ} u_{aa}{}^{\circ} + (u_a{}' u_{aa}{}^{\circ} + u_a{}^{\circ} u_{aa}{}') + u_a{}' u_{aa}{}'] \ . \tag{1.53}$$

Since $u' << u^{\circ}$ we may neglect the second and third terms on the right hand side of (1.53) in comparison with the first term and hence to a first approximation the equation of motion reduces to

$$\rho_0 \ddot{u}' - \alpha u_{aa}{}' = \delta u_a{}^{\circ} u_{aa}{}^{\circ} \ . \tag{1.54}$$

Substituting the trial solutions given in Eqs. (1.49) and (1.50) into Eq. (1.54) we obtain the relation

$$\left.\begin{aligned} &-4\rho_0\omega^2 Ba \sin 2(ka - \omega t) - 4\rho_0\omega^2 Ca \cos 2(ka - \omega t) \\ &- 2\alpha kB \cos 2(ka - \omega t) - 2\alpha kB \cos 2(ka - \omega t) \\ &+ 4\alpha k^2 Ba \sin 2(ka - \omega t) + 2\alpha kC \sin 2(ka - \omega t) \\ &+ 2\alpha kC \sin 2(ka - \omega t) + 4\alpha k^2 Ca \cos 2(ka - \omega t) \\ &\quad = -\delta \frac{k^3}{2} A^2 \sin 2(ka - \omega t) . \end{aligned}\right\} \tag{1.55}$$

Equating the coefficients of $\sin 2(ka - \omega t)$ and $\cos 2(ka - \omega t)$ we find that

$$\left.\begin{aligned} -4\rho_0\omega^2 Ba + 4\alpha k^2 Ba + 4\alpha kC &= -(\delta k^3 A^2/2) \\ -4\rho_0\omega^2 Ca - 4\alpha kB + 4\alpha k^2 Ca &= 0 \end{aligned}\right\} \tag{1.56}$$

Recalling that $\alpha = \rho_0 C_0^2$ from Eq. (1.52) and that the angular frequency ω, the wave number k, and the phase velocity C_0 are related by $\omega = C_0 k$, Eqs. (1.56) reduce to

$$B = 0, \quad C = -[(kA)^2\delta/8\rho_0 C_0^2] . \tag{1.57}$$

Thus after one iteration we have the approximation solution

$$u(a,t) = A \sin(ka - \omega t) - [(kA)^2\delta/8\rho_0 C_0^2]a \cos 2(ka - \omega t) \tag{1.58}$$

which involves the second harmonic. If additional iterations are performed, higher harmonic terms will be obtained (but higher-order elastic constants would be introduced into the expression for $\phi(n)$, of course).

Breazeale and Ford[39] have applied the results of finite amplitude wave analysis, as worked out for fluids, to pure mode longitudinal nonlinear elastic waves in cubic single crystals. They write the equation of motion equivalent to Eq. (1.47) in the form

$$\rho_0 u_{tt} = K_2(u_{aa} + 3u_a u_{aa}) + K_3 u_a u_{aa} \tag{1.59}$$

where for the [100] direction

$$K_2 = C_{11} \text{ and } K_3 = C_{111} \tag{1.60}$$

using Brugger's notation for the TOE constants and subscript t denoting time differentiation. Comparison shows that Eq. (1.47) is identical with Eq. (1.59) if we set

$$\alpha = K_2 \quad \text{and} \quad \delta = 3K_2 + K_3 \, . \tag{1.61}$$

If we recall that $\rho_0 C_0^2 = \alpha$ from Eq. (1.52) and substitute this solution along with Eqs. (1.61) into Eq. (1.58) we have

$$u(a,t) = A \sin(ka - \omega t) - \frac{(3K_2 + K_3)}{8K_2} (kA)^2 a \cos 2(ka - \omega t) \tag{1.62}$$

which is also the expression given by Breazeale and Ford. The nonlinearity parameter $\beta = -\dfrac{3K_2 + K_3}{K_2}$ can be recognized in the second harmonic amplitude in Eq. (1.62).

The equations of motion and their solutions obtained above can readily be specialized to wave propagation in isotropic solids. Thus we see that a pure mode longitudinal nonlinear elastic wave may propagate along the [100] axis or in an isotropic solid, but such a wave generates

higher harmonics and the waveform distorts. A pure mode transverse nonlinear elastic wave cannot propagate without the simultaneous existence of a longitudinal wave.

b. Plane wave propagation along [110] direction. Let us consider the propagation of plane finite amplitude waves along the [110] direction, and rotate our coordinate axes from a = [100], b = [010], c = [001] to a' = [110], b' = [$\bar{1}$10], c' = c = [001]. Thus the coordinate transformation is given by

$$\begin{bmatrix} a' \\ b' \\ c' \end{bmatrix} = (R) \begin{bmatrix} a \\ b \\ c \end{bmatrix} \tag{1.63}$$

where the transformation matrix is

$$R = \begin{bmatrix} 1/\sqrt{2} & 1/\sqrt{2} & 0 \\ -1/\sqrt{2} & 1/\sqrt{2} & 0 \\ 0 & 0 & 1 \end{bmatrix} . \tag{1.64}$$

With respect to the new coordinate axes, the displacement components are

$$\left.\begin{aligned} u' &= u'(a',t) \\ v' &= v'(a',t) \\ w' &= w'(a',t) \end{aligned}\right\} . \tag{1.65}$$

Hence J' and J'* are given by (1.31) and (1.32) with the appropriate primes inserted, and the nonvanishing Lagrangian strain components in the primed coordinate system are of the same form as (1.34), namely

$$\left.\begin{aligned} \eta_{11}' &= u_a' + \frac{1}{2}\left(u_a'^2 + v_a'^2 + w_a'^2\right) \\ \eta_{12}' &= \eta_{21}' = \frac{1}{2} v_a' \\ \eta_{13}' &= \eta_{31}' = \frac{1}{2} w_a' \end{aligned}\right\} \tag{1.66}$$

Since the expression for the strain energy as given by (1.3) is written in terms of the unprimed coordinate system, we must transform the strain components into the primed system in order to use equations (1.66). Making use of the transformation matrix (1.64), we transform the strain components by

$$(\eta) = (R^*)(\eta')(R) \tag{1.67}$$

to obtain

$$\left.\begin{aligned} \eta_{11} &= \frac{1}{2}\left(\eta_{11}' - \eta_{12}' - \eta_{21}'\right) \\ \eta_{12} &= \frac{1}{2}\left(\eta_{11}' + \eta_{12}' - \eta_{21}'\right) \\ \eta_{13} &= 1/\sqrt{2}\ \eta_{13}' \\ \eta_{21} &= \frac{1}{2}\left(\eta_{11}' - \eta_{12}' + \eta_{21}'\right) \\ \eta_{22} &= \frac{1}{2}\left(\eta_{11}' + \eta_{12}' + \eta_{21}'\right) \\ \eta_{23} &= 1/\sqrt{2}\ \eta_{13}' \\ \eta_{31} &= 1/\sqrt{2}\ \eta_{31}' \\ \eta_{32} &= 1/\sqrt{2}\ \eta_{31}' \\ \eta_{33} &= 0\ . \end{aligned}\right\} \tag{1.68}$$

Substituting (1.68) into (1.3) we obtain

$$\phi = \frac{1}{4} C_{11}[\eta_{11}'^2 + (\eta_{12}' + \eta_{21}')^2]$$
$$+ \frac{1}{4} C_{12}[\eta_{11}'^2 - (\eta_{12}' + \eta_{21}')^2]$$
$$+ \frac{1}{2} C_{44}[\eta_{11}'^2 + (\eta_{12}' - \eta_{21}')^2 + 2(\eta_{13}'^2 + \eta_{31}'^2)]$$
$$+ \frac{1}{4} C_{111}[\eta_{11}'^2 + 3\eta_{11}'(\eta_{12}' + \eta_{21}')^2]$$
$$+ \frac{1}{4} C_{112}[\eta_{11}'^3 - \eta_{11}'(\eta_{12}' + \eta_{21}')^2]$$
$$+ \frac{1}{4} C_{144}\, \eta_{11}'(\eta_{13}'^2 + \eta_{31}'^2)$$
$$+ \frac{1}{4} C_{166}[\eta_{11}'^3 + \eta_{11}'(\eta_{12}' - \eta_{21}')^2 + \eta_{11}'(\eta_{13}'^2 + \eta_{31}'^2)]$$
$$+ \frac{1}{2} C_{456}\eta_{11}'\eta_{13}'\eta_{31}' \cdot \qquad (1.69)$$

Differentiating (1.69) with respect to strains, and using the relations $\eta_{ij} = \eta_{ji}$ and $\eta_{ij}' = \eta_{ji}'$ we get

$$\frac{\partial \phi}{\partial \eta_{11}'} = \frac{1}{2}(C_{11} + C_{12} + 2C_{44})\,\eta_{11}' + \frac{3}{4} C_{111}(\eta_{11}'^2 + 4\eta_{12}'^2)$$
$$+ \frac{1}{4} C_{112}(3\eta_{11}'^2 - 4\eta_{12}'^2) + \frac{1}{2} C_{144}\eta_{13}'^2$$
$$+ \frac{1}{4} C_{166}(3\eta_{11}'^2 + 2\eta_{13}'^2) + \frac{1}{2} C_{456}\eta_{13}'^2$$

$$\frac{\partial \phi}{\partial \eta_{21}'} = (C_{11} - C_{12})\eta_{12}' + 3C_{111}\eta_{11}'\eta_{12}' - C_{112}\eta_{11}'\eta_{12}'$$

$$\frac{\partial \phi}{\partial \eta_{31}'} = 2C_{44}\eta_{13}' + \frac{1}{2} C_{144}\eta_{11}'\eta_{13}' + \frac{1}{2} C_{166}\eta_{11}'\eta_{13}'$$
$$+ \frac{1}{4} C_{456}\eta_{11}'\eta_{13}' \cdot \qquad (1.70)$$

Substituting from Eqs. (1.31) with primes inserted, and from Eqs. (1.70) and (1.66) into Eqs. (1.39) with primes inserted, we obtain the

following expressions for T_{11}', T_{21}' and T_{31}':

$$\left.\begin{aligned}
T_{11}' &= \tfrac{1}{2}(C_{11} + C_{12} + 2C_{44})(u_{a'}' + \tfrac{3}{2}u_{a'}'^{2} + \tfrac{1}{2}v_{a'}'^{2} + \tfrac{1}{2}w_{a'}'^{2}) \\
&\quad + \tfrac{3}{4}C_{111}(u_{a'}'^{2} + v_{a'}'^{2}) + \tfrac{1}{4}C_{112}(3u_{a'}'^{2} - v_{a'}'^{2}) \\
&\quad + \tfrac{1}{8}C_{144}w_{a'}'^{2} + \tfrac{1}{4}C_{166}(3u_{a'}'^{2} + \tfrac{1}{2}w_{a'}'^{2}) + \tfrac{1}{8}C_{456}w_{a'}'^{2} \\
T_{21}' &= \tfrac{1}{2}(C_{11} + C_{12} + 2C_{44})u_{a'}'v_{a'}' + \tfrac{1}{2}(C_{11} - C_{12})v_{a'}' \\
&\quad + \tfrac{1}{2}(3C_{111} - C_{112})u_{a'}'w_{a'}' \\
T_{31}' &= \tfrac{1}{2}(C_{11} + C_{12} + 2C_{44})u_{a'}'w_{a'}' + C_{44}w_{a'}' \\
&\quad + \tfrac{1}{4}(C_{144} + C_{166} + C_{456})u_{a'}'w_{a'}'
\end{aligned}\right\} \qquad (1.71)$$

where we have neglected terms greater than quadratic in the displacement gradients. Again we use the reduced forms of the component equations of motion given by Eqs. (1.41) with primes inserted since we are only concerned with waves propagating along a' = [110]. After differentiation of Eqs. (1.71), substitution into (1.41) primed, and rearrangement, we obtain the equations of motion

$$\left.\begin{aligned}
\rho_0\ddot{u} - \alpha u_{aa} &= \delta u_a u_{aa} + \gamma v_a v_{aa} + \gamma^* w_a w_{aa} \\
\rho_0\ddot{v} - \chi v_{aa} &= \gamma(u_a v_{aa} + v_a u_{aa}) \\
\rho_0\ddot{w} - \chi^* w_{aa} &= \gamma^*(u_a w_{aa} + w_a u_{aa})
\end{aligned}\right\} \qquad (1.72)$$

where we have dropped the primes with the understanding that in Eqs. (1.72) u and a are along [110], v and b are along $[\bar{1}10]$ and w and c are along [001]. Again we have collected the linear terms on the left

of the equality and the nonlinear on the right. Moreover, in Birch's notation,

$$\alpha = \frac{1}{2}(C_{11} + C_{12} + 2C_{44})$$

$$\delta = \frac{3}{2}[(C_{11} + C_{12} + 2C_{44}) + (C_{111} + C_{112} + C_{166})]$$

$$\gamma = \frac{1}{2}[(C_{11} + C_{12} + 2C_{44}) + (3C_{111} - C_{112})]$$

$$\gamma^* = \frac{1}{4}[2(C_{11} + C_{12} + 2C_{44}) + (C_{144} + C_{166} + C_{456})]$$

$$\chi = \frac{1}{2}(C_{11} - C_{12})$$

$$\chi^* = C_{44} \tag{1.73}$$

or in Brugger's notation

$$\delta = \frac{3}{2}(C_{11} + C_{12} + 2C_{44}) + \frac{1}{4}(C_{111} + 3C_{112} + 12C_{166})$$

$$\gamma = \frac{1}{2}(C_{11} + C_{12} + 2C_{44}) + \frac{1}{4}(C_{111} - C_{112}) \tag{1.74}$$

$$\gamma^* = \frac{1}{2}(C_{11} + C_{12} + 2C_{44} + C_{144} + C_{166} + 2C_{456}) .$$

Since we attempt to propagate a pure mode longitudinal wave, Eqs. (1.72) reduce to the form of (1.47) given by

$$\rho_0 \ddot{u} - \alpha u_{aa} = \delta u_a u_{aa} . \tag{1.75}$$

If we rearrange Eq. (1.75) and use Eqs. (1.61) we can rewrite (1.75) in the form used by Breazeale and Ford, namely

$$\rho_0 \ddot{u} = K_2(u_{aa} + 3u_a u_{aa}) + K_3 u_a u_{aa} \tag{1.76}$$

where for the [110] direction

$$K_2 = \alpha = \frac{1}{2}(C_{11} + C_{12} + 2C_{44})$$
$$K_3 = \delta - 3\alpha = \frac{1}{4}(C_{111} + 3C_{112} + 12C_{166}) \tag{1.77}$$

using Brugger's notation for TOE constants. Thus, we see that in this case also a pure mode longitudinal nonlinear wave may propagate with the generation of a second harmonic given by (1.62), with K_2 and K_3 substituted from (1.77). In addition, the waveform will be distorted. As in the linear case, two uniquely polarized pure mode transverse waves can propagate but in the nonlinear case each of these pure transverse waves will be accompanied by a different longitudinal wave.

c. Plane wave propagation along [111] direction. Let us consider the propagation of plane finite amplitude waves along the [111] direction, and rotate the coordinate axes from a = [100], b = [010], c = [001] to a' = [111], b' = [11$\bar{2}$], c' = [$\bar{1}$10]. Thus, the coordinate transformation is given by

$$\begin{pmatrix} a' \\ b' \\ c' \end{pmatrix} = (R) \begin{pmatrix} a \\ b \\ c \end{pmatrix} \tag{1.78}$$

where the transformation matrix is

$$R = \frac{1}{\sqrt{6}} \begin{pmatrix} \sqrt{2} & \sqrt{2} & \sqrt{2} \\ 1 & 1 & -2 \\ -\sqrt{3} & \sqrt{3} & 0 \end{pmatrix} .$$

With respect to the new coordinate axes, the displacement components are

$$\left.\begin{aligned} u' &= u'(a',t) \\ v' &= v'(a',t) \\ w' &= w'(a',t) \end{aligned}\right\} \tag{1.80}$$

Hence the nonvanishing Lagrangian strain components in the primed coordinate system are the same as those in Eqs. (1.66), namely

$$\left.\begin{aligned} \eta_{11}' &= u_{a'}' + \frac{1}{2}\left(u_{a'}'^{2} + v_{a'}'^{2} + w_{a'}'^{2}\right) \\ \eta_{12}' &= \gamma_{21}' = \frac{1}{2} v_{a'}' \\ \eta_{13}' &= \gamma_{31}' = \frac{1}{2} w_{a'}' \end{aligned}\right\} \tag{1.81}$$

Since the expression for the strain energy as given by (1.3) is written in terms of the unprimed coordinate system, we must transform the strain components into primed system in order to use Eqs. (1.81). Making use of the transformation matrix, Eq. (1.79), and transforming according to (1.67) we obtain

$$\left.\begin{aligned} \eta_{11} &= \frac{1}{6}\left(\sqrt{2}\,\eta_{21}' - \sqrt{6}\,\eta_{13}' + \sqrt{2}\,\eta_{12}' - \sqrt{6}\,\eta_{13}' + 2\eta_{11}'\right) \\ \eta_{12} &= \frac{1}{6}\left(\sqrt{2}\,\eta_{21}' - \sqrt{6}\,\eta_{31}' + \sqrt{2}\,\eta_{12}' + \sqrt{6}\,\eta_{13}' + 2\eta_{11}'\right) \\ \eta_{13} &= \frac{1}{6}\left(\sqrt{2}\,\eta_{21}' - \sqrt{6}\,\eta_{31}' - 2\sqrt{2}\,\eta_{12}' + 2\eta_{11}'\right) \\ \eta_{21} &= \frac{1}{6}\left(\sqrt{2}\,\eta_{21}' + \sqrt{6}\,\eta_{31}' + \sqrt{2}\,\eta_{12}' - \sqrt{6}\,\eta_{13}' + 2\eta_{11}'\right) \\ \eta_{22} &= \frac{1}{6}\left(\sqrt{2}\,\eta_{21}' + \sqrt{6}\,\eta_{31}' + \sqrt{2}\,\eta_{12}' + \sqrt{6}\,\eta_{13}' + 2\eta_{11}'\right) \\ \eta_{23} &= \frac{1}{6}\left(\sqrt{2}\,\eta_{21}' + \sqrt{6}\,\eta_{31}' - 2\sqrt{2}\,\eta_{12}' + 2\eta_{11}'\right) \\ \eta_{31} &= \frac{1}{6}\left(-2\sqrt{2}\,\eta_{21}' + \sqrt{2}\,\eta_{12}' - \sqrt{6}\,\eta_{13}' + 2\eta_{11}'\right) \end{aligned}\right\} \tag{1.82}$$

$$\eta_{32} = \frac{1}{6}\left(-2\sqrt{2}\,\eta_{21}' + \sqrt{2}\,\eta_{12}' + \sqrt{6}\,\eta_{13}' + 2\eta_{11}'\right)$$

$$\eta_{33} = \frac{1}{6}\left(-2\sqrt{2}\,\eta_{21}' - 2\sqrt{2}\,\eta_{12}' + 2\eta_{11}'\right)$$

Substituting Eqs. (1.82) into Eq. (1.3) we get the expression for strain energy as

$$\begin{aligned}
\phi = {} & \frac{1}{6} C_{11}[\eta_{11}'^2 + (\eta_{21}' + \eta_{12}')^2 + (\eta_{31}' + \eta_{13}')^2] \\
& + C_{12}[\tfrac{1}{3}\eta_{11}'^2 - \tfrac{1}{6}(\eta_{21}' + \eta_{12}')^2 - \tfrac{1}{6}(\eta_{31}' + \eta_{13}')^2] \\
& + \tfrac{2}{3} C_{44}[\eta_{11}'^2 + \eta_{31}'^2 + \eta_{13}'^2 - \eta_{31}'\eta_{13}' + \eta_{21}'^2 + \eta_{12}'^2 - \eta_{21}'\eta_{12}'] \\
& + C_{111}[\tfrac{1}{9}\eta_{11}'^3 + \tfrac{1}{3}\eta_{11}'(\eta_{21}' + \eta_{12}')^2 + \tfrac{1}{3}\eta_{11}'(\eta_{31}' + \eta_{13}')^2 \\
& - \tfrac{\sqrt{2}}{18}(\eta_{21}' + \eta_{12}')^3 + \tfrac{\sqrt{2}}{6}(\eta_{21}' + \eta_{12}')(\eta_{31}' + \eta_{13}')^2] \\
& + C_{112}[\tfrac{2}{9}\eta_{11}'^3 + \tfrac{\sqrt{2}}{18}(\eta_{21}' + \eta_{12}')^3 - \tfrac{\sqrt{2}}{6}(\eta_{21}' + \eta_{12}')(\eta_{31}' + \eta_{13}')^2] \\
& + C_{144}[\tfrac{1}{9}\eta_{11}'^3 - \tfrac{1}{3}\eta_{11}'(\eta_{21}'\eta_{12}' + \eta_{31}'\eta_{13}') \\
& + \tfrac{\sqrt{2}}{36}(\eta_{21}'^3 + \eta_{12}'^3 - 3\eta_{21}'^2\eta_{12}' - 3\eta_{12}'^2\eta_{21}') \\
& + \tfrac{\sqrt{2}}{12}\{\eta_{21}'(\eta_{13}'^2 + 2\eta_{31}'^2\eta_{13}' - \eta_{31}'^2) + \eta_{12}'(\eta_{31}'^2 + 2\eta_{31}'\eta_{13}' - \eta_{13}'^2)\}] \\
& + C_{166}[\tfrac{2}{9}\eta_{11}'^3 + \tfrac{1}{3}\eta_{11}'(\eta_{21}'^2 + \eta_{12}'^2 + \eta_{31}'^2 + \eta_{13}'^2) \\
& + \tfrac{\sqrt{2}}{36}(-\eta_{21}'^3 - \eta_{12}'^3 + 3\eta_{21}'^2\eta_{12}' + 3\eta_{12}'^2\eta_{21}') \\
& + \tfrac{\sqrt{2}}{12}\{\eta_{21}'(\eta_{31}'^2 - 2\eta_{31}'\eta_{13}' - \eta_{13}'^2) + \eta_{12}'(-\eta_{31}'^2 - 2\eta_{31}'\eta_{13}' + \eta_{13}'^2)\}] \\
& + C_{123}[\tfrac{1}{27}\eta_{11}'^3 - \tfrac{1}{18}\eta_{11}'(\eta_{21}' + \eta_{12}')^2 - \tfrac{1}{18}\eta_{11}'(\eta_{31}' + \eta_{13}')^2 \\
& - \tfrac{\sqrt{2}}{54}(\eta_{21}' + \eta_{12}')^3 + \tfrac{\sqrt{2}}{18}(\eta_{21}' + \eta_{12}')(\eta_{31}' + \eta_{13}')^2]
\end{aligned}$$

$$+ C_{456}\left[\frac{2}{27}\eta_{11}'^{3} + \frac{1}{9}\eta_{11}'(-\eta_{31}'^{2} - \eta_{13}'^{2} + \eta_{31}'\eta_{13}')\right.$$

$$+ \frac{1}{9}\eta_{11}'(-\eta_{21}'^{2} - \eta_{12}'^{2} + \eta_{21}'\eta_{12}')$$

$$+ \frac{\sqrt{2}}{54}(-2\eta_{21}'^{3} - 2\eta_{12}'^{3} + 3\eta_{21}'\eta_{12}'^{2} + 3\eta_{12}'\eta_{21}'^{2})$$

$$\left. - \frac{\sqrt{2}}{18}\{\eta_{21}'(\eta_{13}'^{2} - 2\eta_{31}'^{2} + 2\eta_{31}'\eta_{13}') + \eta_{12}'(\eta_{31}'^{2} - 2\eta_{13}'^{2} + 2\eta_{31}'\eta_{13}')\}\right] \tag{1.83}$$

Differentiating Eq. (1.83) with respect to strains and using the symmetry relations $\eta_{ij} = \eta_{ji}$ and $\eta_{ij}' = \eta_{ji}'$, we have

$$\frac{\partial\phi}{\partial\eta_{11}'} = \frac{1}{3}(C_{11} + 2C_{12} + 4C_{44})\eta_{11}' + \frac{1}{3}C_{111}(\eta_{11}'^{2} + 4\eta_{21}'^{2} + 4\eta_{31}'^{2})$$

$$+ \frac{2}{3}C_{112}\eta_{11}'^{2} + \frac{1}{3}C_{144}(\eta_{11}'^{2} - \eta_{21}'^{2} - \eta_{31}'^{2})$$

$$+ \frac{2}{3}C_{166}(\eta_{11}'^{2} + \eta_{21}'^{2} + \eta_{31}'^{2})$$

$$+ \frac{1}{9}C_{123}(\eta_{11}'^{2} - 2\eta_{21}'^{2} - 2\eta_{31}'^{2}) + \frac{1}{9}C_{456}(2\eta_{11}'^{2} - \eta_{31}'^{2} - \eta_{21}'^{2})$$

$$\frac{\partial\phi}{\partial\eta_{21}'} = \frac{2}{3}(C_{11} - C_{12} + 2C_{44})\eta_{21}' + \frac{2}{3}C_{111}(2\eta_{11}'\eta_{21}'$$

$$- \sqrt{2}\,\eta_{21}'^{2} + \sqrt{2}\,\eta_{31}'^{2}) + \frac{2\sqrt{2}}{3}C_{112}(\eta_{21}'^{2} - \eta_{31}'^{2})$$

$$+ \frac{1}{6}C_{144}(-2\eta_{11}'\eta_{21}' - \sqrt{2}\,\eta_{21}' + \sqrt{2}\,\eta_{31}'^{2})$$

$$+ \frac{1}{6}C_{166}(4\eta_{11}'\eta_{21}' + \sqrt{2}\,\eta_{21}'^{2} - \sqrt{2}\,\eta_{31}'^{2})$$

$$+ \frac{2}{9}C_{123}(-\eta_{11}'\eta_{21}' - \sqrt{2}\,\eta_{21}'^{2} + \sqrt{2}\,\eta_{31}'^{2})$$

$$+ \frac{1}{18}C_{456}(-2\eta_{11}'\eta_{21}' + \sqrt{2}\,\eta_{21}' - \sqrt{2}\,\eta_{31}'^{2})$$

$$\frac{\partial \Phi}{\partial \eta_{31}'} = \frac{2}{3}(C_{11} - C_{12} + C_{44})\eta_{31}' + \frac{4}{3}C_{111}(\eta_{11}'\eta_{31}' + \sqrt{2}\,\eta_{21}'\eta_{31}')$$

$$- \frac{4\sqrt{2}}{3}C_{112}\eta_{21}'\eta_{31}'$$

$$+ \frac{1}{3}C_{144}(-\eta_{11}'\eta_{31}' + \sqrt{2}\,\eta_{21}'\eta_{31}') + \frac{1}{3}C_{166}(2\eta_{11}'\eta_{31}' - \sqrt{2}\,\eta_{21}'\eta_{31}')$$

$$+ \frac{2}{9}C_{123}(-\eta_{11}'\eta_{31}' + 2\sqrt{2}\,\eta_{21}'\eta_{31}')$$

$$+ \frac{1}{9}C_{456}(-\eta_{11}'\eta_{31}' + \sqrt{2}\,\eta_{21}'\eta_{31}' - 2\sqrt{2}\,\eta_{21}'\eta_{31}') \quad . \tag{1.84}$$

Substituting from Eqs. (1.31) with primes inserted and from Eqs. (1.84) and from Eqs. (1.81) into Eqs. (1.39) with primes inserted, we obtain

$$T_{11}' = \frac{1}{3}(C_{11} + 2C_{12} + 4C_{44})(u_a',_1 + \frac{3}{2}u_a',_1^2 + \frac{1}{2}v_a',_1^2 + \frac{1}{2}w_a',_1^2)$$

$$+ \frac{1}{3}C_{111}(u_a',_1^2 + v_a',_1^2 + w_a',_1^2) + \frac{2}{3}C_{112}u_a',_1^2$$

$$+ \frac{1}{3}C_{144}(u_a',_1^2 - \frac{1}{4}v_a',_1^2 - \frac{1}{4}w_a',_1^2) + \frac{2}{3}C_{166}(u_a',_1^2 + \frac{1}{4}v_a',_1^2 + \frac{1}{4}w_a',_1^2)$$

$$+ \frac{1}{9}C_{123}(u_a',_1^2 - \frac{1}{2}v_a',_1^2 - \frac{1}{2}w_a',_1^2) + \frac{1}{9}C_{456}(2u_a',_1^2 - \frac{1}{4}v_a',_1^2 - \frac{1}{4}w_a',_1^2)$$

$$T_{21}' = \frac{1}{3}(C_{11} - C_{12} + C_{44})v_a',_1 + \frac{1}{3}(C_{11} + 2C_{12} + 4C_{44})u_a',_1v_a',_1$$

$$+ \frac{2}{3}C_{111}(u_a',_1v'_a,_1 - \frac{\sqrt{2}}{4}v_a',_1^2 + \frac{\sqrt{2}}{4}w_a',_1^2)$$

$$+ \frac{\sqrt{2}}{6}C_{112}(v_a',_1^2 - w_a',_1^2) + \frac{1}{6}C_{144}(-u_a',_1v_a',_1 - \frac{\sqrt{2}}{4}v_a',_1^2 + \frac{\sqrt{2}}{4}w_a',_1^2)$$

$$+ \frac{1}{6}C_{166}(2u_a',_1v_a',_1 + \frac{\sqrt{2}}{4}v_a',_1^2 - \frac{\sqrt{2}}{4}w_a',_1^2)$$

$$+ \frac{1}{9}C_{123}(-u_a',_1v_a',_1 - \frac{\sqrt{2}}{2}v_a',_1^2 + \frac{\sqrt{2}}{2}w_a',_1^2)$$

$$+ \frac{1}{18}C_{456}(-u_a',_1v_a',_1 + \frac{\sqrt{2}}{4}v_a',_1^2 - \frac{\sqrt{2}}{4}w_a',_1^2)$$

$$T_{31}' = \frac{1}{3}(C_{11} - C_{12} + C_{44})w_a', + \frac{1}{3}(C_{11} + 2C_{12} + 4C_{44})u_a', w_a',$$
$$+ \frac{1}{3} C_{111}(2u_a', w_a', + \sqrt{2}\, v_a', w_a',) - \frac{\sqrt{2}}{3} C_{112} v_a', w_a',$$
$$+ \frac{1}{6} C_{144}(-u_a', w_a', + \frac{\sqrt{2}}{2} v_a', w_a',) + \frac{1}{3} C_{166}(u_a', w_a', - \frac{\sqrt{2}}{4} v_a', w_a',)$$
$$+ \frac{1}{9} C_{123}(-u_a', w_a', + \sqrt{2}\, v_a', w_a',) + \frac{1}{18} C_{456}(-u_a', w_a', - \frac{\sqrt{2}}{2} v_a', w_a',) \qquad (1.85)$$

where we have neglected terms higher than the quadratic in the displacement gradients.

We can use the reduced forms of the component equations given by (1.41) with primes inserted because we are only concerned with waves propagating along the a' = [111] direction. After differentiation of Eq. (1.85), substitution into Eqs. (1.41) primed, and rearrangement, we obtain the equations of motion as follows:

$$\left.\begin{aligned} \rho_0 \ddot{u} - c u_{aa} &= \cdot u_a u_{aa} + \cdot (u_a v_{aa} + w_a w_{aa}) \\ \rho_0 \ddot{v} - \cdot v_{aa} &= \cdot (u_a v_{aa} + v_a u_{aa}) + \cdot (w_a w_{aa} - v_a v_{aa}) \\ \rho_0 \ddot{w} - \cdot w_{aa} &= \cdot (u_a w_{aa} + w_a u_{aa}) + \cdot (v_a w_{aa} + w_a v_{aa}) \end{aligned}\right\} \qquad (1.86)$$

where we have dropped the primes with the understanding that in Eqs. (1.86) u and a are along [111], v and b are along $[11\bar{2}]$ and w and c are along $[\bar{1}10]$. As before, we have collected the linear terms on the left of the equality and the nonlinear on the right. In Birch's notation of TOE constants

$$\left.\begin{aligned}
\alpha &= \frac{1}{3}\,(C_{11} + 2C_{12} + 4C_{44}) \\
\delta &= \frac{1}{9}\,[9(C_{11} + 2C_{12} + 4C_{44}) + 6C_{111} + 12C_{112} + 6C_{144} \\
&\qquad + 12C_{166} + 2C_{123} + 4C_{456}] \\
\gamma &= \frac{1}{18}\,[6(C_{11} + 2C_{12} + 4C_{44}) + 12C_{111} - 3C_{144} + 6C_{166} - 2C_{123} - C_{456}] \\
\chi &= \frac{1}{3}\,(C_{\quad} - C_{12} + C_{44}) \\
\varepsilon &= \frac{\sqrt{2}}{36}\,(12C_{111} - 12C_{112} + 3C_{144} - 3C_{166} + 4C_{123} - C_{456})
\end{aligned}\right\} \tag{1.87}$$

or in Brugger's notation

$$\left.\begin{aligned}
\delta &= (C_{11} + 2C_{12} + 4C_{44}) + \frac{1}{9}\,(C_{111} + 6C_{112} + 12C_{144} + 24C_{166} \\
&\qquad + 2C_{123} + 16C_{456}) \\
\gamma &= \frac{1}{3}\,(C_{11} + 2C_{12} + 4C_{44}) + \frac{1}{9}\,(C_{111} - 3C_{144} + 6C_{166} - C_{123} - 2C_{456}) \\
\varepsilon &= \frac{\sqrt{2}}{18}\,(C_{111} - 3C_{112} + 3C_{144} - 3C_{166} + 2C_{123} - 2C_{456})
\end{aligned}\right\} \tag{1.88}$$

If we attempt to propagate a pure mode longitudinal wave only, Eqs. (1.86) reduce to the form of Eq. (1.47) given by

$$\rho_0\ddot{u} - \alpha u_{aa} = \delta u_a u_{aa} \,. \tag{1.89}$$

If we rearrange Eq. (1.89) and use Eqs. (1.61), we may rewrite Eq. (1.86) in the form used by Breazeale and Ford, namely,

$$\rho_0\ddot{u} = K_2(u_{aa} + 3u_a u_{aa}) + K_3\, u_a u_{aa} \tag{1.90}$$

where for the [111] direction

$$\left.\begin{aligned} K_2 &= \alpha = \frac{1}{3}\,(C_{11} + 2C_{12} + 4C_{44}) \\ K_3 &= \delta - 3\alpha = \frac{1}{9}\,(C_{111} + 6C_{112} + 12C_{144} + 24C_{166} + 2C_{123} + 16C_{456}) \end{aligned}\right\} \tag{1.91}$$

using Brugger's notation for TOE constants. Thus, we see that in this case also a pure mode longitudinal nonlinear wave may propagate with the generation of a second harmonic given by Eq. (1.62) with K_2 and K_3 substituted from (1.91). Due to the presence of ε terms, transverse wave propagation is more complicated than the previous [100] and [110] cases.

Summarizing the results obtained in the above three sections we can say that in the principal directions in cubic crystals the equations of motion for plane finite amplitude longitudinal waves are described by equations of motion of the form (Eqs. 1.47, 1.75 and 1.89)

$$\rho_0 \ddot{u} - \alpha u_{aa} = \delta u_a u_{aa} \tag{1.92}$$

or in the form (Eqs. 1.59, 1.76 and 1.90)

$$\rho_0 \ddot{u} = K_2(u_{aa} + 3u_a u_{aa}) + K_3 u_a u_{aa} \tag{1.93}$$

given by Breazeale and Ford. In the above two equations the constants are related by

$$\left.\begin{aligned} K_2 &= \alpha \\ \text{and} \\ K_3 &= \delta - 3\alpha \end{aligned}\right\} \tag{1.94}$$

The values of K_2 and K_3 along the three pure mode directions are given in Table I (Eqs. 1.61, 1.77 and 1.91).

Table 1. Values of the quantities K_2 and K_3 for longitudinal wave propagation along the pure mode directions in a cubic crystal

Direction of Wave Propagation	K_2	K_3
[100]	C_{11}	C_{111}
[110]	$\frac{1}{2}(C_{11} + C_{12} + 2C_{44})$	$\frac{1}{4}(C_{111} + 3C_{112} + 12C_{166})$
[111]	$\frac{1}{3}(C_{11} + C_{12} + 4C_{44})$	$\frac{1}{9}(C_{111} + 6C_{112} + 12C_{144} + 24C_{166} + 2C_{123} + 16C_{456})$

The ultrasonic nonlinearity parameter, as defined in Section 2, is the negative of the ratio of the nonlinear term to the linear term in the wave equation (1.92 or 1.93), namely,

$$\beta = -\frac{3K_2 + K_3}{K_2} \quad . \tag{1.95}$$

For an initially sinusoidal disturbance at a = 0, the solutions are of the form (Eqs. 1.62)

$$u = A_1 \sin(ka - \omega t) + \frac{A_1^2 k^2 a\beta}{8} \cos 2(ka - \omega t) \tag{1.96}$$

where A_1 is the fundamental wave amplitude and $A_2 = \frac{A_1^2 k^2 a\beta}{8}$ is the second harmonic amplitude. A_2 contains the nonlinearity parameter β. In terms of A_1 and A_2, β is given by

$$\beta = \frac{8}{3}\left(\frac{A_2}{A_1^2}\right)\frac{1}{k^2 a} = -\frac{1}{3}\left(3 + \frac{K_3}{K_2}\right) \quad . \tag{1.97}$$

Obviously a is the propagation distance and $k = 2\pi/\lambda$ is the wave vector. So a measurement of A_1 and A_2 leads to β which can be used to evaluate K_3 which are combinations of TOE constants.

CHAPTER II

APPARATUS AND MEASUREMENTS

The ultrasonic nonlinearity parameters are determined by measuring the amplitudes of both the fundamental component and the generated second harmonic component of a longitudinal wave propagating along the three symmetry directions of the sample. In the theory of finite amplitude distortion in solids the ratio (A_2/A_1^2), as given in (1.97), is independent of A_1 only in the limit of infinitesimal amplitude. So the smallest amplitude consistent with useful signal to noise ratio are used. The proportionality between the second harmonic amplitude and square of the fundamental amplitude holds strictly true[39] for infinite discontinuity distance which is equivalent to infinitesimal amplitude. So measurements with the smallest fundamental amplitude most exactly satisfy the assumptions made in the theory.

The frequency of the fundamental signal is chosen as 30 MHz as a compromise between the two following considerations: The generation of the second harmonic amplitude A_2 is directly proportional to the square of the frequency. So higher frequencies produce an improvement in the signal to noise ratio. At the same time, attenuation and effects of nonparallelism of the sample faces also increase with frequency. 30 MHz frequency is found to be most favorable. In the nonlinearity measurements the pulse-echo technique is used, allowing one wave pocket to die out before the next one is introduced. The pulse repetition rate is kept down to about 60 Hz to minimize sample heating. The largest ultrasonic displacement amplitudes attained at 30 MHz are of the order

of 10 A°. From Eq. (1.96) it can be estimated that the second harmonic amplitude will be about 1 percent of that of the fundamental. Thus a detector is needed of sensitivity sufficient to measure displacement amplitudes of the order of 10^{-9} cm.

1. Room Temperature Apparatus

(a) The Capacitive Detector. A capacitive detector has been developed[40] to measure displacement amplitudes as small as 10^{-12} cm ($\simeq 10^{-4}$ A°). A simplified diagram of the capacitive detector assembly is shown in Figure 1. The assembly consists of a detecting electrode held in place by a fused silica optical flat so that it is insulated from the outer ground ring which forms the ground of the electrical system. The detector and ground ring are made optically flat to an accuracy of half a wavelength of helium discharge light. The detector electrode is positioned at the center of the ground ring. It is recessed slightly with respect to the surface of the ground ring. The sample faces are also made optically flat to the same accuracy. The sample rests on the outer ground ring. The assembly is aligned properly so that the sample face and the electrode surface form a parallel plate capacitor. Typical gap spacing between the sample face and the electrode is of the order of 5-10 microns, resulting in a capacitance of 100-75 PF for a detector diameter of 0.916 cm. A bias voltage of the order of 100-150 volts is applied to the electrode, producing very high electric field (1000 kV/cm) in the capacitor gap. When a plane longitudinal wave impinges on the sample face, causing it to vibrate, the gap spacing is changed correspondingly and an alternating voltage is induced between the electrode and ground. The exact alignment of the sample, electrode

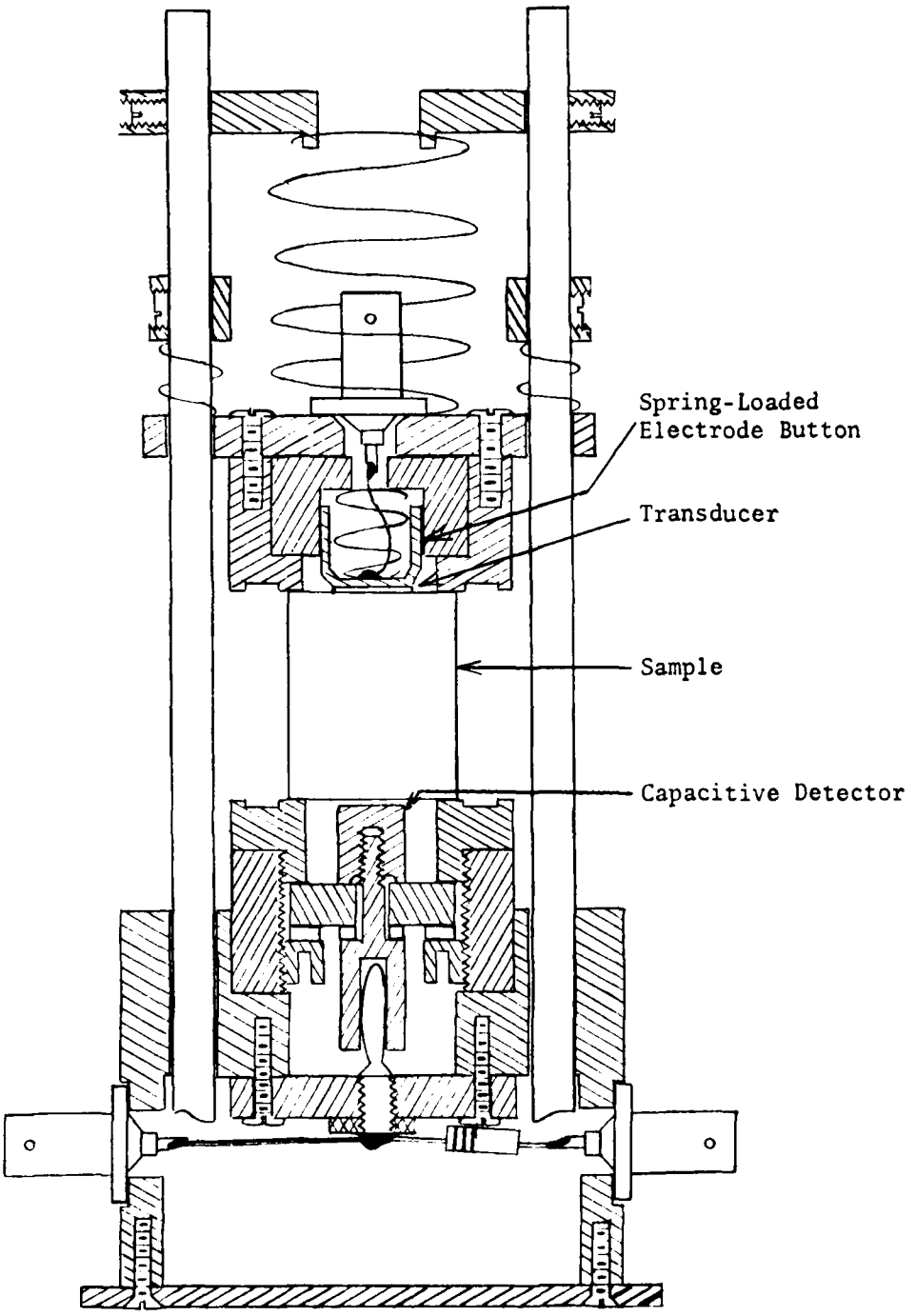

Figure 1. Cross sectional view of the room temperature apparatus.

button and ground ring is very important because a slight misalignment can result in shorting between the sample face and the electrode. For perfect alignment, the electrode is fixed at the center of the ground ring, and an optical flat is used in monochromatic light to produce fringes on the ring and electrode. Alignment of the fringes assures parallelism of the ground ring and the electrode.

Onto the top of the sample a piezoelectric X-cut quartz transducer of fundamental frequency 30 MHz is attached with stopcock grease as the bonding material. The transducers used are of diameter 1.27 cm. A copper electrode separated (electrically insulated) from the outer portion of the assembly by a teflon ring is pressed against the transducer by a spring. The spring provides electrical connection between the electrode and the BNC connector through which the electrical pulse is applied. The entire system is aligned and held in position by steel pins. The outer parts of both the detector and the generator transducer assembly make good contact with the sample surfaces so that electrical shielding is obtained which is very essential for accurate measurements. A photograph of the assembled room temperature apparatus is shown in Figure 2.

b. Calibration Procedure. Calibration of the capacitive detector and subsequent absolute amplitude measurements are done by introducing a substitutional signal in place of the acoustical signal. Provision is made in the experimental setup to connect a substitutional signal generator and an RF voltmeter to the detector button. The assembly is made in such a way that the capacitive detector need not be removed from the circuit during calibration measurements. The equivalent circuit for

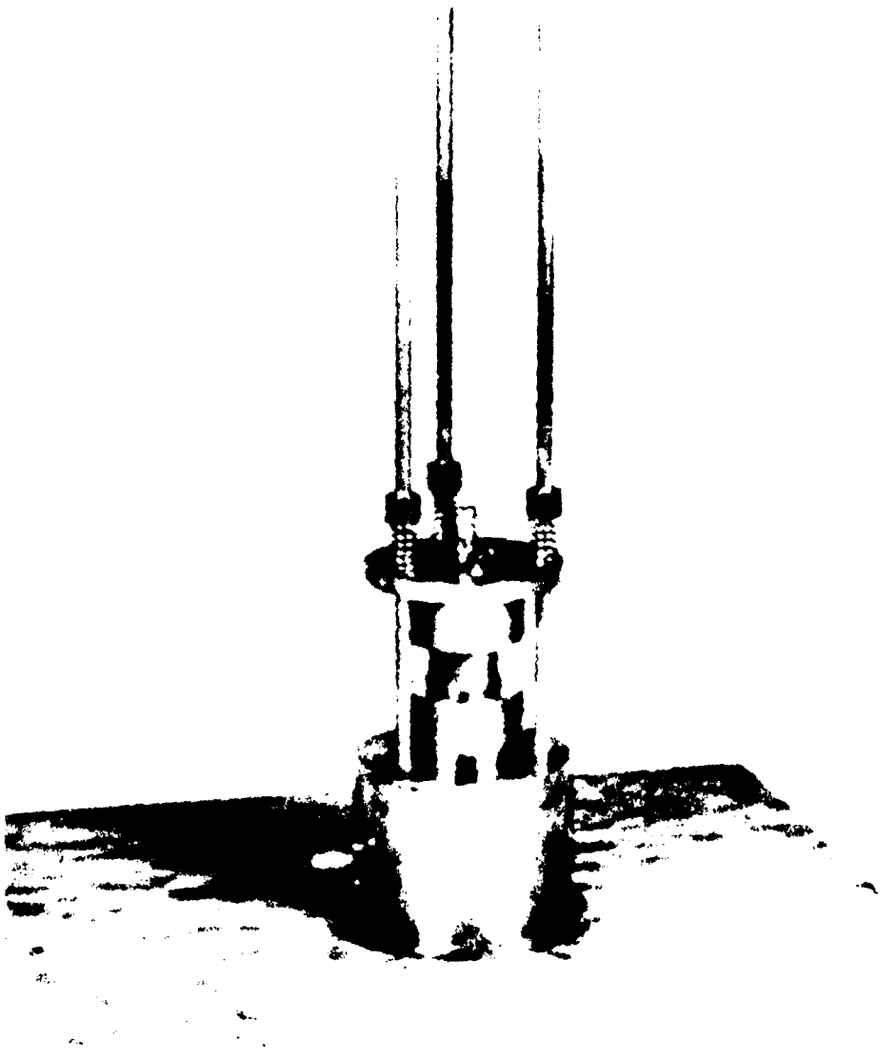

Figure 2. The room temperature apparatus.

the detector is the Norton equivalent. The equivalent circuit for the detector is shown in Figure 3. When the acoustic signal is turned off, the imaginary switch S_1 is opened, and the switch S_2 is closed by connecting the substitutional signal generator to the detector assembly. The series combination of the inductance L, the amplifier input impedance in parallel with the detector capacitance C_D and stray capacitance C_S form the total impedance of the detector circuit. The substitutional signal current i_s flows through the same impedance as the acoustical signal current i_s. The inductance L is the inductance of the wire leading from the banana jack to the BNC connector (see Figure 1). The inductance of the connector between the banana jack and the bottom of the detector can be neglected due to the large diameter of this connector.

If the end of the sample vibrates sinusoidally at an angular frequency ω with amplitude 2A, where A is the acoustic wave amplitude in the sample, then the gap spacing changes with time according to the relation

$$S = S_0 + 2A \sin \omega t \ . \tag{2.1}$$

The factor 2 enters in the amplitude because the vibration amplitude of the sample is twice the wave amplitude inside the sample. This results from reflection of the wave at the stress-free surface of the sample. Thus, the capacitance of the detector, considered as a parallel plate capacitor, responds as

$$1/C = 1/C_0\left(1 + \frac{2A}{S_0} \sin \omega t\right) \tag{2.2}$$

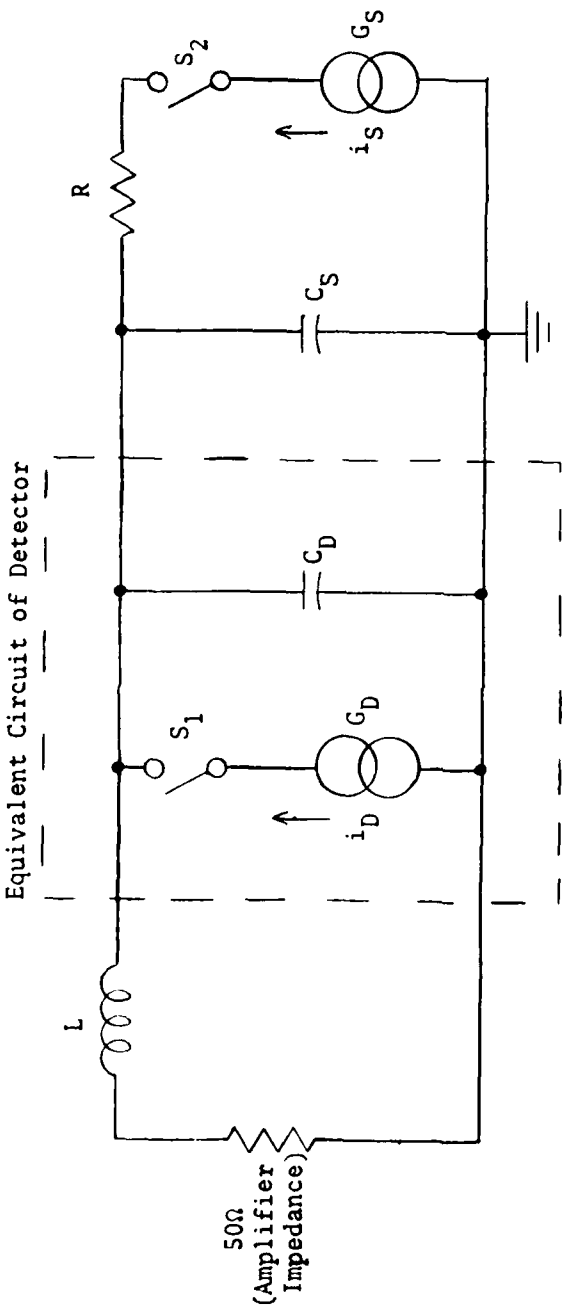

Figure 3. Equivalent circuit of the room temperature apparatus for absolute amplitude measurements.

where C_0 is the static capacitance of the receiver which is given by

$$C_0 = \frac{\varepsilon\alpha}{S_0} \tag{2.3}$$

where α is the area of cross section of the electrode button, ε is the dielectric constant of the medium (=1 in our case because the medium is air) and S_0 is the static gap spacing. If V_b is the bias voltage applied to the detector, the equivalent voltage V of the detector can easily be obtained as

$$V = \frac{2AV_b}{S_0} \tag{2.4}$$

where A is the amplitude of the ultrasonic wave. The derivation of this expression with the help of an equivalent circuit is given in Appendix A1.

In the equivalent circuit given in Figure 3, G_D and G_S represent the ultrasonic and substitutional signal generators. Since the voltage V is related to i_D by $i_D = V\omega C_D$ where ω is the angular frequency of the ultrasonic wave, we have

$$i_D = \frac{2AV_b\omega C_D}{S_0} \quad . \tag{2.5}$$

The substitutional current generator G_S is adjusted to give the same output from the amplifier as with the acoustic signal. When this connection is satisfied

$$i_D = i_S \quad . \tag{2.6}$$

Practically, voltages are much easier to measure than currents and so the voltage across G_S is measured and the current i_S is calculated from this voltage and a knowledge of the impedance through which the current flows. The resistor R does not act as a pure resistance at high frequencies. So the impedance of the resistor R must be measured at each frequency used in the calibration measurements. These measurements are made with a vector voltmeter. The sample, detector assembly and bottom plate are removed from the apparatus and a 50Ω precision terminator is placed on the "signal out" BNC connector as shown in Figure 4. Both vector voltmeter probes (with isolator tips) are placed at point 1 and the phase angle between the signals is zeroed and the amplitudes are measured. Probe A of the voltmeter is then left at point 1 while probe B is moved to point 2. The generator is readjusted to obtain the same reading of the A channel amplitude as before, and the amplitude of the B channel and the phase between the probes are recorded. This is done at each frequency used in the calibration measurements. The impedance Z of the resistor R can be calculated from

$$Z = \left[j\omega C + \frac{1}{R + j\omega L_1} \right]^{-1} \frac{V_{B1} - V_{B2}e^{i\phi}}{V_{B2}e^{i\phi}} \qquad (2.7)$$

where V_{B1} is the amplitude measured by probe B at point 1, V_{B2} is the amplitude measured by probe B at point 2, C is the stray capacitance which appears at point 2 (this includes the probe tip capacitance), R_1 is the resistance of the precision terminator (measured to 0.01Ω with an impedance bridge), ω is the angular frequency, ϕ is the phase angle

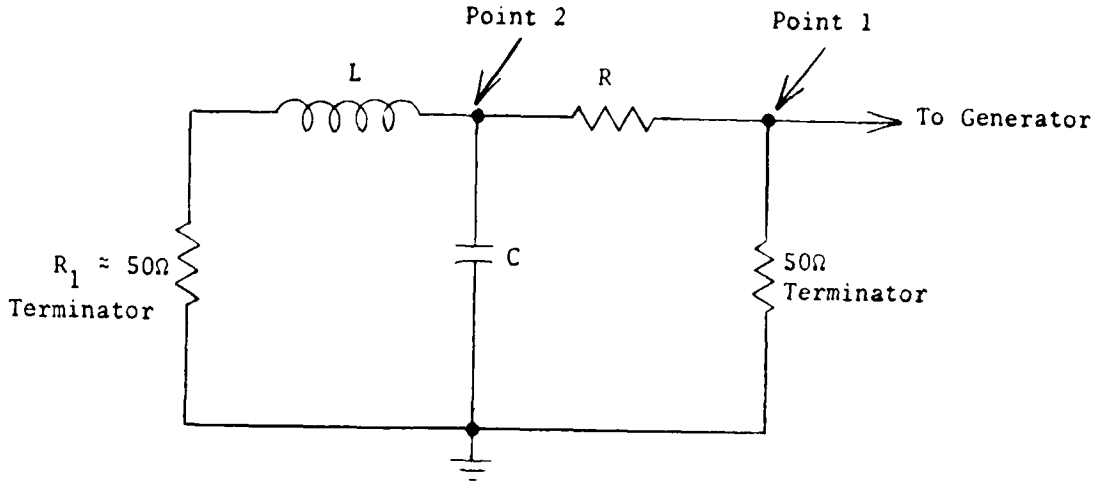

Figure 4. Equivalent circuit of the room temperature apparatus for the measurement of the impedance of R.

between V_{B1} and V_{B2} and $j^2 = -1$. A plot of the real and imaginary values of Z versus frequency, around the fundamental and second harmonic frequencies are shown in Figure 5.

The substitutional current i_S is then calculated by

$$i_S = \frac{V_S}{Z + [j\omega(C_D+C_S) + \frac{1}{50+j\omega L}]^{-1}} \qquad (2.8)$$

where V_S is the voltage across the current generator G_S. The resistor R has a value of approximately 10 KΩ; therefore Z is much larger than the other impedances in the apparatus, so that the other impedances do not have to be known very accurately in order to calculate i_S accurately. Also, the large value of Z gives a large voltage V_S which can be easily measured.

c. The Experimental Setup. The block diagram of the experimental setup for the room temperature nonlinearity measurements is given in Figure 6. A stable RF oscillator is used to drive a gated amplifier. The pulses are passed through a matching network and a 30 MHz bandpass filter which insures spectral purity of the ultrasonic wave even if the quartz transducer is driven off resonance. The transducer has been well bonded to the sample with nonag stopcock grease. The signal from the capacitive detector is fed to either the 30 MHz or 60 MHz bandpass amplifiers and the amplitudes of the signals are measured accurately with the boxcar integrator and vector voltmeter. The silicon samples not being good conductors, do not sufficiently shield the RF pulse at the transducer from the detector so that a 30 MHz direct feedthrough pulse is received at the detector by radiation before the ultrasonic

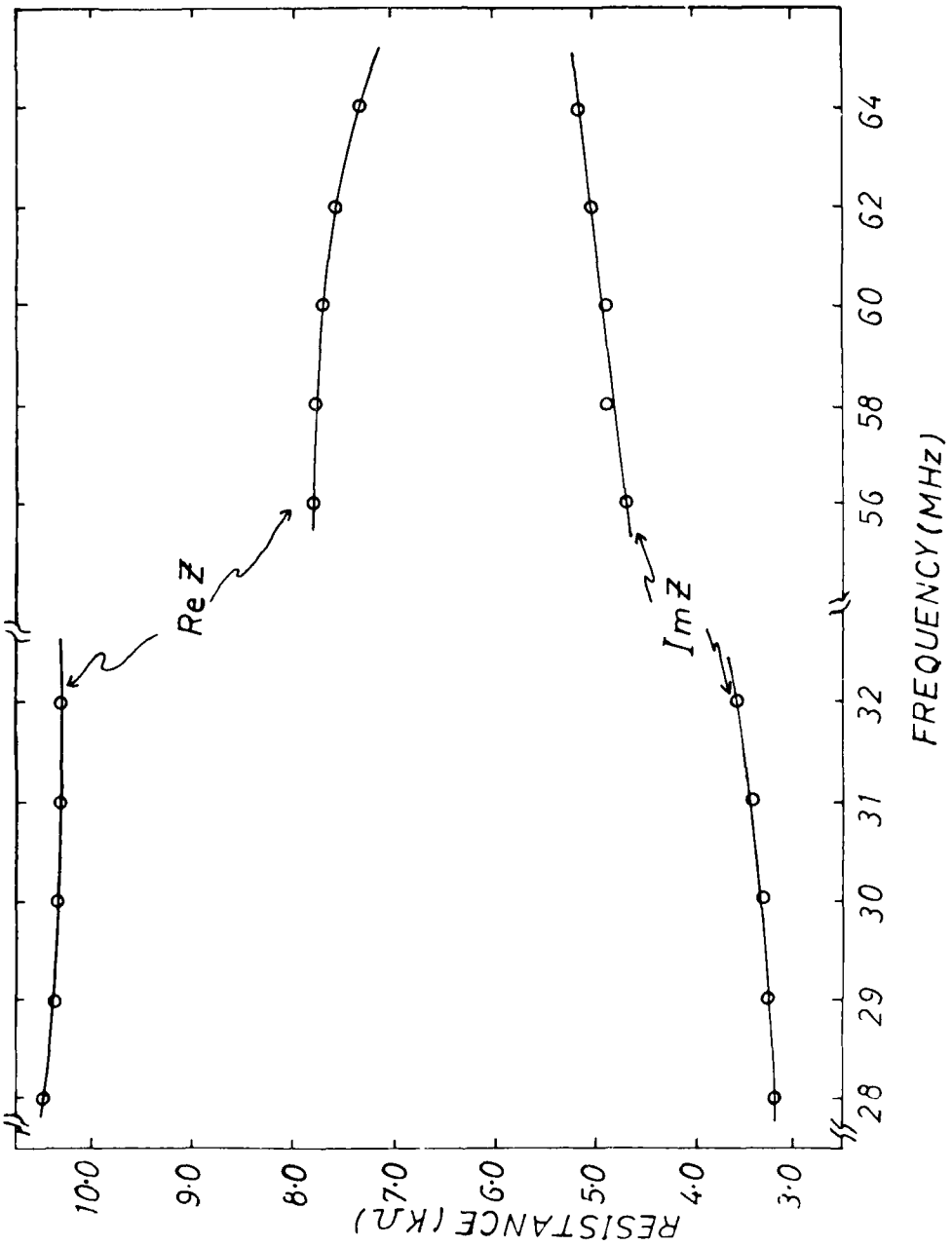

Figure 5. Real and imaginary values of the impedance of R drawn as a function of frequency.

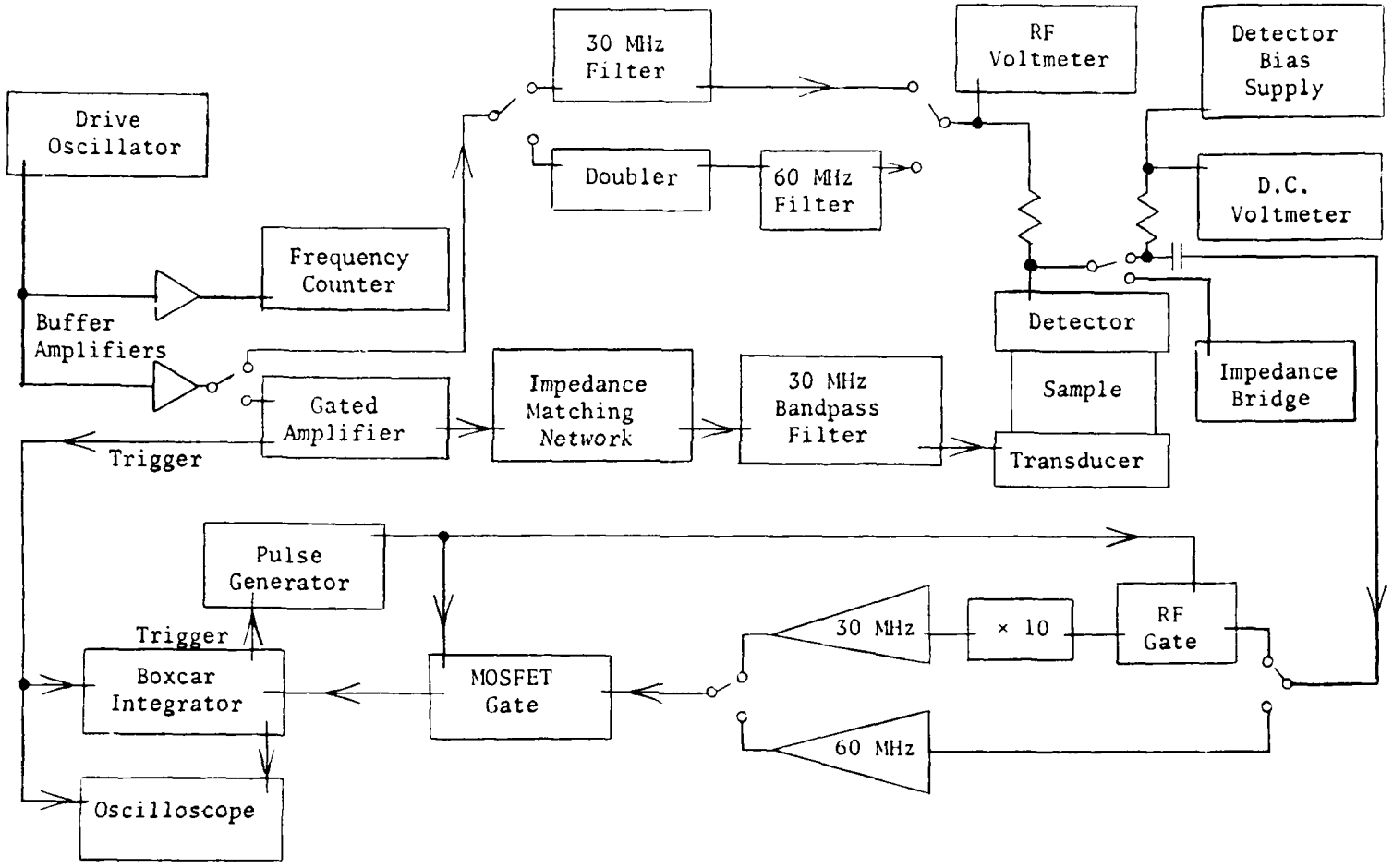

Figure 6. Block diagram for the room temperature nonlinearity measurements.

signal reaches the detector. This feedthrough pulse is oftentimes much larger than the echo of interest and although it can be separated in time from the echo to be measured, it can overload the 30 MHz amplifier and the boxcar integrator. The recovery time of the 30 MHz amplifier and the boxcar integrator would be too long to allow proper measurement of the first echo if they are overloaded by the feedthrough pulse. Whenever the feedthrough is excessive to make measurements difficult, an RF gate is used to detect the acoustic echo and a MOSFET gate is used to prevent overloading of the boxcar integrator. Descriptions of the RF gate and MOSFET gate along with their circuits are given in Appendix A2.

2. Room Temperature Measurements

The 30 MHz fundamental and the 60 MHz second harmonic signals have been measured by the boxcar integrator and then the continuous wave 30 MHz substitutional signal is introduced at the detector. A 30 MHz filter is used between the generator buffer amplifier and the detector to insure spectral purity of the signal. The signal amplitude of the substitutional signal is adjusted with attenuators so that the readings on the boxcar integrator coincides with the readings corresponding to the acoustical signal. The 60 MHz substitutional signal is derived by doubling the 30 MHz signal with a ring bridge mixer and filtering the output with a 60 MHz bandpass filter. The circuit and description of the frequency doubler are also given in Appendix A2. The continuous wave substitutional signals in both cases are measured accurately with an RF voltmeter. The bias voltage applied to the detector is noted and the gap spacing of the receiver is measured by

measuring its capacitance with an impedance bridge. From these the amplitudes of the fundamental and second harmonic signals are determined.

The measurements have been repeated for different values of fundamental signal amplitudes, the measurements being done on [100], [110] and [111] silicon samples.

3. Velocity Measurements

In order to determine the K_2 values given in Table 1 (p. 46) or the SOE constants of silicon, measurements of velocity of longitudinal waves along the three symmetry directions have been made using the pulse overlap technique with the capacitive receiver described before as the detector. A typical experimental setup for pulse overlap technique is shown in Figure 7. The gated amplifier produces a series of pulses that overlap in the sample. As the frequency of the CW generator is changed the echoes go through interference maxima and minima. The number of minima (or maxima) are counted and their frequencies noted. A typical interference pattern obtained using this technique is given in Figure 8. Interference minima are preferred rather than maxima in order to minimize envelope effects in shift in the position of the peaks due to nonconstant amplitude response of the electronic equipment as a function of frequency. The velocity C is then calculated from

$$C = \frac{2\Delta f L}{\Delta n} \tag{2.9}$$

where Δf is the change in frequency corresponding to a change in peak number Δn and L is the length of the sample. The velocities of longitudinal waves along the three symmetry directions are given by

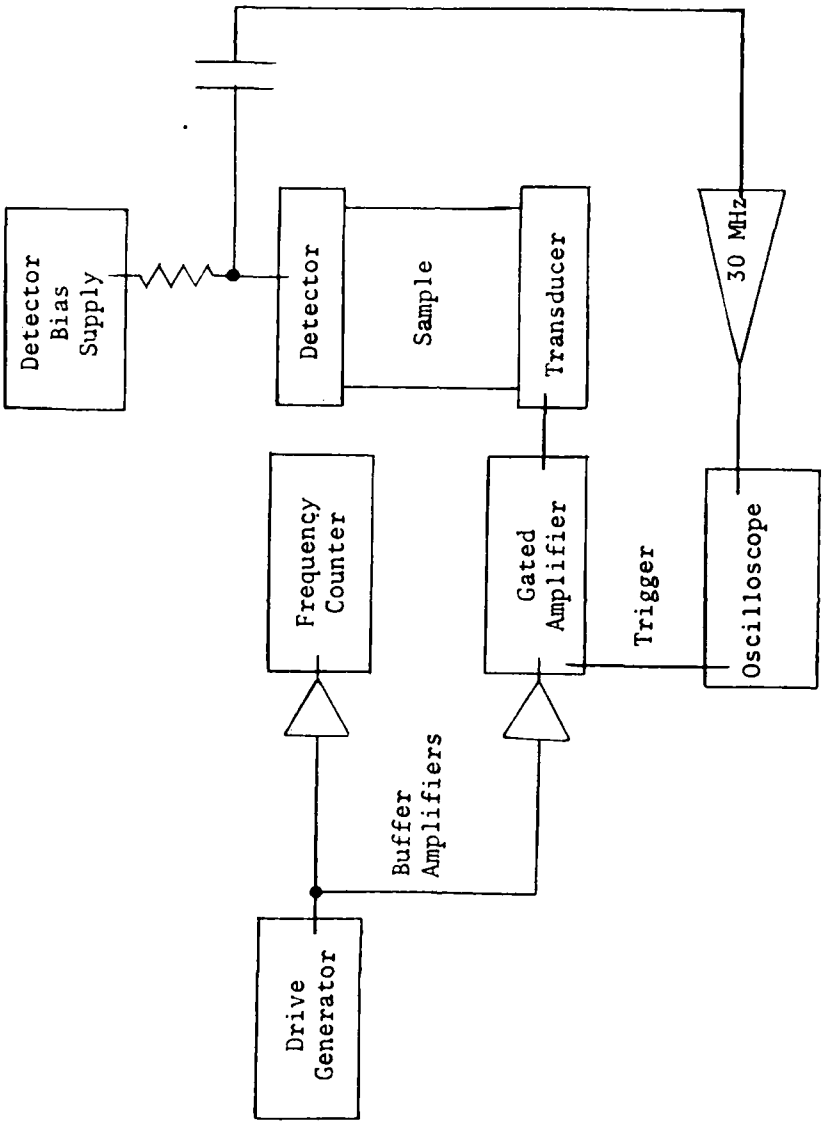

Figure 7. Block diagram for the velocity measurements using the pulse overlap technique.

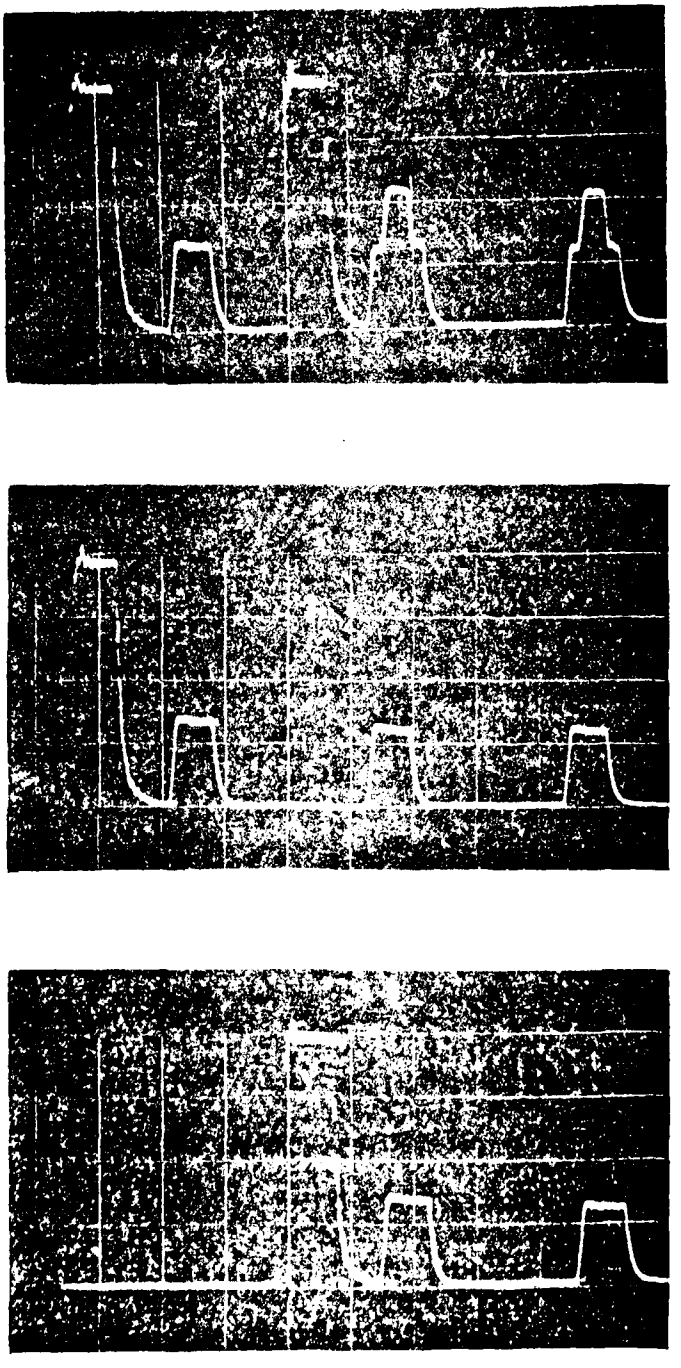

Figure 8. [illegible] obtained with the pulse overlap [illegible] ate pulse trains which interfere to [illegible]

$$\left.\begin{aligned} C[100] &= C_{11} = K_2\,[100] \\ C(110] &= \tfrac{1}{2}\,(C_{11} + C_{12} + 2C_{44}) = K_2\,[110] \\ C[111] &= \tfrac{1}{3}\,(C_{11} + 2C_{12} + 4C_{44}) = K_2\,[111] \end{aligned}\right\} \qquad (2.10)$$

So a measurement of velocities leads directly to the K_2 values given in Table 1 (p. 46). The measured values are compared with the values reported by McSkimin[53] and are found to agree very well within experimental uncertainties.

4. Samples

The samples used in the measurements are single crystals of silicon cut along the [100], [110] and [111] symmetry directions having lengths 2.5171 cm, 2.5222 cm and 2.5248 cm, respectively. The sample ends are made optically flat to less than 15" of arc by hand lapping and polishing. The end faces are then made electrically conductive by coating a copper coating of approximately 1000 A° thick onto them by vacuum evaporation.

5. The Cryogenic Apparatus

A general cross sectional view of the cryogenic system is shown in Figure 9. The dewar used is a conventional glass type incorporating two vacuum chambers with silver coated surfaces. The cryogenic fluid chambers are shown as V_1 and V_2 in the figure. For operation between room temperature and 77K, liquid nitrogen is used as the cooling agent in both the chambers. Near room temperature, it is convenient to operate with liquid in V_2 only and have dry nitrogen gas in the usually

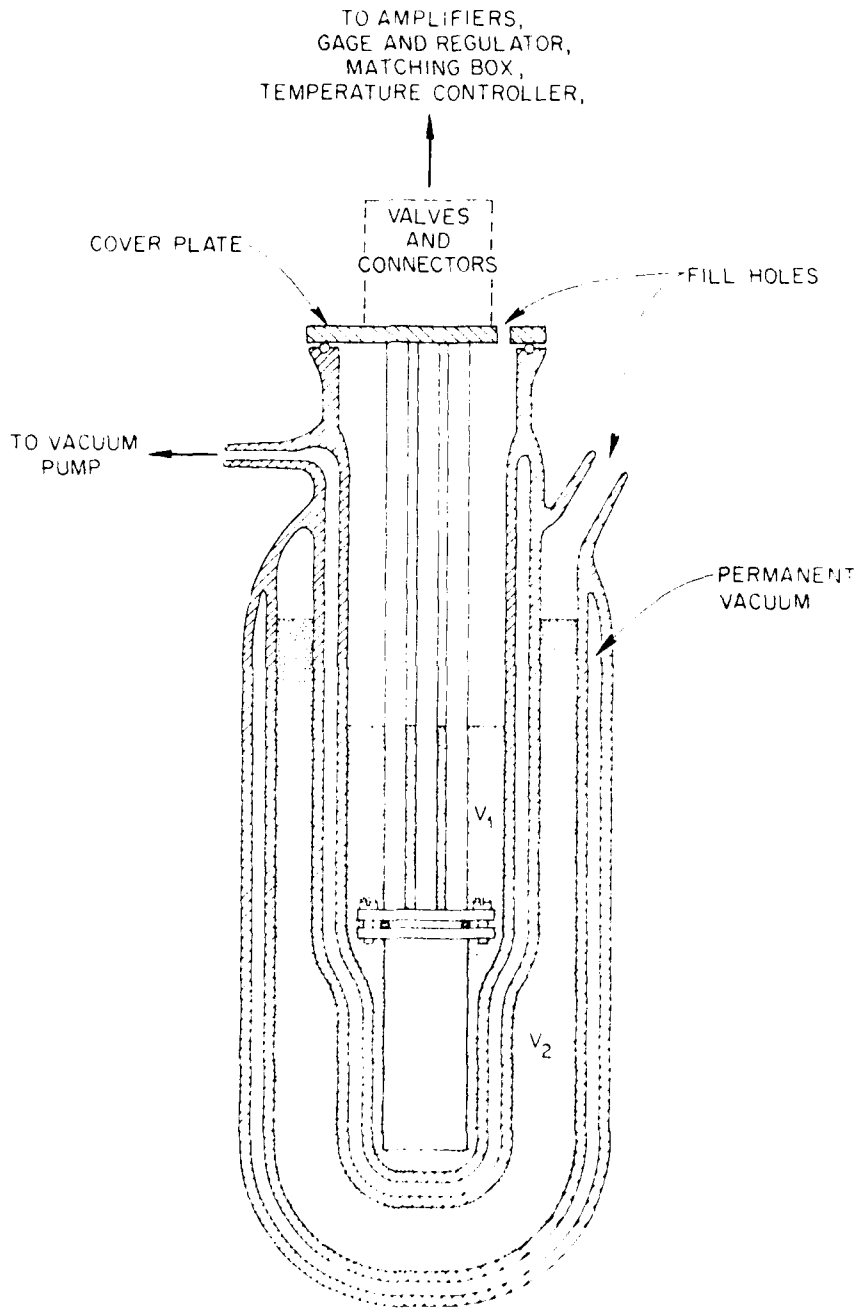

Figure 9. Cryostat used for the measurement of the temperature dependence of the nonlinearity parameters of single crystals.

evacuated space between V_1 and V_2. To operate between 77 and 3K, liquid helium is used as the cooling agent, maintaining liquid helium in V_1 and keeping V_2 filled with liquid nitrogen. It has been observed that by pumping on the liquid nitrogen in the inner chamber, the temperature can be brought down to about 65°K thus avoiding the use of expensive liquid helium between 77 and 65K.

The sample assembly is surrounded by two stainless steel cans. The inner one surrounds the sample and control assemblies, and the outer one which is concentric with the inner one provides a means of controlling the amount of heat transfer between the system and the coolant. The outer can is in immediate contact with the coolant. The space between the two cans is evacuated to provide an insulating jacket around the inner can. The cans are well polished to reduce radiation losses. The cans are supported by three thin-walled cupro-nickel tubes, each of which serves multiple purposes. Two of the tubes have smaller thin-walled cupro-nickel tubes inside them to form a coaxial transmission line: one for the signal input to the transducer and the other for the output from the detector. The tube sizes are chosen to make a 50Ω transmission line. These two tubes are also used as vacuum lines. The tube that houses the transmission line connector to the transducer is the vacuum line for the space surrounding the sample (the inside space of the inner can). The tube that houses the transmission line connector from the detector is also the vacuum lining to evacuate the space surrounding the detector button of the capacitive detector. Photographs showing the cryogenic apparatus are given in Figure 10.

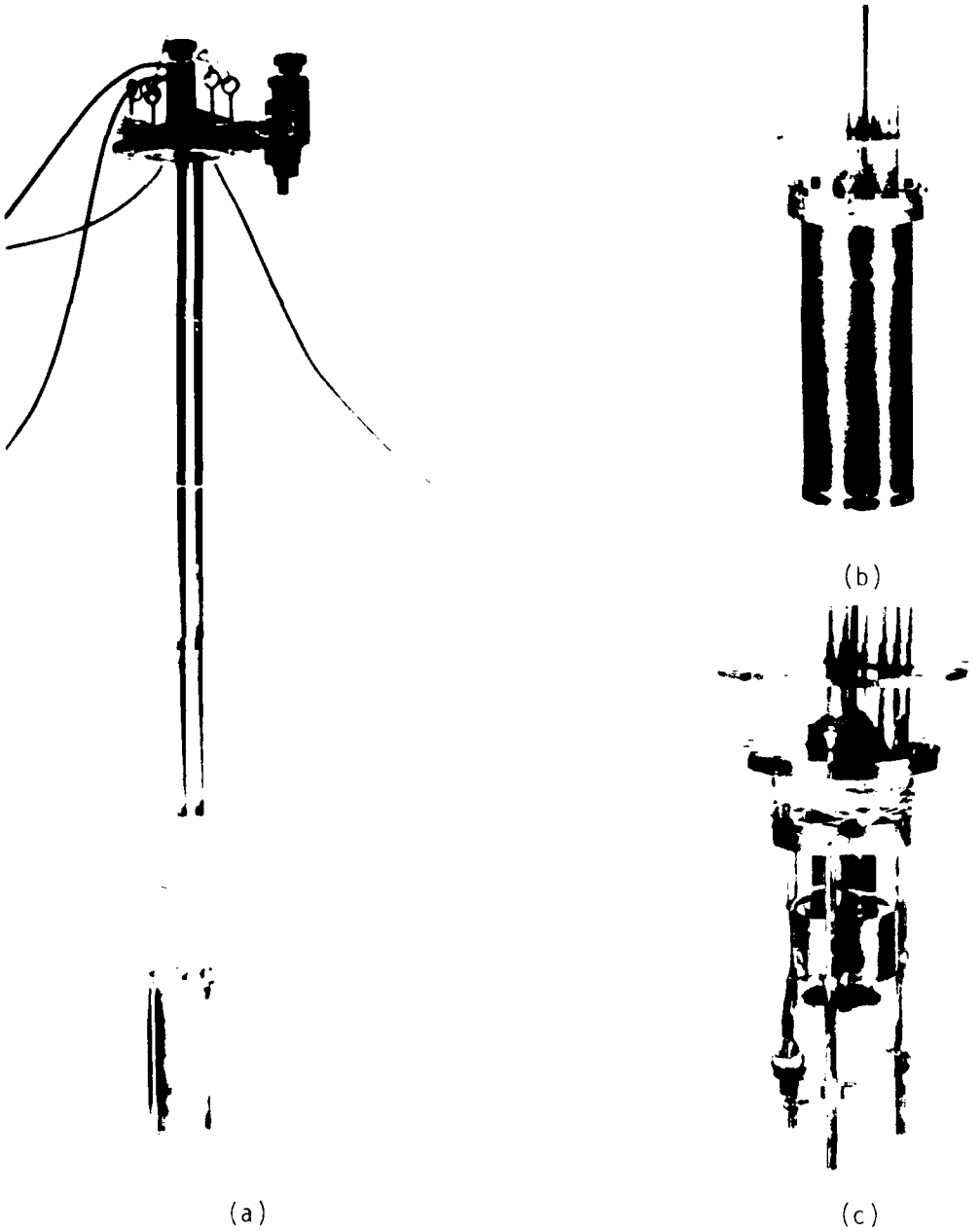

(a) (b) (c)

Figure 10. The cryogenic apparatus. (a) The complete apparatus; (b) apparatus with outer can removed; (c) apparatus with both cans removed.

The capacitive detector used for low temperature measurements is similar to that used in the room temperature apparatus, with the additional feature that the gap spacing between the detector button and sample surface can be controlled pneumatically. The cross sectional view of the variable gap capacitive detector is shown in Figure 11. The lapped ground ring against which the sample rests is undercut to make it a flexible diaphragm approximately 0.04 cm thick. The detector space is evacuated through the tube which houses the transmission line for the signal from the detector. The gap spacing is controlled pneumatically by regulating the pressure in the inner can. A cut-away view of the sample assembly is shown in Figure 12. The capacitive receiver, the inner can and the outer can are bolted in place with indium O-ring seals so as to have good vacuum in the detector space, inner can and outer can. Dry nitrogen or helium gas can be admitted into the space surrounding the sample which helps to prevent unwanted precipitation in the sample space. The gap spacing is adjusted pneumatically by letting in or pumping out nitrogen or helium gas in the sample space. The variable gap capacitive detector makes it possible to have a constant detector capacitance for the detector when the temperature is varied. The effects due to differential thermal expansion of the sample and the associated assembly are thus compensated by regulating the pressure in the inner can.

Once the sample has been cooled to liquid nitrogen or liquid helium temperature, the temperature can be increased with an electrical heater. Two sets of heater coils are wound, one above and one below the sample so that uniform heating of the sample takes place. The temperature

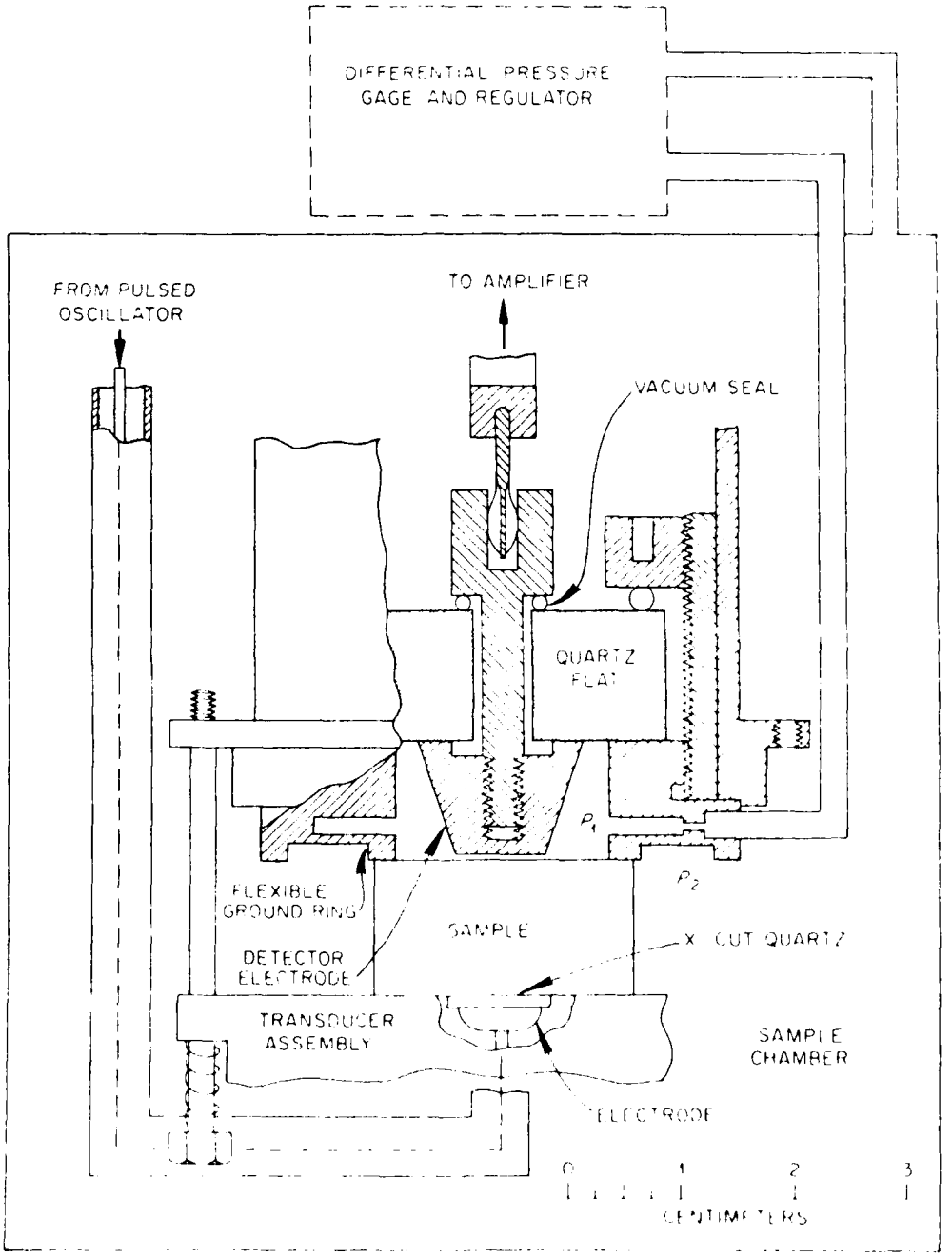

Figure 11. Variable gap capacitive detector.

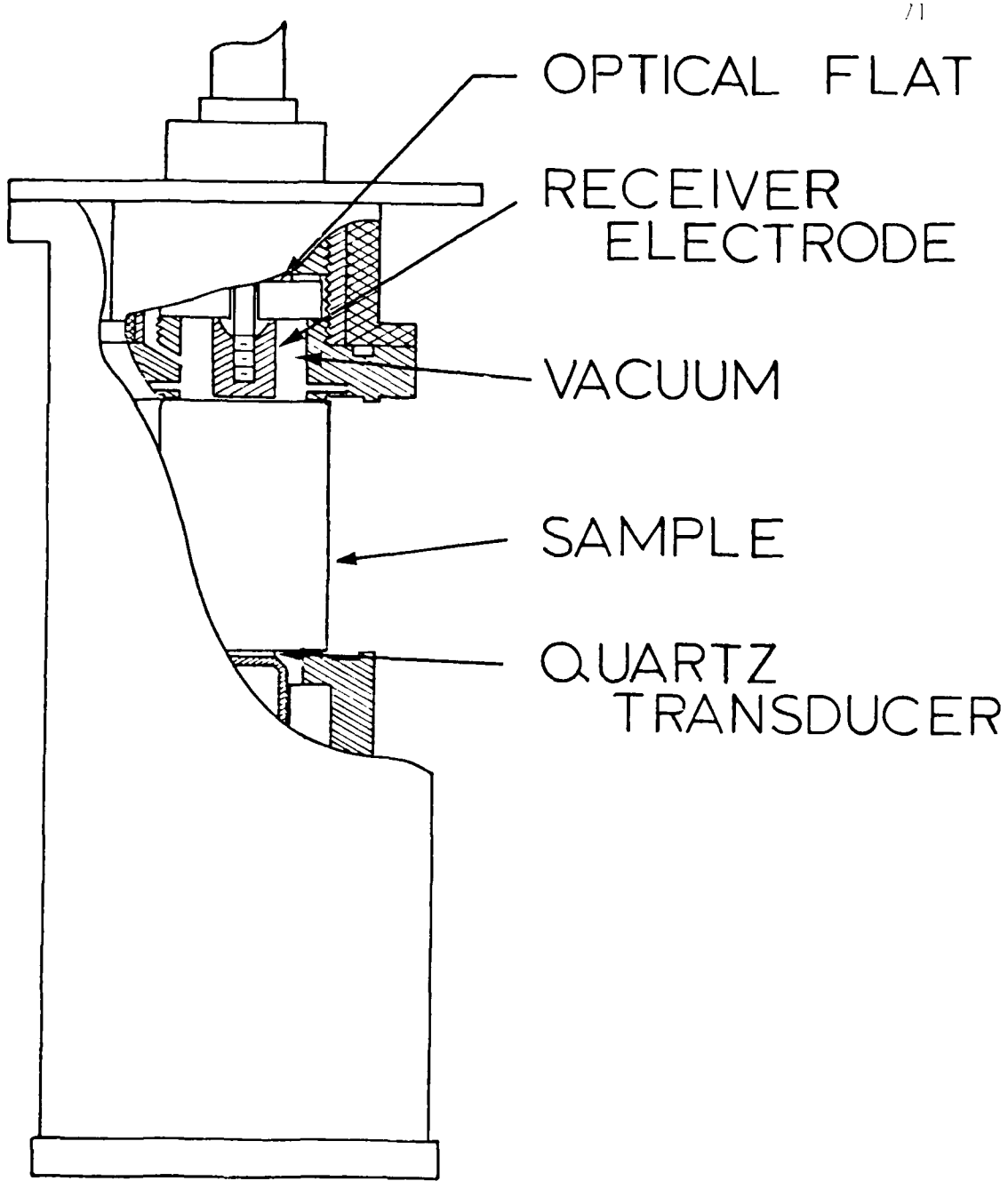

Figure 12. Cut-away view of the low temperature sample assembly.

of the sample is measured with a germanium or platinum sensor. A germanium sensor with negative temperature coefficient of resistance is used below ~ 20 K and a platinum sensor with positive temperature coefficient of resistance is used at higher temperatures. The electrical output from the sensor controls the power delivered to the heater, this being accomplished with an Artronix temperature controller. The temperature controller contains a bridge circuit. One of the arms of the bridge is the temperature sensor. If the bridge is unbalanced, the controller provides more or less power to the heater which tends to balance the bridge. The deviation of the temperature from the set point, and the voltage on the heater are monitored on a dual pen strip chart recorder. Monitoring the heater voltage allows one to determine when thermal equilibrium has been established in the sample chamber. The system allows one to increase the temperature slowly and measure it accurately. A block diagram of the temperature measurement and control system is given in Figure 13.

To facilitate accurate temperature measurements, the measurements are done with different sensors than the temperature control sensors. A constant current generator, shown in Figure 14, supplies a current to the sensor (either platinum or germanium), and the voltage is measured across the sensor. A four-wire connection is made to the sensors so that the voltage measurement is made by a path which does not carry current. This prevents lead resistance from affecting the sensor resistance measurement. A voltmeter which has an input impedance of ~ 1000 m is used for measurement so that negligible current is drawn. The voltmeter is also used to measure the current by measuring

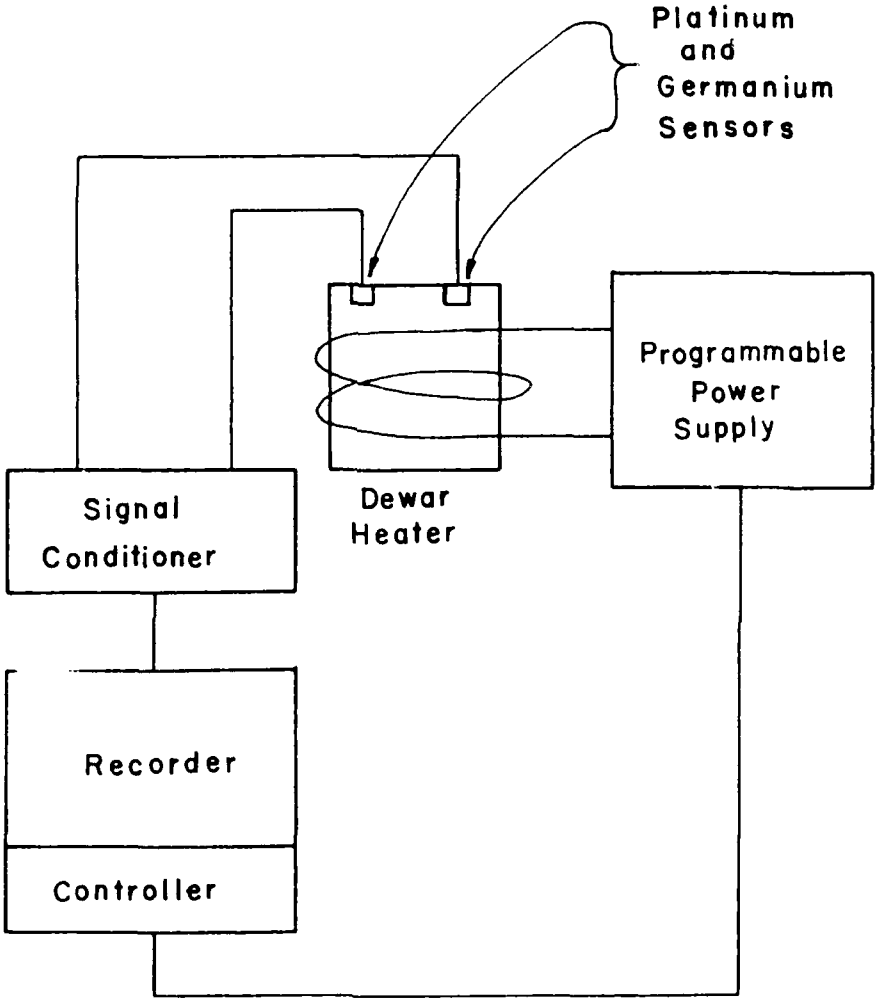

Figure 13. Temperature measurement and control system.

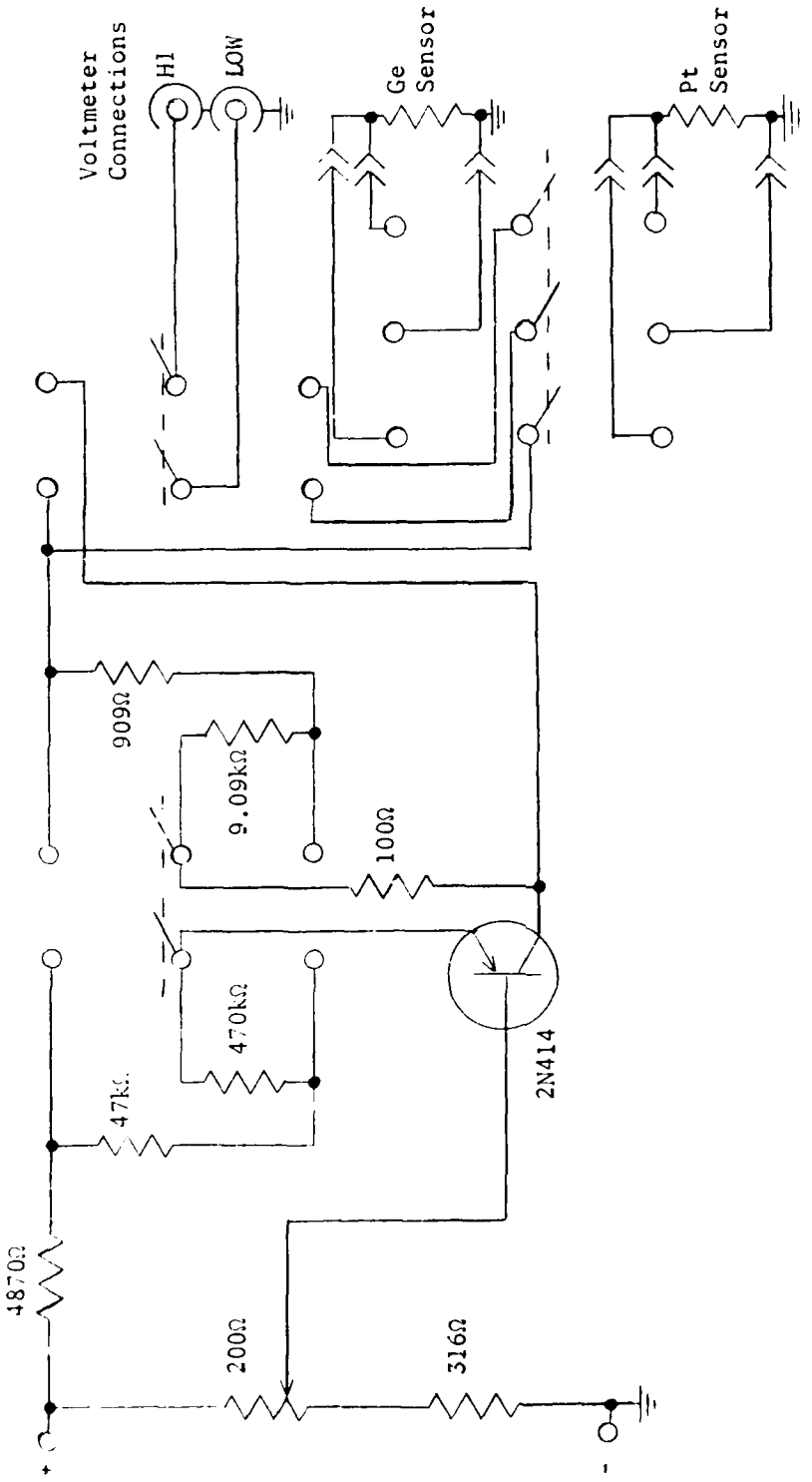

Figure 14. The constant current generator used for temperature control.

the voltage across a known resistance in series with the current-carrying lead. The constant current generators is required because the heater current also flows through the ground of the apparatus. When a simple resistive network is used to supply current, the noisy heater current is large enough to change the voltage with respect to ground which changes the sensor current by a noticeable amount. The resistance measurement can still be made, in principle, as the sensor voltage changes when the sensor current is changed, but since the measurements cannot be made simultaneously the heater noise makes measurements difficult. The single transistor constant-current generator is very effective in holding the current constant regardless of voltage changes with respect to ground. The voltages measured are of the order of 1 mV so that contact potentials and thermal potentials need be taken into account. An effective way to do this is to take two or more resistance measurements using different currents. Then the sensor resistance R is found by

$$R = \frac{V_2 - V_1}{I_2 - I_1} \tag{2.11}$$

where V_1 and V_2 are two voltages and I_1 and I_2 are the corresponding currents.

6. Cryogenic Nonlinearity Measurements

The block diagram of the apparatus used for low temperature ultrasonic nonlinearity measurements is shown in Figure 15. The signal path is the same as that for room temperature measurements with the exceptions that (1) the substitutional signal capability is absent

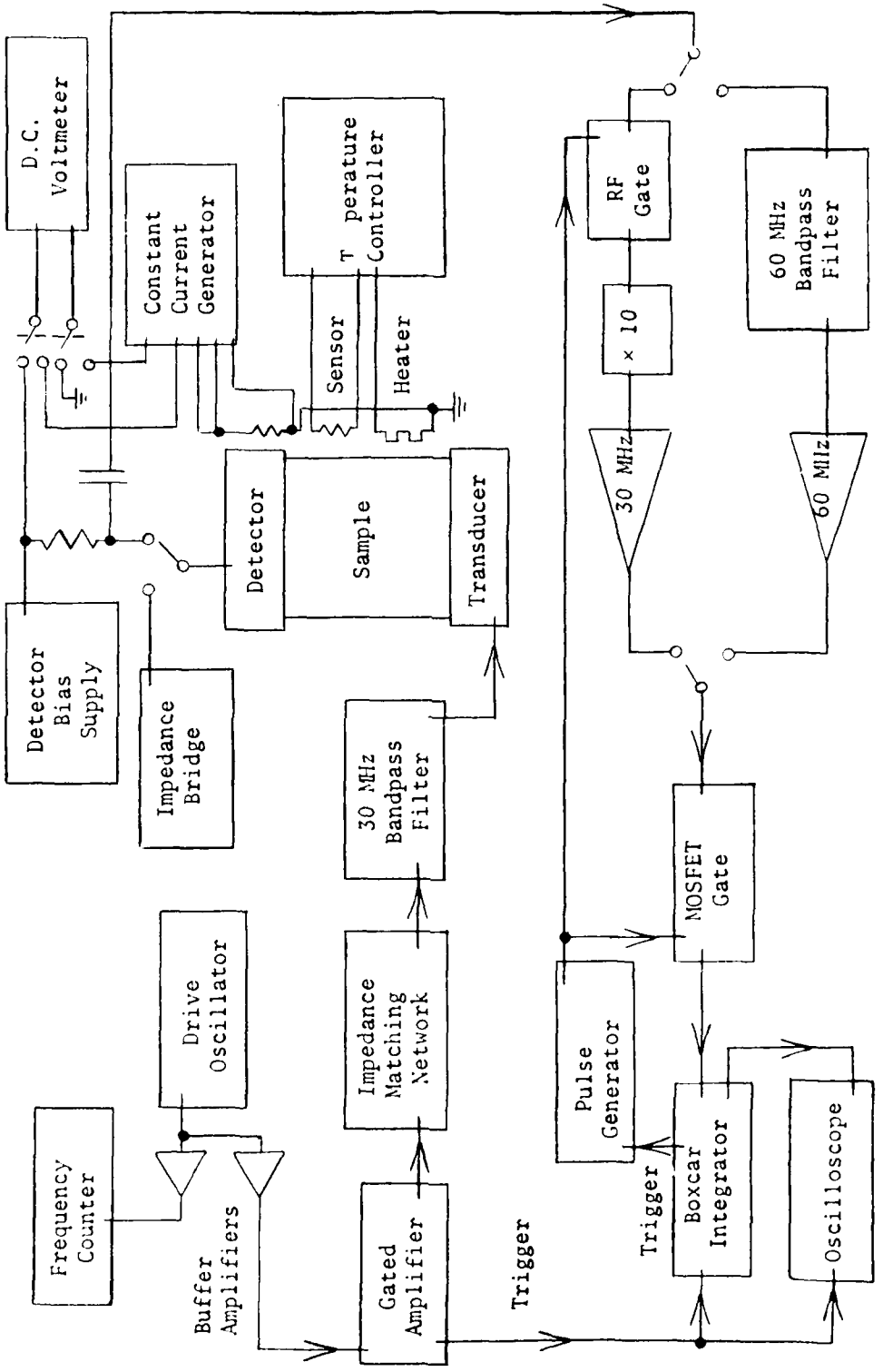

Figure 15. Block diagram of the cryogenic nonlinearity measurements.

because only relative amplitudes need be measured and (2) a 60 MHz broadband filter is introduced between the capacitive detector and the 60 MHz amplifier in addition to themostat gates. The feedthrough problem is much worse in the cryogenic measurements than in the room temperature measurements. In the room temperature apparatus, the sample could be adjusted manually until proper sample seating, principally on the transducer end, is achieved resulting in the reduction of feedthrough signal. In the low temperature apparatus, the sample is inaccessible to such adjustments and so the two gates are important in the cryogenic measurements to insure that the amplifiers are not overloaded. Under these severe conditions the 60 MHz amplifier can be overloaded by the 30 MHz feedthrough. So the 60 MHz filter is used to attenuate the feedthrough while passing the 60 MHz signal. Since the filter is a completely passive network, harmonics cannot be generated by it. In Figure 16 a photograph of the entire low temperature system is given.

The low temperature nonlinearity measurements are done using a comparison technique because the 30 MHz and 60 MHz amplifiers have gains which can be functions of the signal amplitude. The procedure is to set the capacitance of the detector to a chosen value. As the temperature is varied, the variations in the capacitance (or spacing) is nullified very conveniently by adjusting the pressure in the inner can with a regulator valve. The bias voltage on the detector is set to some predetermined value ($\simeq$ 150 volts). The RF power applied to the quartz transducer is adjusted to obtain some predetermined reading of the 30 MHz signal on the boxcar integrator. The detector bias voltage

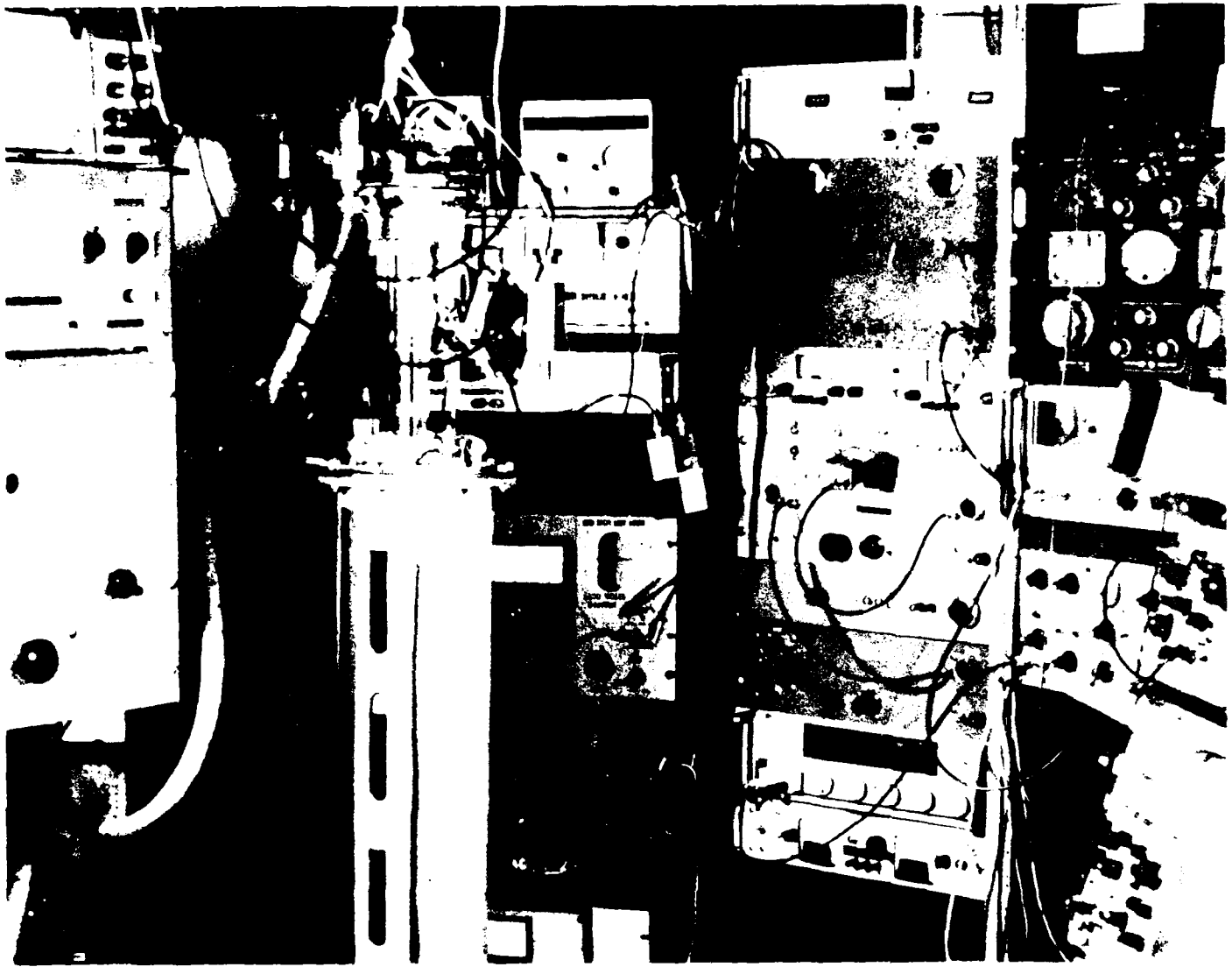

Figure 16. Assembled apparatus.

is then changed until the 60 MHz second harmonic signal reaches the predetermined boxcar integrator reading. The pulse repetition rate, pulse length and gains of the 30 MHz and 60 MHz amplifiers should be kept undisturbed during the entire experiment. In order to avoid the trouble of considering the frequency dependence of the equipment, the frequency of the CW generator is also kept constant.

Always the bias voltage of the fundamental signal remains the same and any deviation of the fundamental signal amplitude from the predetermined boxcar integrator reading is compensated by adjusting the input signal to the transducer. The second harmonic bias voltage is then varied to obtain the predetermined second harmonic boxcar integrator reading. So the only variable in the entire temperature cycling is the second harmonic bias voltage. The output of the 60 MHz amplifier is proportional to the amplitude of the second harmonic A_2 and the detector bias voltage V_b. If this output is held constant and the measurements are made at two temperatures T_1 and T_2,

$$A_2^{T_1} V_b^{T_1} = A_2^{T_2} V_b^{T_2} \tag{2.12}$$

where the different subscripts indicate the temperature corresponding to the value. Therefore

$$A_2^{T_2} = A_2^{T_1} \frac{V_b^{T_1}}{V_b^{T_2}} . \tag{2.13}$$

The measurements are made relative to the room temperature values. The relative nonlinearity parameters of silicon along the three symmetry

directions have been measured between room temperature and 3°K by this technique.

7. Transducer Bonding for Low Temperature Nonlinearity Measurements

The nonlinearity measurements are made with X-cut 30 MHz transducers of diameter 1.27 cm bonded to the sample. For room temperature measurements nonaq stopcock grease is used as the bonding material. This bonding material fails at low temperatures. So for low temperature measurements a cellulose tape adhesive is used as the bonding material. A cellulose tape manufactured by Technical Trade Corp., Carbondale, Illinois, under the designation 7510-551-9818, LT90C Type 1, Class A is used for the purpose. The adhesive is applied as follows. A piece of plastic film with a hole slightly larger in diameter than the transducer is centered over the sample end and a piece of the cellulose tape is applied which sticks to the sample through the hole. The tape is smoothed down to remove all air bubbles and a drop of water is applied to the back of the tape. When the tape turns cloudy (3-5 minutes), the water is blotted away and the plastic film is gently lifted. The backing of the tape separates cleanly from the adhesive everywhere except at the edge of the hole. The adhesive stretches between the sample face and the plastic film at the edge of the hole and is very carefully severed with a sharp blade so that the backing is gently lifted away without disturbing the adhesive bonded to the sample. All traces of moisture on the bond are removed by keeping the sample in vacuum for approximately three hours. The transducer is then carefully placed on the adhesive and all air bubbles are removed by firm but careful

rubbing with the eraser at the end of a pencil. This bond is found to work very well over the entire temperature range.

CHAPTER III

RESULTS AND DISCUSSION

In this chapter we report the results of the measurements made on silicon samples to determine their ultrasonic nonlinearity parameters at room temperature as well as the temperature dependence of the nonlinearity parameters between room temperature and liquid helium temperature. Temperature variation of some more combinations of TOE constants are also determined and reported. The strain generalized Grüneisen parameters of silicon calculated along the symmetry directions from nonlinearity parameters are also evaluated and presented.

a. Room Temperature Nonlinearity Measurements of Silicon

The results of the absolute amplitude measurements at room temperature for silicon along the three principal directions are given in Table 2. In order to satisfy the theoretical assumption of infinitesimal amplitudes, these measurements are made at low amplitudes which give good signal to noise ratio. Irrespective of the value of A_1, it may be noted from the table that the value of A_2/A_1^2 is a constant. The variation of the absolute amplitude of the second harmonic with the square of the fundamental amplitude for all the three orientations are plotted in Figure 17. The straight lines show a well-defined linear variation of A_2 with A_1^2. The lines do not pass through the origin because of the residual noise of the experimental setup. The slope of the lines, in the least square sense, is the best fit to the value of the quantity

Table 2. Amplitudes of Ultrasonic Wave Components for Silicon at Room Temperature

Sample Orientation	Frequency Used (MHz)	Fundamental Amplitude $A_1 \times 10^{-10}$ M	Second Harmonic Amplitude $A_2 \times 10^{-13}$ M	A_2/A_1^2 $\times 10^7$ M^{-1}	$\beta = \frac{8}{3}\left(\frac{A_2}{A_1^2}\right)\frac{1}{k^2 a}$
[100]	30.41	7.1677	16.5192	0.321536	0.6657
		7.0557	15.7156	0.315683	0.6536
		6.7944	14.7334	0.319154	0.6608
		6.5704	12.9475	0.299918	0.6210
		6.0105	12.3224	0.341094	0.7062
		5.6745	10.8937	0.338314	0.7005
		5.3385	9.3758	0.328980	0.6812
		4.5918	6.9649	0.330331	0.6839
		4.2558	5.8933	0.325384	0.6737
		3.6585	4.7325	0.353577	0.7321
[110]	30.24	3.1279	6.0989	0.623370	1.5303
		3.0614	5.9663	0.636579	1.5184
		2.9282	5.3034	0.618519	1.5997
		2.7508	4.9056	0.648297	1.5628
		2.7064	4.7731	0.651653	1.5944
		2.6842	4.7731	0.662477	1.5915
		2.5955	4.3753	0.649480	1.6263
		2.3958	3.5798	0.623674	1.5311
		2.1296	2.8373	0.625618	1.5358
		2.1075	2.7843	0.626875	1.5389
[111]	30.30	3.4860	5.9676	0.4910717	1.2555
		3.4442	5.8433	0.492585	1.2594
		3.3190	5.3460	0.485305	1.2408
		3.2563	5.1719	0.4877545	1.2470
		3.2150	5.0973	0.4931491	1.2608
		3.0267	4.4757	0.488565	1.2491
		2.9015	4.1027	0.4873316	1.2460
		2.7345	3.6054	0.482167	1.2328
		2.6301	3.3568	0.4852672	1.2407
		2.3590	2.7352	0.491520	1.2567
		2.1918	2.3622	0.4917165	1.2572

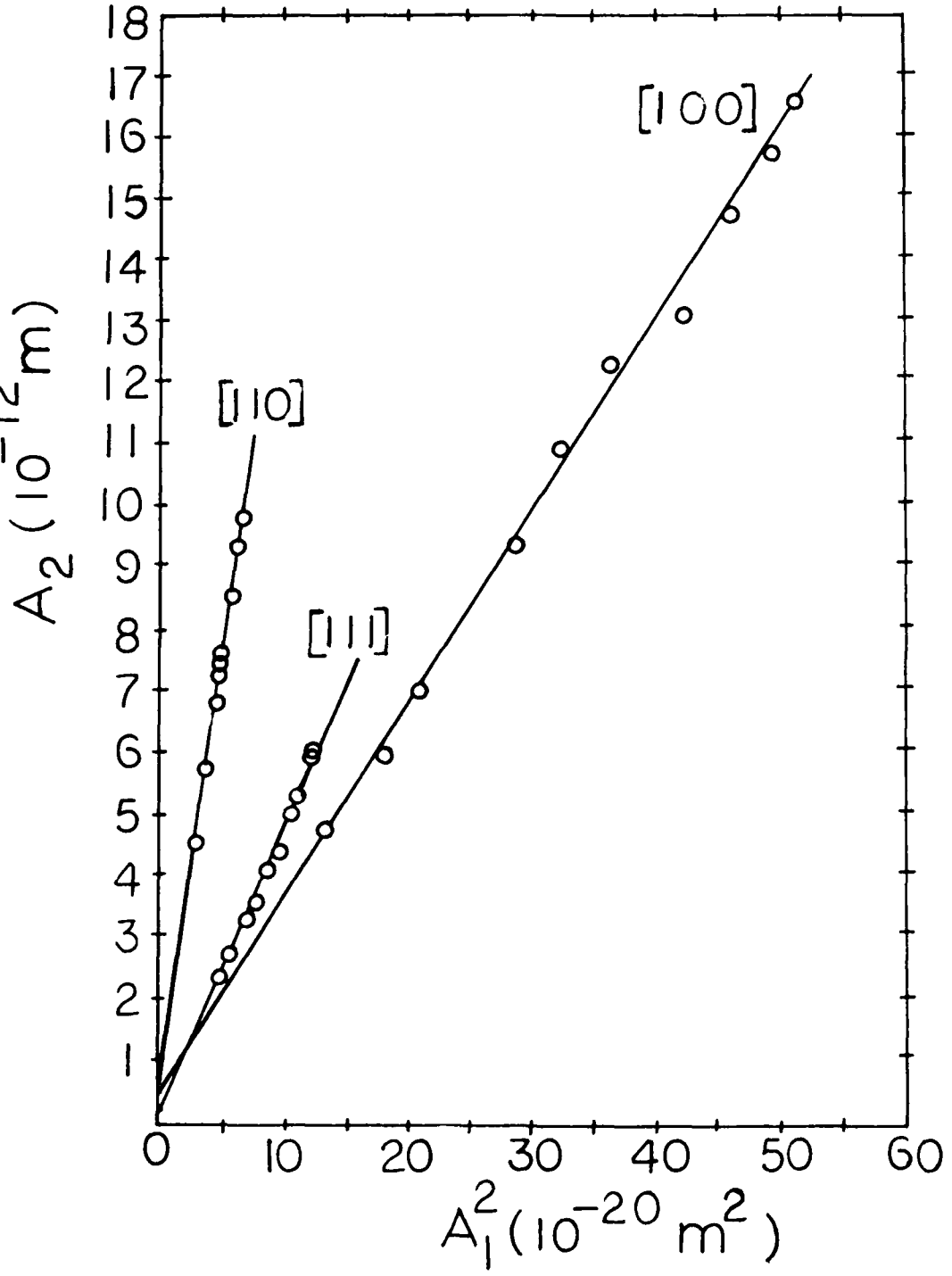

Figure 17. Variation of A_2 with A_1^2 at room temperature for silicon.

$$\frac{3}{8}\beta k^2 a = k^2 a\left[-\frac{3K_2 + K_3}{8K_2}\right] \tag{3.1}$$

which involves the nonlinearity parameter β. The role played by the power lost from the fundamental to the second harmonic is examined in Appendix 3. If this effect is taken into account, the quantity $\frac{3}{8}\beta k^2 a$ is given by

$$\frac{3}{8} k^2 a\beta = \frac{\ell n(A_2 + \sqrt{A_1^2 + A_2^2}) - \ell n A_1}{\sqrt{A_1^2 + A_2^2}} \tag{3.2}$$

rather than A_2/A_1^2. For the entire range of amplitudes given in Table 2, the difference between A_2/A_1^2 and the quantity calculated from Eq. (3.2) is negligible.

In Figure 18 we have plotted the dimensionless parameter β calculated for various values of the fundamental amplitude. The scattering of points in Figure 18 is well within experimental error in view of the fact that the measurements depend on absolute measurements of displacement amplitudes of the order of 10^{-3} Å. In Table 3 we tabulate the values of β obtained by a least squares fit to the data from all the plotted points for all the three principal directions. The standard deviation from the least square fit calculated by

$$\sigma = \frac{\sqrt{\sum_i \beta_i^2 - \frac{1}{n}(\sum_i \beta_i)^2}}{n - 1} \tag{3.3}$$

is included in the β values.

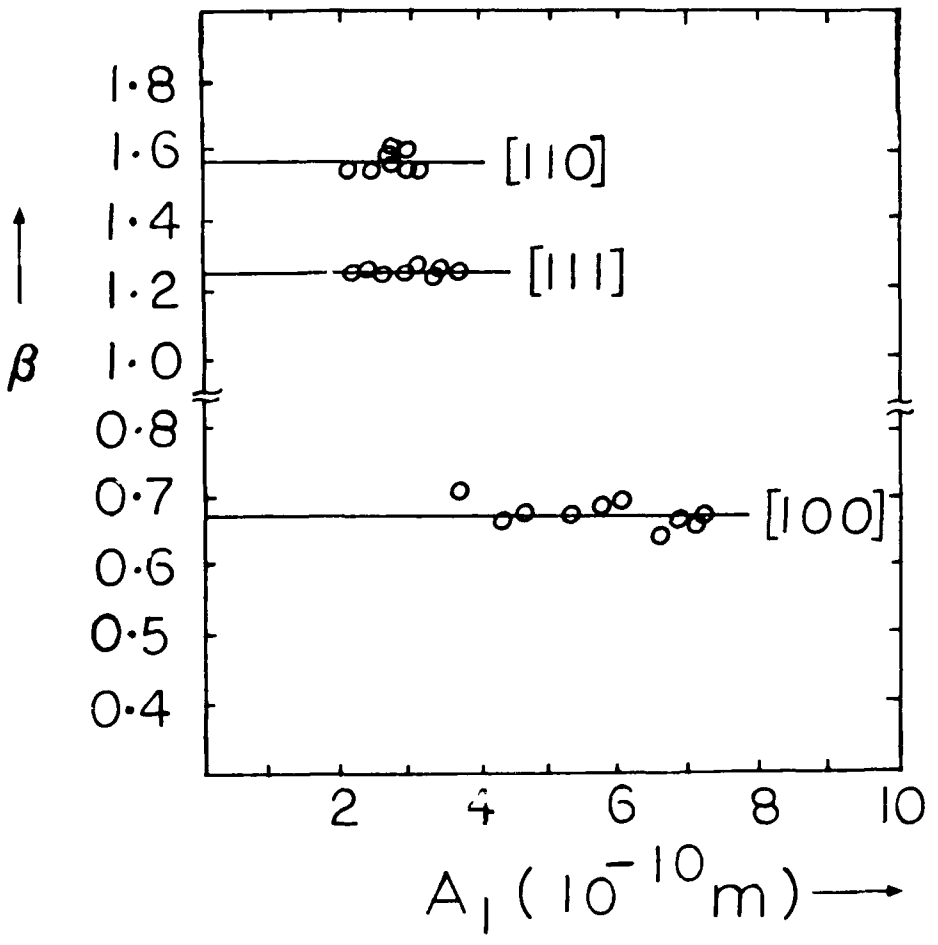

Figure 18. The nonlinearity parameter β plotted as a function of A_1 for silicon at room temperature.

Table 3. Values of the Nonlinearity Parameter β (Least Square Fit)

Sample Orientation	Sample Length (cm)	β
[100]	2.5171	?.0336
[110]	2.5222	4.6887
[111]	2.5248	3.7500

AD-A097 724 TENNESSEE UNIV KNOXVILLE ULTRASONICS LAB F/G 20/11
A DETAILED STUDY OF ULTRASONIC NONLINEARITY IN RELATION TO OTHE--ETC(U)
MAR 81 J PHILIP N00014-76-C-0177
UNCLASSIFIED TR-19 NL

2 OF 2
AD A
097724

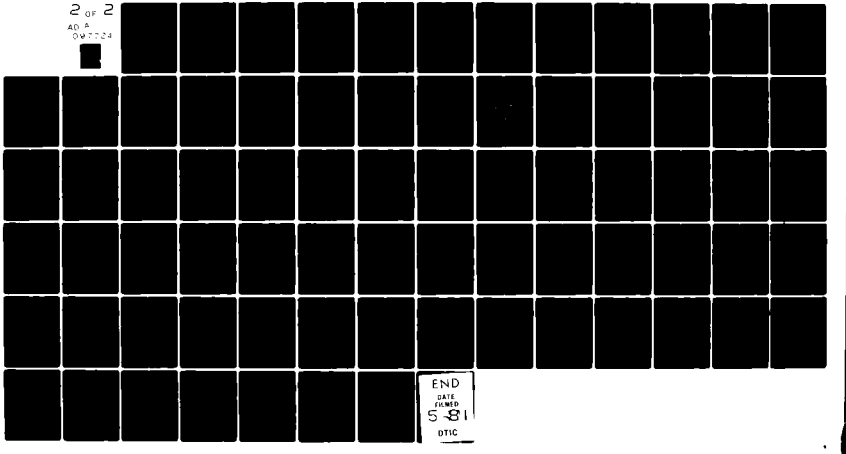

END
DATE FILMED
5-81
DTIC

The parameters K_3, which are combinations of TOE constants, along the three directions are evaluated from the β values by Eq. (1.95)

$$K_3 = (3 + \beta)K_2 \tag{3.4}$$

and are tabulated in Table 4. The K_2 values used in the calculation are evaluated from the SOE constants of silicon reported by McSkimin and Andreatch.[54] We have measured the velocities and verified that our values of SOE constants agree very well with those of McSkimin and Andreatch.[54] The K_2 values used in the evaluation of K_3 are also given in Table 4. The room temperature TOE constants of silicon have been measured earlier by hydrostatic and uniaxial pressure technique by McSkimin et al.[26] The K_3 values calculated from their TOE constants are also tabulated in Table 4 for comparison. It may be noted that the K_3 values obtained from these two entirely different techniques agree very well within experimental inaccuracies. Keating[55] has theoretically evaluated all the six TOE constants of both silicon and germanium in terms of three anharmonic first and second neighbor force constants and two harmonic force constants on the basis of central potential. We have calculated the K_3 values from these theoretical TOE constants and these values are also presented in Table 4. The agreement between experimental and theoretical K_3 values shows that Keating's model is a very good approximation for silicon and other diamond-like solids.

b. Strain Generalized Grüneisen Parameters of Silicon

In this section we derive the relationship between the strain generalized Grüneisen parameters and ultrasonic nonlinearity parameter

Table 4. The K_2 and K_3 Values of Silicon Along the Principal Directions at Room Temperature

Sample Orientation	$K_2 \times 10^{11}$ (dynes/cm^2)	$K_3 \times 10^{12}$ dynes/cm^2		
		Present Experiment	Experimental Values of McSkimin et al.[a]	Theoretical Values of Keating[b]
[100]	16.5779	- 8.34 ± 0.11	- 8.25	- 8.21
[110]	19.4470	-14.95 ± 0.22	-14.75	-15.68
[111]	20.4031	-13.77 ± 0.12	-13.31	-13.58

[a]Reference 26.

[b]Reference 55.

for solids. Since the medium is not stressed in the determination of nonlinearity parameter by harmonic generation technique, the generalized Grüneisen tensor calculated from the nonlinearity parameters is purely isentropic.

Let us rewrite Eq. (1.24) in the form

$$\frac{\partial^2 P_j}{\partial t^2} = \frac{\mu_j}{\rho_0}\left(1 + \frac{\nu_{jjj}}{\mu_j}\frac{\partial P_j}{\partial a_1}\right)\frac{\partial^2 P_j}{\partial a_1^2} . \tag{3.5}$$

When the ultrasonic nonlinearity parameter β_j defined by (1.28) is zero, Eq. (3.5) reduces to a linear differential equation describing infinitesimal amplitude wave propagation of velocity

$$C_j = (\mu_j/\rho_0)^{1/2} . \tag{3.6}$$

For finite amplitude waves β_j is nonzero and it is convenient to define the natural wave velocity by[23]

$$W(j,N) = \left[\frac{\mu_j}{\rho_0}\left(1 + \frac{\nu_{jjj}}{\mu_j}\frac{\partial P_j}{\partial a_1}\right)\right]^{1/2} = C_j\left(1 - \beta_j \frac{\partial P_j}{\partial a_1}\right)^{1/2} . \tag{3.7}$$

So β_j is a direct measure of the nonlinearity of the solid with respect to elastic wave propagation.

The isentropic generalized Grüneisen parameter $\gamma^S_{rs}(j,\vec{N})$ describing the frequencies $\omega(j,\vec{N})$ are defined by

$$\gamma^{s}_{rs}(j,\vec{N}) = -\left(\frac{1}{\omega(j,N)}\right)\frac{\partial\omega(j,N)}{\partial\bar{\eta}_{rs}}\Big)_{s,\eta=0} \tag{3.8}$$

where $\bar{\eta}$ refers to the original coordinate system and s is the entropy. The strain derivatives in the original coordinate system may be expressed in terms of the derivatives with respect to the displacement gradients $\partial p_j/\partial a_l$ in the transformed coordinates by using chain-rule differentiation. Hence, we may write

$$\left(\frac{\partial}{\partial\bar{\eta}_{rs}}\right)_{s,\eta=0} = \left(\frac{\partial\eta_{pq}}{\partial\bar{\eta}_{rs}}\frac{\partial(\partial u_k/\partial a_l)}{\partial\eta_{pq}}\frac{\partial(\partial p_j/\partial a_l)}{\partial(\partial u_k/\partial a_l)} \times \frac{\partial}{\partial(\partial p_j/\partial a_l)}\right)_{s,\bar{\eta}} . \tag{3.9}$$

Using Eqs. (1.14) and (1.22) and the relation

$$\left(\frac{\partial(\partial u_k/\partial a_l)}{\partial\eta_{pq}}\right)_{s,\bar{\eta}=0} = \frac{1}{2}\left(\delta_{kp}\delta_{lq} + \delta_{kq}\delta_{lp}\right) \tag{3.10}$$

where δ_{ij} are Kronecker deltas, we can express Eq. (3.9) in the form

$$\left(\frac{\partial}{\partial\bar{\eta}_{rs}}\right)_{s,\bar{\eta}=0} = \frac{1}{2}\delta_{kj}(R_{kr}R_{ls} + R_{lr}R_{ks})\left(\frac{\partial}{\partial(\partial p_j/\partial a_l)}\right)_{s,\partial p_j/\partial a_l=0} . \tag{3.11}$$

Substituting (3.11) into (3.8) we obtain

$$\gamma^{s}_{rs}(j,\vec{N}) = -\frac{1}{2}\delta_{kj}(R_{kr}R_{ls} + R_{lr}R_{ks})\left(\frac{1}{\omega(j,\vec{N})} \times \frac{\partial\omega(j,N)}{\partial(\partial p_j/\partial a_l)}\right)_{s,\partial p_j/\partial a_l=0} . \tag{3.12}$$

In the Debye model, the lattice vibrational frequencies $\omega(j,\vec{N})$ are related for any state of strain to the natural velocity by[56]

$$\omega(j,\vec{N}) \propto W(j,N) \ . \tag{3.13}$$

Hence, using Eqs. (3.7) and (3.13) we may write

$$\left(\frac{1}{\omega(j,N)} \frac{\partial\omega(j,N)}{\partial(\partial p_j/\partial a_1)}\right)_{s,\partial p_j/\partial a_1=0} = \frac{1}{W(j,N)} \left(\frac{\partial W(j,N)}{\partial(\partial p_j/\partial a_1)}\right)_{s,\partial p_j/\partial a_1=0} = -\frac{1}{2}\beta_j \ . \tag{3.14}$$

Substituting (3.14) into (3.12) we obtain the general relationship between the (γ,s) component of the isentropic strain generalized Grüneisen tensor and the solid nonlinearity parameter β_j to be

$$\gamma^s_{rs}(j,N) = \frac{1}{4}\beta_j S_{kj}(R_{kr}R_{ls} + R_{ls}R_{ks}) \ . \tag{3.15}$$

From this equation we find that the (1,1) components of the isentropic strain generalized Grüneisen tensors for the case of longitudinally polarized (j=1) waves propagating in the symmetry directions[57] are

$$\left.\begin{aligned} \gamma^s_{11}(1, [100]) &= \frac{1}{2}\beta_1 \quad \text{for the [100] direction} \\ \gamma^s_{11}(1, [110]) &= \frac{1}{4}\beta_1 \quad \text{for the [110] direction, and} \\ \gamma^s_{11}(1, [111]) &= \frac{1}{6}\beta_1 \quad \text{for the [11] direction.} \end{aligned}\right\} \tag{3.16}$$

In Table 5 we list room temperature values of the (1,1) components of the experimentally measured isentropic strain generalized Grüneisen tensors for the pure mode directions of silicon and germanium crystals. The corresponding mixed state strain generalized Grüneisen parameters parameters calculated from the theory of Brugger[58] using experimental values of elastic constants are also given in the table. For silicon

Table 5. Room Temperature Values of the Isentropic Strain Generalized Grüneisen Parameters along Symmetry Directions for Silicon and Germanium

Sample	Grüneisen γ from β Measured in the Present Experiment			Grüneisen γ from Brugger's Theory		
	$\gamma_{11}^{S}(1,[100])$	$\gamma_{11}^{S}(1,[110])$	$\gamma_{11}^{S}(1,[111])$	$\gamma_{11}^{S}(1,[100])$	$\gamma_{11}^{S}(1,[110])$	$\gamma_{11}^{S}(1,[111])$
Silicon	1.01	1.17	0.63	0.99	1.40	1.08
Germanium	1.5	1.5	0.9	1.4	1.5	1.1

the TOE constant data of McSkimin et al.[54] and our measured nonlinearity parameters are used. For germanium the TOE constant data of Bateman et al.[22] and nonlinearity parameters data of Bains et al.[46] are used.

It must be pointed out that exact agreement between the isentropic strain generalized Gruneisen parameters γ_{rs}^{s} and the Brugger-Grüneisen parameters γ_{rs}^{B} is not to be expected because the former are of a pure thermodynamic state whereas the latter are of a mixed thermodynamic state. The difference between the two may be of the same order as the difference between adiabatic and isothermal elastic constants. An examination of Table 5 reveals that for the [100] direction for both silicon and germanium the agreement between γ_{rs}^{s} and γ_{rs}^{B} is good. They agree reasonably well for the [110] direction but do not agree for the [111] direction for either silicon or germanium. Further work in this direction is underway to trace the reason for the disagreement in the results along the [111] direction.

c. Temperature Dependence of the Nonlinearity of Silicon

The measured values of $|\beta|$ down to approximately 3°K are given in Table 6 along with the ratio of $|\beta|$ to the room temperature $|\beta|$. The room temperature value is the most probable average value obtained from Table 3. These data for all the three directions are listed. The K_3 values calculated from β are also tabulated in Table 6 between 300 and 3°K. In Figure 19 we have plotted the data obtained for the parameter K_3 for the three orientations as a function of temperature. The SOE constants of silicon as a function of temperature have been plotted by McSkimin[53] from room temperature to 77°K. We measured the velocities

Table 6. Measured Relative Values of β and the K_3 Values of Silicon as a Function of Temperature

Temperature T°K	K_2 x10^{12} dyn/cm^2	Bias Voltage of the Second Harmonic V_b	$\lvert\frac{\beta}{\beta_R}\rvert$	$\lvert\beta\rvert$	$-K_3$ x10^{12} dyn/cm^2
		[100] direction			
3.10	1.6755	150.01	1.1086	0.7509	8.8005
4.02	1.6755	150.05	1.1087	0.7508	8.8004
6.00	1.6755	150.15	1.1079	0.7503	8.7994
10.57	1.6755	150.85	1.1028	0.7468	8.7803
16.14	1.6755	152.51	1.0908	0.7387	8.7396
20.11	1.6755	153.00	1.0873	0.7363	0.7275
24.93	1.6755	153.00	1.0873	0.7363	8.7275
35.08	1.6753	153.55	1.0833	0.7336	8.7129
47.82	1.6753	155.12	1.0725	0.7263	8.6762
59.25	1.6752	158.80	1.0477	0.7095	8.5913
66.33	1.6750	160.88	1.0343	0.7004	8.5445
77.60	1.6747	163.21	1.0195	0.6904	8.4927
86.84	1.6743	163.45	1.0177	0.6892	8.4847
101.57	1.6740	163.58	1.0163	0.6882	8.4781
119.92	1.6732	163.82	1.0140	0.6867	8.4666
131.51	1.6723	164.08	1.0118	0.6852	8.4545
147.89	1.6713	164.05	1.0113	0.6849	8.4479
167.99	1.6700	164.22	1.0093	0.6835	8.4343
181.11	1.6689	164.25	1.0083	0.6828	8.4253
197.93	1.6674	164.35	1.0067	0.6817	8.4122
216.08	1.6654	164.62	1.0051	0.6807	8.3971
231.91	1.6637	164.41	1.0042	0.6800	8.3850
250.29	1.6617	164.42	1.0031	0.6793	8.3715
266.30	1.6601	164.41	1.0022	0.6787	8.3604
272.48	1.6594	164.45	1.0017	0.6784	8.3554
Room temp.	1.6566	164.48	1.0000	0.6772	8.3353
		[110] direction			
2.98	1.9641	150.05	1.2742	1.9922	17.6286
4.02	1.9641	150.08	1.2740	1.9913	17.6256
4.90	1.9641	152.55	1.2534	1.9591	17.3915
8.41	1.9641	155.65	1.2284	1.9200	17.2055
10.57	1.9641	156.48	1.2219	1.9098	17.1454
14.00	1.9641	157.85	1.2113	1.8933	17.0482
16.14	1.9639	158.38	1.2072	1.8869	17.0087
24.93	1.9639	161.22	1.1858	1.8534	16.8114
35.08	1.9637	165.55	1.1547	1.8048	16.5234
47.82	1.9635	170.08	1.1241	1.7570	16.2401
56.82	1.9634	174.66	1.0946	1.7109	15.9686
64.58	1.9633	177.12	1.0796	1.6874	15.8285
77.79	1.9629	178.65	1.0704	1.6730	15.7405

Table 6 (continued)

Temperature T°K	K_2 x10^{12} dyn/cm^2	Bias Voltage of the Second Harmonic V_b	$\lvert\frac{\beta}{\beta_R}\rvert$	$\lvert\beta\rvert$	$-K_3$ x10^{12} dyn/cm^2
		[110] direction (continued)			
84.02	1.9627	179.92	1.0627	1.6610	15.6682
94.75	1.9623	180.89	1.0564	1.6512	15.6073
107.28	1.9618	181.55	1.0520	1.6443	15.5628
118.77	1.9614	182.46	1.0464	1.6355	15.5078
129.77	1.9606	182.78	1.0441	1.6319	15.4803
136.76	1.9602	183.21	1.0414	1.6277	15.4525
147.89	1.9594	183.56	1.0389	1.6238	15.4232
160.87	1.9585	184.52	1.0329	1.6144	15.3609
173.35	1.9575	185.21	1.0284	1.6074	15.3120
184.10	1.9563	185.98	1.0235	1.5997	15.2574
194.91	1.9552	186.38	1.0206	1.5952	15.2224
206.38	1.9542	186.78	1.0179	1.5910	15.1900
223.37	1.9522	187.24	1.0145	1.5857	15.1434
241.70	1.9501	187.98	1.0094	1.5777	15.0803
260.13	1.9480	188.66	1.0074	1.5746	15.0460
272.48	1.9464	188.86	1.0031	1.5678	14.9939
Room temp.	1.9433	189.18	1.0000	1.5630	14.9420
		[111] direction			
3.97	2.0601	150.12	1.0575	1.3219	14.3500
4.90	2.0601	150.08	1.0577	1.3221	14.3513
7.03	2.0601	150.03	1.0581	1.3226	14.3544
10.08	2.0601	149.89	1.059	1.3239	14.3624
17.00	2.0600	150.26	1.0565	1.3206	14.3413
24.50	2.0600	150.58	1.0543	1.3179	14.3246
30.70	2.0599	150.81	1.0526	1.3158	14.3109
36.99	2.0599	150.98	1.0513	1.3141	14.3004
43.55	2.0598	151.77	1.0459	1.3074	14.2583
50.47	2.0596	152.55	1.0406	1.3008	14.2162
59.25	2.0595	152.76	1.0394	1.2993	14.2062
66.33	2.0593	152.81	1.0390	1.2988	14.2018
70.15	2.0592	153.81	1.0323	1.2904	14.1492
77.79	2.0592	155.00	1.0245	1.2806	14.0886
86.84	2.0587	155.62	1.0199	1.2749	14.0500
92.49	2.0585	155.82	1.0185	1.2731	14.0375
103.85	2.0581	156.02	1.0166	1.2708	14.0206
114.16	2.0576	156.44	1.0136	1.2670	13.9937
129.77	2.0566	156.68	1.0113	1.2641	13.9690
139.68	2.0561	156.48	1.0121	1.2651	13.9718
147.89	2.0553	157.08	1.0080	1.2600	13.9349
157.32	2.0546	156.83	1.0093	1.2616	13.9400
167.99	2.0537	156.45	1.0111	1.2639	13.9481
174.54	2.0532	156.45	1.0109	1.2636	13.9429

Table 6 (continued)

Temperature T°K	K_2 $\times 10^{12}$ dyn/cm^2	Bias Voltage of the Second Harmonic V_b	$\left\|\frac{\beta}{\beta_R}\right\|$	$\|\beta\|$	$-K_3$ $\times 10^{12}$ dyn/cm^2
		[111] direction (continued)			
181.71	2.0525	156.45	1.0105	1.2631	13.9350
197.93	2.0508	156.48	1.0092	1.2615	13.9137
212.44	2.0492	156.48	1.0086	1.2608	13.8985
227.03	2.0476	156.75	1.0061	1.2576	13.8680
244.15	2.0457	156.66	1.0057	1.2571	13.8520
260.13	2.0436	156.89	1.0034	1.2543	13.8207
272.48	2.0421	156.82	1.0032	1.2540	13.8087
Room temp.	2.0388	157.11	1.0000	1.2500	13.7619

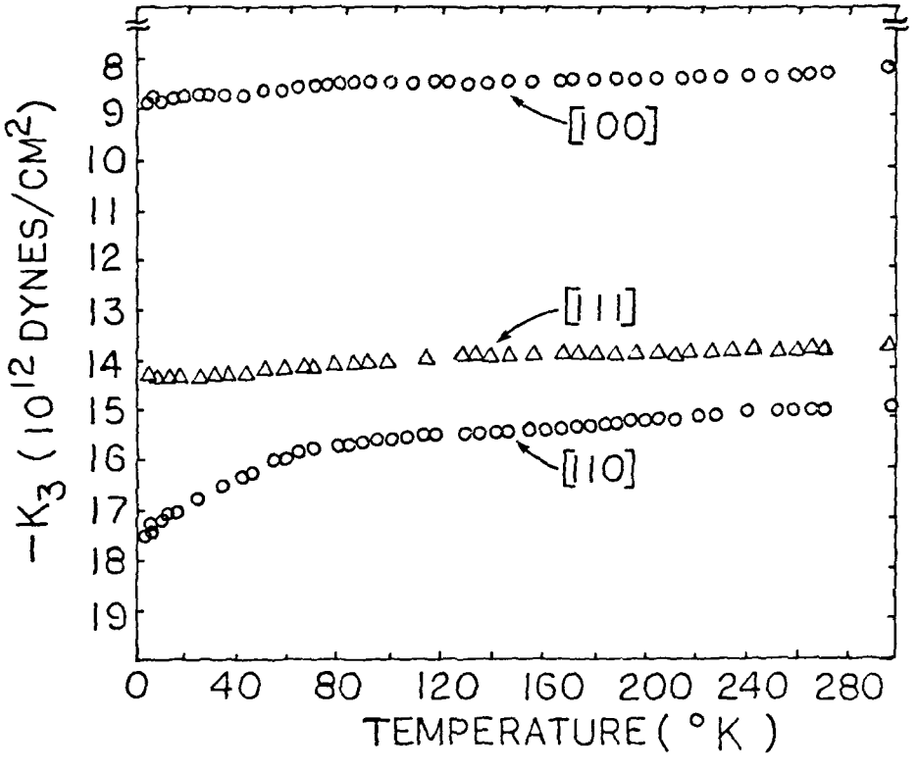

Figure 19. Temperature variation of the parameter K_3 of silicon for the three principal directions.

and hence the K_2 values at different temperatures below 77 K and found that these values agree with the curves of McSkimin extrapolated to 0°K. For calculations of K_3 as a function of temperature the K_2 values have been evaluated as a function of temperature. They are also tabulated in Table 6.

From Figure 19 it may be noted that the K_3 values undergo noticeable temperature variation below 77 K especially K_3 [110]. Between room temperature and 3°K, the K_3 values for the [100], [110], and [111] directions vary by 5.3%, 15.2%, and 4.1%, respectively. The data for the [100] and [111] directions are quite smooth and are nearly parallel to the temperature axis. The variation is maximum for the [110] direction between 77 and 3 K, the variation being as high as 11%. Since β is a direct measure of the anharmonicity (nonlinearity), a large change in β (and therefore K_3) at low temperatures is not surprising in view of the thermal expansion data which shows that there is a large change in the anharmonicity of silicon and other diamond-like solids below liquid nitrogen temperature (thermal expansion becomes negative).

The TOE constant C_{111} appears in the K_3 values along all the directions. It can be subtracted out from K_3 [110] and K_3 [111]. In this way we can get two more combinations of TOE constants, namely $(C_{112} + 4C_{166})$ and $(C_{123} + 6C_{144} + 8C_{456})$ and their temperature variation can be studied. The temperature variation of these two combinations along with that of C_{111} are plotted in Figure 20. As can be seen from Figure 20, the variation of these combinations as a function of temperature is not very great down to 77 K. But between 77 and 3 K, there is a considerable variation in some of them. In particular, the

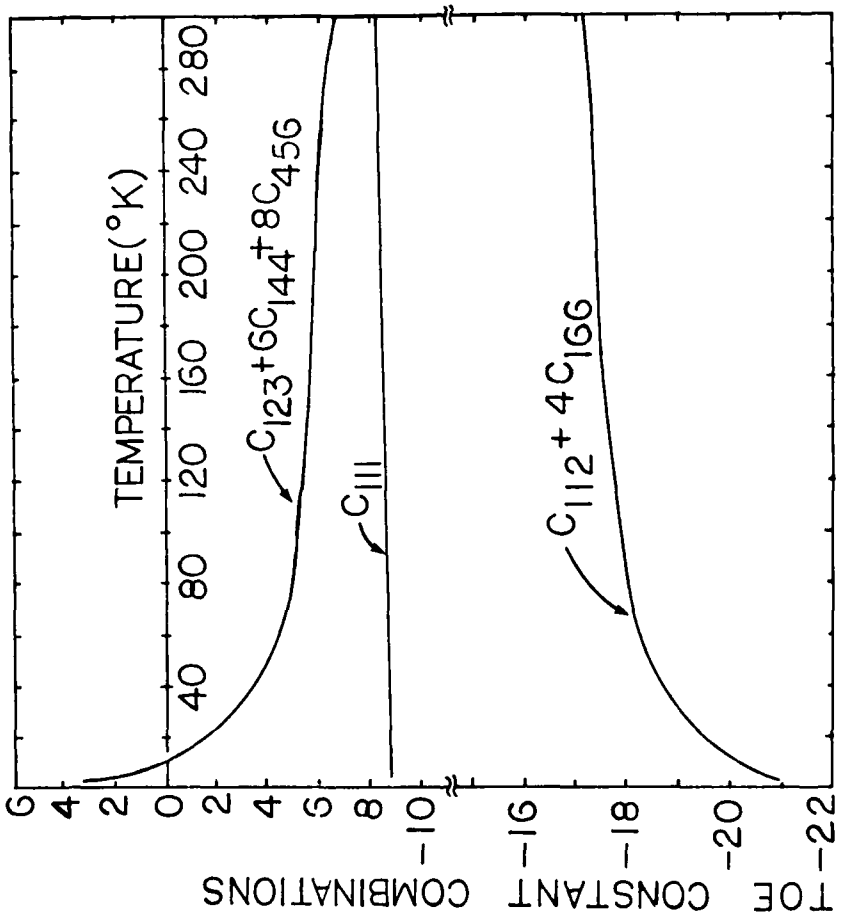

Figure 20. Variation of some combinations of TOE constants of silicon with temperature.

combination ($C_{123} + 6C_{144} + 8C_{456}$) crosses zero at about 8°K and becomes positive below that temperature. Since these are the TOE constants which would play a significant role in the propagation of transverse modes, the lack of agreement between the theoretically calculated value of thermal expansion from elastic data and measured thermal expansion values might be attributed to the theoretical assumption that the TOE constants are independent of temperature.

d. Temperature Dependence of the Nonlinearity of Germanium

In order to supplement the necessary data for the work to be described in the next chapter, we reproduce here the data on the temperature variation of the K_3 values of germanium. In Table 7 we present the measured values of the nonlinearity parameter β and calculated values of K_3 of germanium between 300 and 3°K. These data are adopted from the Ph.D. dissertation of J. A. Bains.[59] In Figure 21 we have plotted the temperature variation of the parameters K_3 of germanium along the pure mode directions between room temperature and 3°K.

Table 7. Measured Values of K_3 of Germanium as a Function of Temperature (Ref. 59)

Sample Orientation	Temperature °K	$K_3 \times 10^{12}$ dyn/cm^2
[100]	2.94	- 8.47
	9.01	- 8.47
	19.30	- 8.47
	27.81	- 8.47
	43.28	- 8.46
	56.72	- 8.46
	68.66	- 8.46
	77.40	- 8.22
	100.51	- 8.29
	124.35	- 8.34
	148.48	- 8.38
	160.53	- 8.36
	184.52	- 8.28
	196.55	- 8.30
	220.51	- 8.30
	245.16	- 8.17
	270.27	- 7.88
	Room temp.	- 7.78
[110]	3.00	-17.21
	9.01	-16.32
	19.30	-15.89
	27.81	-15.54
	43.28	-14.91
	56.72	-14.35
	68.66	-14.57
	77.68	-14.62
	100.51	-14.54
	124.34	-14.45
	148.43	-14.46
	160.50	-14.27
	184.57	-14.24
	196.52	-14.13
	220.51	-14.15
	245.11	-14.20
	270.28	-14.15
	Room temp.	-14.10
[111]	3.01	-13.28
	9.11	-13.61
	19.38	-13.84
	27.78	-13.72
	43.22	-13.59
	56.78	-13.56
	68.69	-13.28

Table 7 (continued)

Sample Orientation	Temperature °K	$K_3 \times 10^{12}$ dyn/cm^2
[111] (continued)	77.48	-13.52
	100.53	-13.31
	124.33	-13.71
	148.46	-13.49
	160.53	-13.40
	184.54	-13.53
	196.58	-13.44
	220.51	-13.47
	245.15	-13.51
	270.28	-13.73
	Room temp.	-13.40

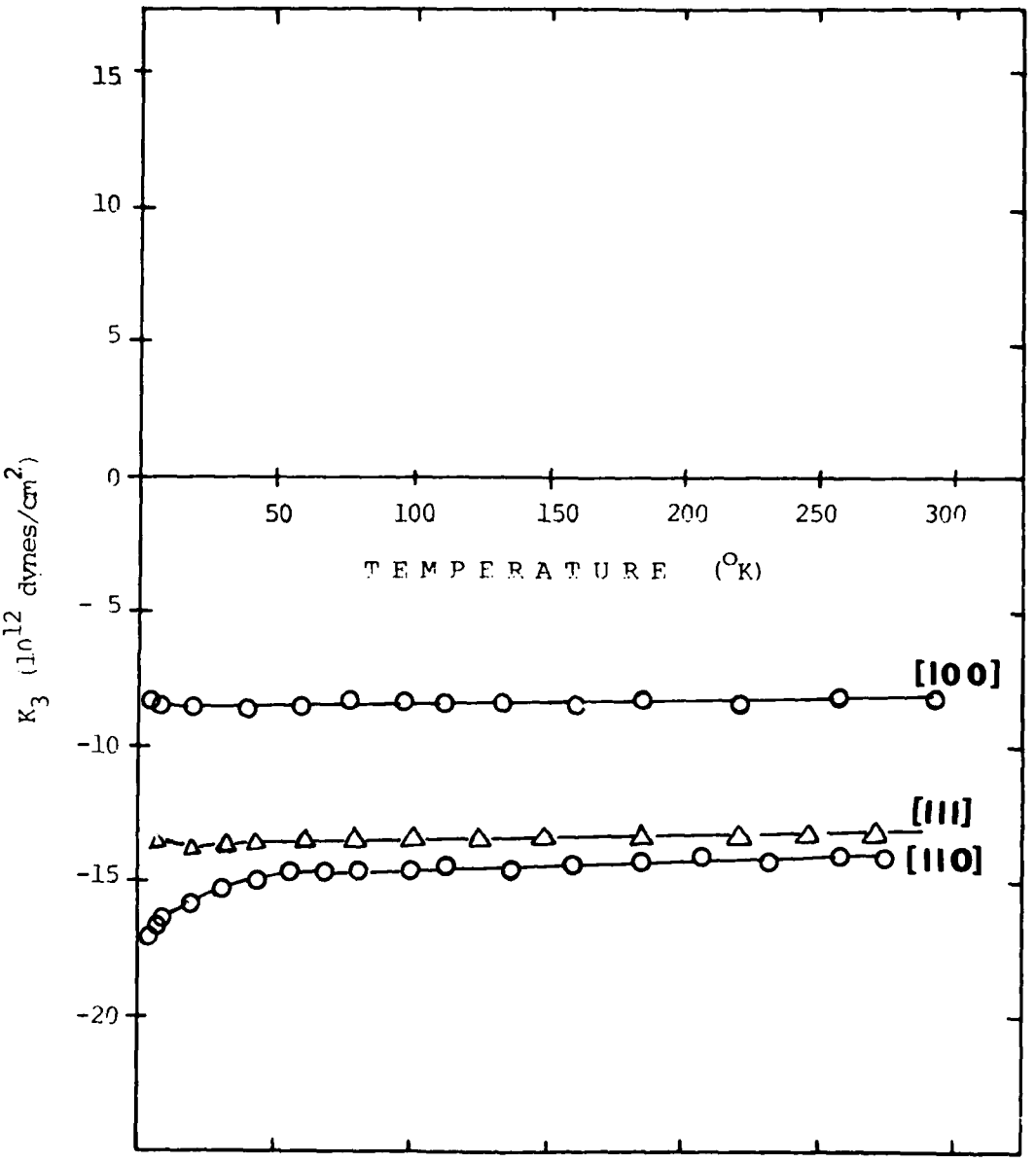

Figure 21. Temperature variation of the K_3 parameters of germanium.

CHAPTER IV

TEMPERATURE VARIATION OF THE TOE CONSTANTS OF SILICON AND GERMANIUM

The SOE constants of a number of solids have been measured as a function of temperature by a number of authors. The first measurement of this kind has been done by McSkimin[53] on silicon, germanium and fused silica from room temperature to liquid nitrogen temperature. Later the measurement has been extended to liquid helium temperature by Fine[60] on germanium. Subsequently measurements have been reported on a number of solids. The results have been reviewed by Hearmon[61] and are not reproduced here.

The measurement of the TOE constants as a function of temperature is much more difficult than in the case of SOE constants. If one uses the McSkimin technique, changes in sound velocity need be measured with the application of pressure and as a function of temperature. Due to experimental difficulties not much work has been done in this direction. Salama and Alers[29] measured the TOE constants of copper at 295, 77 and 4.2°K. Sarma and Reddy[62] measured the TOE constants of nickel at 298 and 80°K. In both cases the technique gave results in which the inaccuracies of the measurement entered at every temperature at which measurements were made. The effect of temperature on TOE constants are found to be comparatively small. The normal tendency is for the stiffness to increase, i.e., to become less negative as the temperature rises. Some authors have reported the results of calculations

based on theoretical considerations. These are also reviewed by Hearmon.[61] As already has been pointed out in the introduction, the ultrasonic harmonic generation measurements can readily be undertaken at low temperatures but until now this technique allows one to measure only three combinations of TOE constants as a function of temperature and not individual TOE constants.

In this chapter we have combined the results of our measurements of the nonlinearity parameters of silicon and germanium with an established lattice dynamical model to arrive at expressions for individual TOE constants in terms of nonlinearity parameters and have studied their variation with temperature. The model used is the central potential model[63,55] introduced by Keating for diamond-like solids. For the first time in literature we have studied the temperature dependence of the individual TOE constants of a solid between 300 and 3°K. The highlights of Keating's theory are given in the next section and in the following section the Keating force constants are expressed in terms of the K_3 parameters along principal directions and expressions for TOE constants are arrived at. Section c is devoted to results. Graphs showing the temperature variation of the TOE constants of silicon and germanium are plotted.

As is well known, the diamond-like solids silicon and germanium exhibit an anomalous thermal expansion behavior at low temperatures.[64,65,66] Thermal expansion of silicon is negative between 120 and 20°K and is again positive below that temperature.[67] Thermal expansion of germanium is negative between 40 and 16°K and is positive below that temperature.[68] The works done have been reviewed by

Carr et al.[69] The Grüneisen parameter follows a similar behavior as thermal expansion.[70] Theoretical calculations based on the quasiharmonic approximation[71,72] using room temperature values of TOE constants do not predict this behavior.[73,74] We have evaluated the Grüneisen parameter at low temperatures using our temperature dependent TOE constants for both silicon and germanium. Results are compared with previous publications. Temperature variation of some more anharmonic properties like pressure derivatives of the SOE constants, the Anderson-Grüneisen parameter, etc. are also studied and the results are reported. The final section constitutes discussion and some concluding remarks.

a. Keating's Model for the Lattice Dynamics of Diamond-Like Solids

The Keating[63,55] model for the diamond-like solids is basically equivalent to the Born-Huang[13] approach of imposing the invariance requirements on the elastic strain energy of the crystal. Keating's theory provides additional insight into the interatomic forces in this group of solids and has more operational advantages over the Born-Huang method. The method demonstrates that all purely first-neighbor interactions are central only. Keating's approach confirms that in the harmonic approximation there are no noncentral purely first-neighbor interactions present in any nonmetallic crystal. In the harmonic approximation treatment to derive expressions for SOE constants, Keating's model involves only two types of interactions, a nearest-neighbor central term and a noncentral second neighbor term.

The basic unit cell of the diamond structure is a rhombohedron with two atoms, atoms 1 and 0 in Figure 22, on its major axis which is

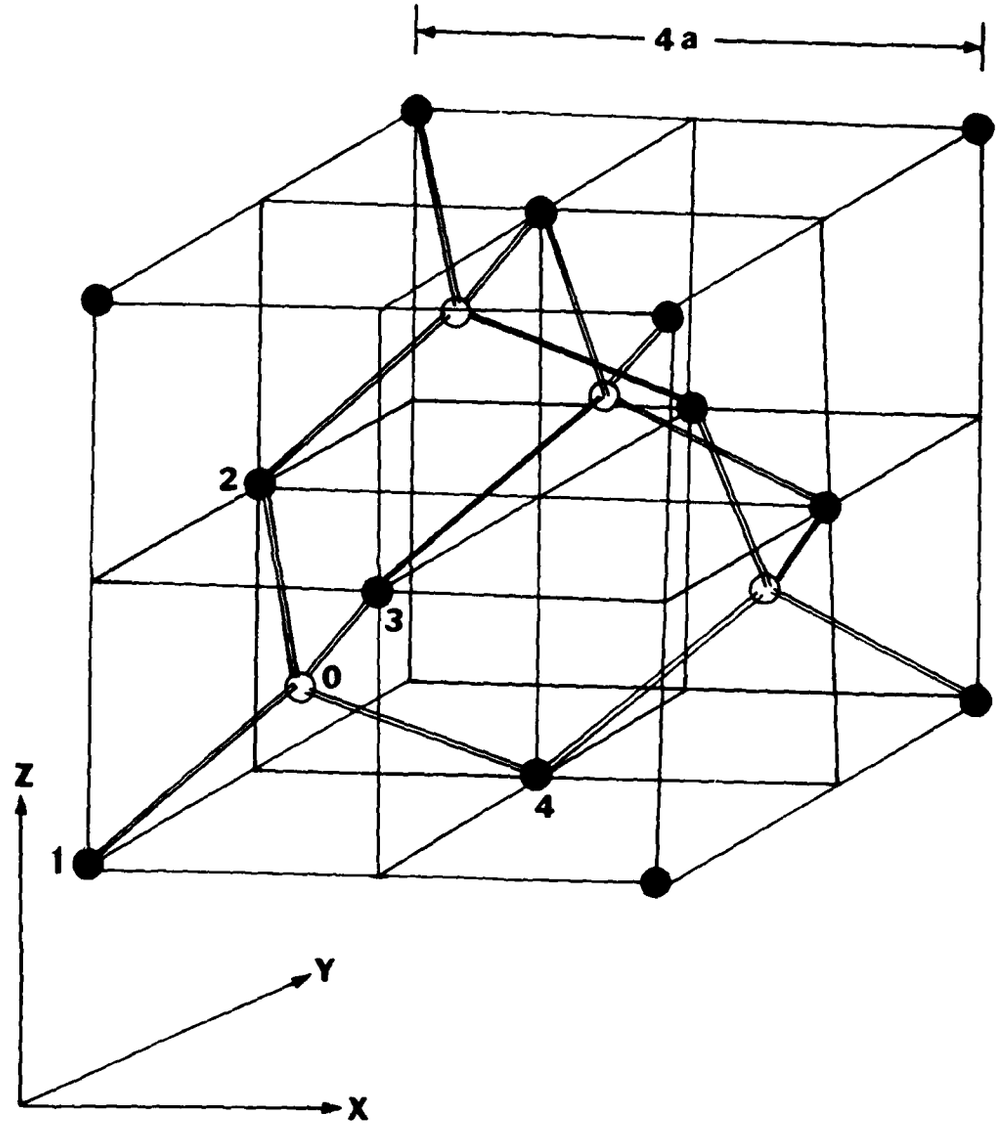

Figure 22. The crystal model of diamond-like solids. The open and filled circles represent the atoms in the two different sublattices.

directed along the [111] direction. The three neighboring unit cells of interest contain atoms 2 and 5, 3 and 6 and 4 and 7, respectively. The expression for the microscopic strain energy in terms of the central first neighbor constant α and the noncentral second neighbor constant β has been written[63] and after imposing crystal symmetry requirements, the expression in the harmonic approximation becomes

$$
\begin{aligned}
u = \frac{\alpha}{32a}\{[(e_d + e_{yz} + e_{zx} + e_{xy} + \frac{u' + v' + w'}{a})^2 \\
+ (e_d + e_{yz} - e_{zx} - e_{xy} + \frac{u' - v' - w'}{a})^2 \\
+ (e_d - e_{yz} - e_{zx} + e_{xy} - \frac{u' + v' - w'}{a})^2 \\
+ (e_d - e_{yz} + e_{zx} - e_{xy} - \frac{u' - v' + w'}{a})^2]\} \\
+ \frac{\beta}{16a}\{[(e_{xx} - e_{yy} - e_{zz} - e_{yz} + \frac{u'}{a})^2 \\
+ (e_{xx} + e_{yy} - e_{zz} - e_{xy} + \frac{w'}{a})^2 + (e_{xx} - e_{yy} - e_{zz} + e_{yz} - \frac{u'}{a})^2 \\
+ (e_{xx} - e_{yy} + e_{zz} - e_{xz} + \frac{v'}{a})^2 + (e_{xx} - e_{yy} + e_{zz} + e_{zx} - \frac{v'}{a})^2 \\
+ (e_{xx} + e_{yy} - e_{zz} + e_{xy} - \frac{w'}{a})^2]\} ,
\end{aligned}
\tag{4.1}
$$

where a is the lattice parameter and e_{ij}'s are the strain parameters with $e_d = e_{xx} + e_{yy} + e_{zz}$. u', v', w' are the atomic displacement components. By imposing the condition

$$
\frac{\partial u}{\partial u'} = \frac{\partial u}{\partial v'} = \frac{\partial u}{\partial w'} = 0 \tag{4.2}
$$

one obtains

$$\left.\begin{aligned} u' &= -a\,\xi\,e_{yz} \\ v' &= -a\,\xi\,e_{zx} \\ \text{and } w' &= -a\,\xi\,e_{xy} \end{aligned}\right\} \tag{4.3}$$

where

$$\xi = (\alpha-\beta)/(\alpha+\beta)\ . \tag{4.4}$$

After substitution for u', etc., and comparing the resulting expression with the well-known macroscopic expression for strain energy for cubic crystals[75], namely

$$u = \frac{1}{2}\,C_{11}(e_{xx}^{\,2} + e_{yy}^{\,2} + e_{zz}^{\,2}) + C_{12}(e_{yy}e_{zz} + e_{zz}e_{xx} + e_{xx}e_{yy}) + \frac{1}{2}\,C_{44}(e_{yz}^{\,2} + e_{zx}^{\,2} + e_{xy}^{\,2})\ , \tag{4.5}$$

we obtain

$$\left.\begin{aligned} C_{11} &= (\alpha + 3\beta)/4a \\ C_{12} &= (\alpha - \beta)/4a \\ C_{44} &= \alpha\beta/a(\alpha + \beta) \end{aligned}\right\} \tag{4.6}$$

These form the expressions for the SOE constants in terms of the harmonic force constants α and β. It can easily be seen that the parameter ξ is given by

$$\xi = \frac{\alpha - \beta}{\alpha + \beta} = \frac{2C_{12}}{(C_{11} + C_{12})} \tag{4.7}$$

A calculation of the TOE constants of silicon, germanium and other diamond-like solids has been presented by Keating[55] which is an

extension of the above method of setting up the expression for the strain energy including the anharmonic terms. Expressions for the six TOE constants are derived in terms of three anharmonic first and second neighbor force constants and the two previously determined harmonic force constants. As has been done before, expressions for the strain energy are set up in the microscopic and macroscopic regimes. Including the anharmonic terms, the expression for macroscopic strain energy can be written as

$$u_{a'} = \frac{1}{6} C_{111}(e_1^3 + e_2^3 + e_3^3) + \frac{1}{2} C_{112}[e_1^2(e_2 + e_3) + e_2^2(e_3 + e_1) + e_3^2(e_1 + e_2)] + C_{123}\, e_1e_2e_3 + \frac{1}{2} C_{144}(e_1e_4^2 + e_2e_5^2 + e_3e_6^2) + \frac{1}{2} C_{166}[e_1^2(e_5^2 + e_6^2) + e_2(e_6^2 + e_4^2) + e_3(e_4^2 + e_5^2)] + C_{456}\, e_4e_5e_6 + \frac{1}{2} C_{11}(e_1^3 + e_2^3 + e_3^3) + \frac{1}{2} C_{12}[e_1^2(e_2 + e_3) + e_2^2(e_3 + e_1) + e_3^2(e_1 + e_2)] \quad (4.8)$$

where $e_1 = e_{xx}$, $e_2 = e_{yy}$, $e_3 = e_{zz}$, $e_4 = e_{xy}$, $e_5 = e_{xz}$, and $e_6 = e_{yz}$.

Considering the microscopic energy density, it should be pointed out that the most important forces between atoms in diamond-like solids are apparently short-range forces mainly due to shell-shell and shell-core interactions. Cochran[76] has obtained a good fit between theoretical and experimental phonon dispersion and elasticity data with the shell model and only short range forces. The shell model reduces to a rigid-ion formulation if only the elasticity is to be considered and excellent agreement has been obtained between theory and experiment using only a

nearest neighbor interaction and a noncentral second neighbor interaction. Since the shell-shell and shell-core effects give only small contributions for third and more distant neighbors, we include interactions out to second neighbors only.

Including the anharmonic terms, the expression for the microscopic strain energy can be written as[55]

$$u_a = [(\gamma' - \delta' + 3\varepsilon')/3 + (\alpha + 3\beta)/8a_0](e_1^3 + e_2^3 + e_3^3)$$

$$+ 2(\gamma' + 3\delta' - \varepsilon')e_1e_2e_3 + [\gamma' - \delta' + \varepsilon'/3 + (\alpha - \beta)/8a_0][e_1^2(e_2 + e_3)$$

$$+ e_2^2(e_3 + e_1) + e_3^2(e_1 + e_2)] + 2\gamma'(1 - \xi)^3e_4e_5e_6$$

$$+ [\gamma'(1 - \xi)^2 + \delta'(1 + \xi)^2 + \frac{1}{3}\varepsilon'(1 + \xi)(3\xi - 1)$$

$$+ \xi^2(\alpha - \beta)/8a_0][e_1e_4^2 + e_2e_5^2 + e_3e_6^2)$$

$$+ [\gamma'(1 - \xi)^2 - \delta'(1 + \xi)^2 + \frac{1}{3}\varepsilon'(1 + \xi)(3 - \xi)$$

$$+ \xi^2(\alpha - \beta)/8a_0][e_1(e_5^2 + e_6^2) + e_2(e_6^2 + e_4^2) + e_3(e_4^2 + e_5^2)] \ . \tag{4.9}$$

γ', δ' and ε' are the anharmonic force constants. The details of the derivation are not given here as it is already available in literature.[55] Comparing the expressions (4.8) and (4.9), the expressions for the TOE constants of diamond-like solids are obtained as

$$
\left.
\begin{aligned}
C_{111} &= \gamma - \delta + 9\varepsilon \\
C_{112} &= \gamma - \delta + \varepsilon \\
C_{123} &= \gamma + 3\delta - 3\varepsilon \\
C_{144} &= \gamma(1 - \varepsilon)^2 + \delta(1 + \varepsilon)^2 + \varepsilon(1 + \varepsilon)(3\varepsilon - 1) + C_{12}\varepsilon^2 \\
C_{166} &= \gamma(1 - \varepsilon)^2 - \delta(1 + \varepsilon)^2 + \varepsilon(1 + \varepsilon)(3 - \varepsilon) + C_{12}\varepsilon^2 \\
C_{456} &= \gamma(1 - \varepsilon)^3
\end{aligned}
\right\} \qquad (4.10)
$$

where $\gamma = 2\gamma'$, $\delta = 2\delta'$ and $\varepsilon = \frac{2}{3}\varepsilon'$ are the redefined anharmonic force constants.

Keating's model has been used to evaluate the TOE constants of silicon and germanium and it is found that the results are in very good agreement with the room temperature experimental values. This agreement is quite remarkable owing to the fact that the model involves only three adjustable parameters and it suggests that the anharmonic force constant model used is a fairly realistic one. The introduction of additional interactions into the strain energy will, of course, allow a much better fit but such a fit then might not be significant physically. The fact that Keating's model involves only three anharmonic parameters has enabled us to isolate all the TOE constants of silicon and germanium from our measured ultrasonic nonlinearity parameters and study their variation as a function of temperature. The Keating model has been applied by Nandanpawar and Rajagopalan[77] to predict the temperature dependence of C_{166} and $3C_{144} + 4C_{456}$ between 73 and 293°K of germanium. Their results agree reasonably well with available experimental values.

b. TOE Constants in Terms of the K_2 and K_3 Parameters

The expressions for the K_2 and K_3 parameters which are combinations of SOE and TOE constants given in Table 1 are reproduced here for the ease of further derivations. These parameters are obtained directly from harmonic generation experiments.

$$\left.\begin{aligned} K_2[100] &= C_{11} \\ K_2[110] &= \tfrac{1}{2}(C_{11} + C_{12} + 2C_{44}) \\ K_2[111] &= \tfrac{1}{3}(C_{11} + 2C_{12} + 4C_{44}) \end{aligned}\right\} \tag{4.11}$$

$$\left.\begin{aligned} K_3[100] &= C_{111} \\ K_3(110] &= \tfrac{1}{4}(C_{111} + 3C_{112} + 12C_{166}) \\ K_3[111] &= \tfrac{1}{9}(C_{111} + 6C_{112} + 12C_{144} + 24C_{166} + 2C_{123} + 16C_{456}) \end{aligned}\right\} \tag{4.12}$$

Substituting for the SOE and TOE constants from Eqs. (4.6) and (4.10) in (4.11) and (4.12), respectively, we can express K_2 and K_3 along the principal directions in terms of the harmonic force constants α and β and the anharmonic force constants γ, δ and ε.

$$\begin{aligned} K_2[100] &= (\alpha + 3\beta)/4a \\ K_2[110] &= \tfrac{1}{2}[(\alpha + 3\beta)/4a + (\alpha - \beta)/4a + 2\alpha\beta/(\alpha + \beta)a] \\ K_2[111] &= \tfrac{1}{3}[(\alpha + 3\beta)/4a + 2(\alpha - \beta)/4a + 4\alpha\beta/(\alpha + \beta)a] \end{aligned} \tag{4.13}$$

A knowledge of the parameter $\xi = (\alpha - \beta)/\alpha + \beta$ is enough for our calculations and so individual α and β are not evaluated. As has been shown in Eq. (4.4)

$$\xi = \frac{(\alpha - \beta)}{\alpha + \beta} = \frac{2C_{12}}{C_{11} + C_{12}} . \tag{4.14}$$

The K_3 parameters can be expressed in terms of γ, δ and ε as follows:

$$K_3[100] = \gamma - \delta + 9\varepsilon \tag{4.15}$$

$$K_3[110] - 3C_{12}\,\xi^2 = D\gamma - E\delta + F\varepsilon \tag{4.16}$$

where

$$D = 1 + 3(1 - \xi)^2$$

$$E = 1 + 3(1 + \xi)^2$$

and

$$F = 3[4 + 2\xi - \xi^2]$$

$$K_3[111] - 4C_{12}\,\xi^2 = H\gamma - P\delta + Q\varepsilon \tag{4.17}$$

where

$$H = 1 + 4(1 - \xi)^2 + \frac{16}{9}(1 - \xi)^3$$

$$P = \frac{1}{9} + \frac{4}{3}(1 + \xi)^2$$

$$Q = 1 + \frac{4}{3}(\xi^2 + 6\xi + 5) .$$

Solving between (4.15), (4.16) and (4.17) we get expressions for ε, δ and γ as follows:

$$\varepsilon = \frac{[R - H \frac{(K_3[100] \cdot E - G)}{(E - D)} + P \frac{(K_3[100] \cdot D - G)}{(E - D)}}{[P \frac{(9D - F)}{(E - D)} + Q - H \frac{(9E - F)}{(E - D)}]} \tag{4.18}$$

where

$$G = K_3[110] - 3C_{12}\,\varepsilon^2$$

and

$$R = K_3[111] - 4C_{12}\,\varepsilon^2$$

$$\delta = \frac{(K_3[100] \cdot D - G)}{(E - D)} - \frac{(9D - F)}{(E - D)}\,\varepsilon \tag{4.19}$$

and

$$\gamma = K_3[100] + \delta - 9\varepsilon\ . \tag{4.20}$$

Substituting these force constants in Eq. (4.10) leads to the six independent TOE constants for diamond-like solids. Evaluation of ε, γ and δ as a function of temperature results in the TOE constants as a function of temperature.

c. Results - Temperature Variation of the TOE Constants of Silicon and Germanium

As described in Chapter III, we have measured the nonlinearity parameters and hence the K_3 parameters along the three principal directions of silicon as a function of temperature from room temperature to 3°K using the ultrasonic harmonic generation technique. The results are given in Chapter III. Using the same technique, the nonlinearity parameters and K_3 parameters of germanium have been measured by Bains[46,59] in the same temperature range. The SOE constants of silicon and germanium have also

been measured in the entire temperature region. From these measured K_2 and K_3 values, substituting in (4.14), (4.18), (4.19) and (4.20) we have evaluated the force constants ξ, ε, γ and δ as a function of temperature for both silicon and germanium. In Table 8 we have tabulated the results.

In Figures 23 and 24 we have drawn the temperature variation of the anharmonic force constants of silicon and germanium. It may be noted from the figures that the force constants are susceptible to considerable temperature variations at low temperatures assuming nearly constant values at higher temperatures. The harmonic force constants do not vary much with temperature. The quantity ξ which is defined by (4.7) appearing in the set of equations (4.10) is almost independent of temperature, as can be seen from Table 8.

The force constants at various temperatures have been substituted in Eqs. (4.10) to evaluate all the six independent TOE constants of silicon and germanium as a function of temperature between 300 and 3°K. In Table 9 we tabulate the results. In Figure 25 we draw the TOE constants C_{111}, C_{112} and C_{166} of silicon as a function of temperature. Temperature variation of C_{123}, C_{144} and C_{456} of silicon are drawn in Figure 26. Similarly, in Figures 27 and 28 we have drawn the TOE constants of germanium as a function of temperature.

In the figures we have plotted both calculated data points and a best fit curve through them to show the effect of error propagation. Even in the curves showing greatest scatter of data, namely the C_{123} curves, the temperature dependence seems very clear. As can be seen

Table 8. Temperature Variation of the Force Constants of Silicon and Germanium

Temperature °K	$\xi = \frac{2C_{12}}{C_{11} + C_{12}}$	$-\varepsilon$ x 10^{12}	δ x 10^{12}	$-\gamma$ x 10^{12}
		Silicon		
4.02	0.5594	0.5630	0.6273	3.1061
10.57	0.5594	0.5327	0.5614	3.4246
16.14	0.5593	0.5174	0.5510	3.5320
24.93	0.5593	0.5089	0.5246	3.6228
35.08	0.5593	0.4940	0.4856	3.7813
43.49	0.5592	0.4926	0.4557	3.8137
51.78	0.5592	0.4742	0.4420	4.0031
61.04	0.5592	0.4434	0.4192	4.1697
77.61	0.5591	0.4342	0.4220	4.1629
100.42	0.5589	0.4364	0.3998	4.1511
118.77	0.5588	0.4378	0.3927	4.1344
131.51	0.5586	0.4343	0.3877	4.1581
147.89	0.5585	0.4396	0.3840	4.1075
167.99	0.5582	0.4301	0.3760	4.1874
197.93	0.5579	0.4254	0.3608	4.2228
223.37	0.5575	0.4268	0.3536	4.1992
241.70	0.5573	0.4233	0.3474	4.2214
260.13	0.5571	0.4247	0.3452	4.1969
272.48	0.5570	0.4225	0.3392	4.2137
Room temp.	0.5567	0.4244	0.3357	4.1800
		Germanium		
3.0	0.5476	0.6893	0.6154	1.6509
9.0	0.5475	0.5985	0.4839	2.5996
19.3	0.5472	0.5401	0.4169	3.1922
27.8	0.5471	0.5494	0.3637	3.1617
43.2	0.5469	0.5476	0.2699	3.2617
56.7	0.5466	0.5331	0.1838	3.4783
68.6	0.5464	0.5932	0.2186	2.9026
77.4	0.5463	0.4776	0.2822	3.6394
100.5	0.5460	0.5356	0.2539	3.2157
124.3	0.5459	0.4745	0.2258	3.8437
148.4	0.5458	0.5279	0.2186	3.4103
160.5	0.5458	0.5319	0.1948	3.3781
184.5	0.5458	0.4550	0.1622	4.0228
196.5	0.5458	0.5029	0.1948	3.5791
220.5	0.5457	0.4968	0.1896	3.6392
245.1	0.5455	0.4522	0.2276	3.8726
270.2	0.5454	0.3221	0.2875	4.6936
Room temp.	0.5459	0.3496	0.3054	4.3302

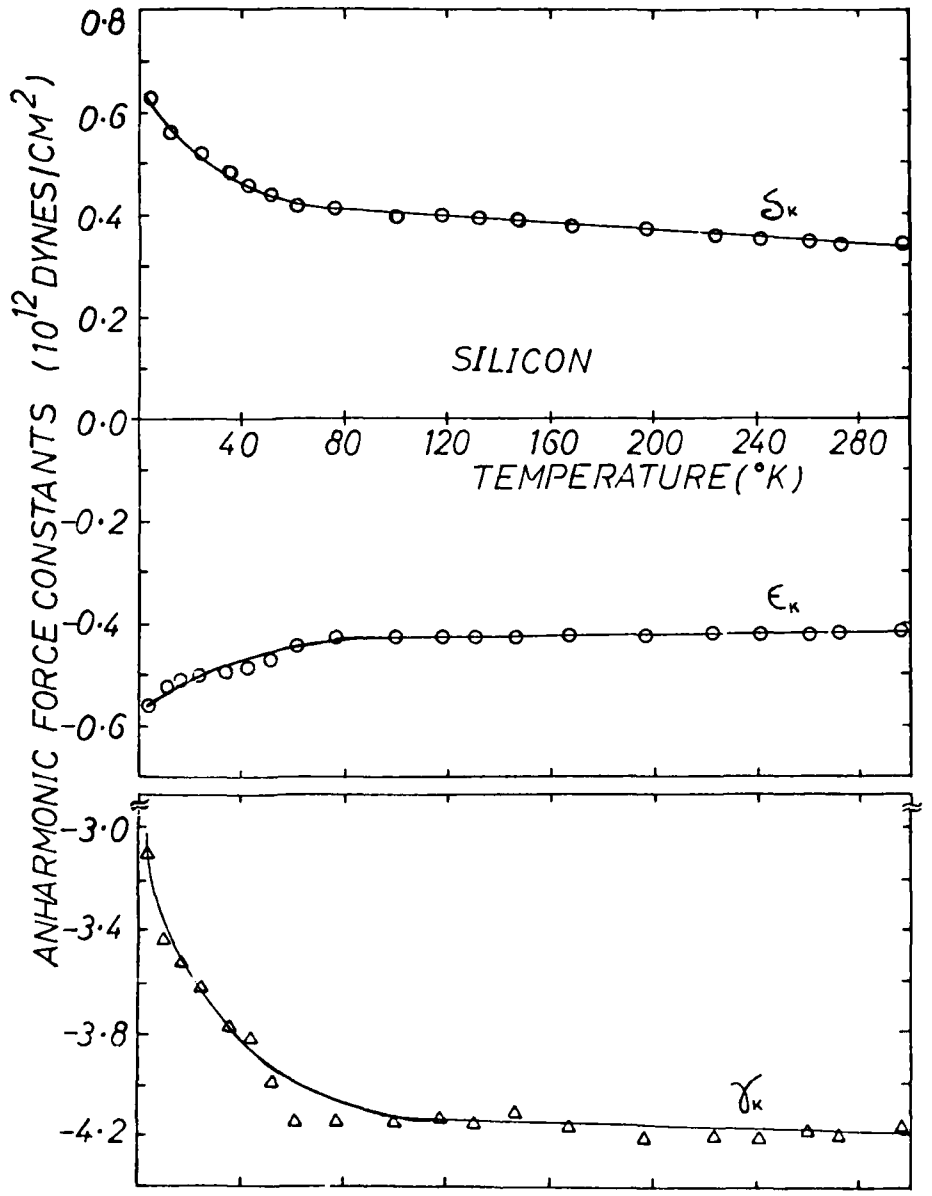

Figure 23. Temperature variation of the Keating anharmonic force constants of silicon.

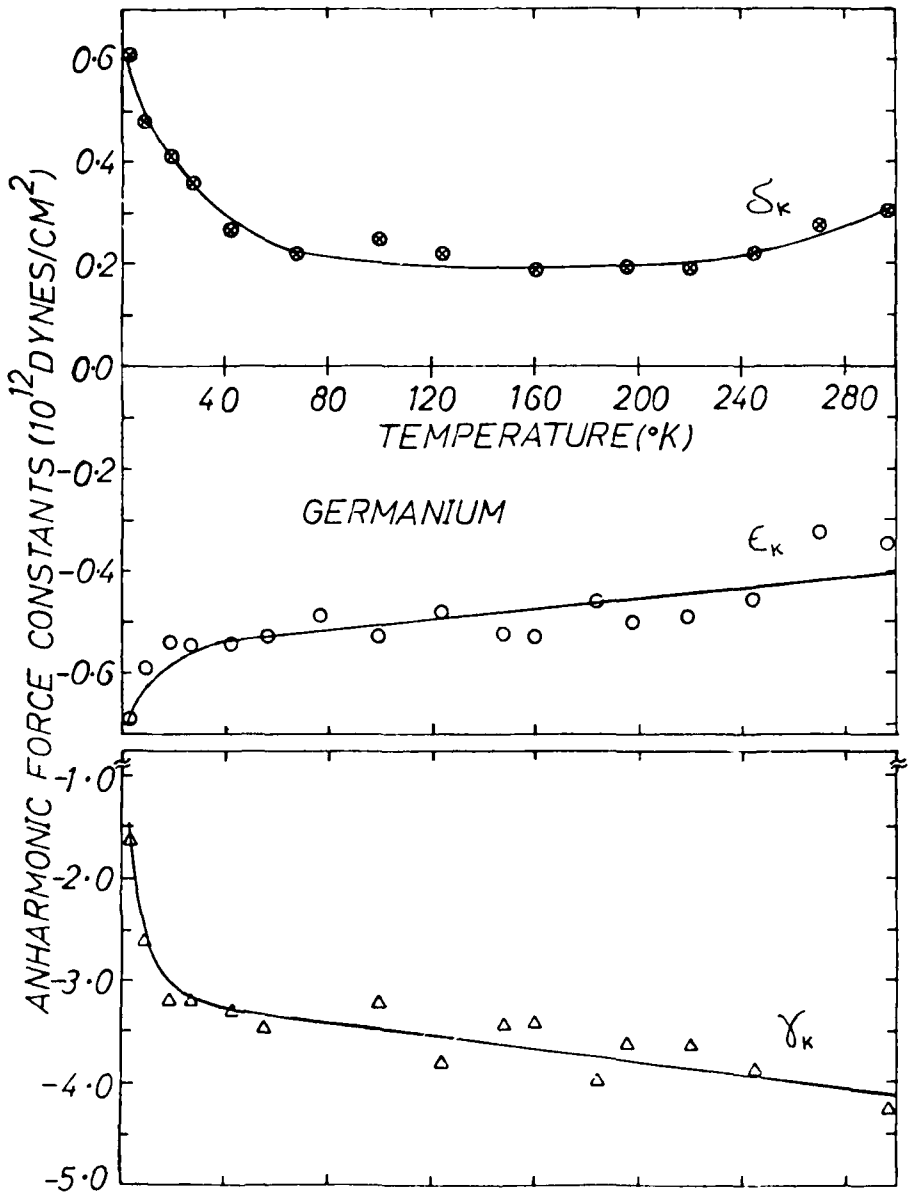

Figure 24. Temperature variation of the Keating anharmonic force constants of germanium.

Table 9. Temperature Variation of the TOE Constants of Silicon and Germanium

Temperature °K	C_{111} $\times 10^{12}$ dyn/cm^2	C_{112} $\times 10^{12}$ dyn/cm^2	C_{123} $\times 10^{12}$ dyn/cm^2	C_{144} $\times 10^{12}$ dyn/cm^2	C_{166} $\times 10^{12}$ dyn/cm^2	C_{456} $\times 10^{12}$ dyn/cm^2
			Silicon			
4.02	-8.8004	-4.2964	0.4648	0.5306	-4.0675	-0.2655
10.57	-8.7803	-4.5187	-0.1423	0.3406	-3.8538	-0.2929
16.14	-8.7396	-4.6004	-0.3268	0.3103	-3.7913	-0.3023
24.93	-8.7275	-4.6563	-0.5223	0.2375	-3.7124	-0.3101
35.08	-8.7129	-4.7609	-0.8425	0.1276	-3.5917	-0.3236
43.49	-8.7028	-4.7620	-0.9688	0.0499	-3.5202	-0.3266
51.78	-8.6445	-4.9193	-1.2545	-0.0010	-3.4537	-0.3429
61.04	-8.5795	-5.0323	-1.5819	-0.0563	-3.3134	-0.3571
77.60	-8.4927	-5.0191	-1.5943	-0.0388	-3.2843	-0.3568
100.42	-8.4785	-4.9873	-1.6425	-0.0937	-3.2372	-0.3563
118.77	-8.4673	-4.9649	-1.6429	-0.1096	-3.2224	-0.3551
131.51	-8.4545	-4.9801	-1.6921	-0.1234	-3.2022	-0.3576
147.89	-8.4479	-4.9311	-1.6367	-0.1287	-3.2040	-0.3535
167.99	-8.4343	-4.9935	-1.7691	-0.1550	-3.1652	-0.3611
197.93	-8.4122	-5.0090	-1.8642	-0.1954	-3.1188	-0.3649
223.37	-8.3940	-4.9796	-1.8580	-0.2114	-3.1036	-0.3638
241.70	-8.3785	-4.9921	-1.9093	-0.2282	-3.0805	-0.3662
260.13	-8.3644	-4.9668	-1.8872	-0.2312	-3.0768	-0.3646
272.48	-8.3554	-4.9754	-1.9286	-0.2473	-3.0576	-0.3663
Room temp.	-8.3353	-4.9400	-1.8997	-0.2526	-3.0511	-0.3641
			Germanium			
3.0	-8.4700	-2.9556	2.2632	0.5993	-4.2789	-0.1529
9.0	-8.4700	-3.6820	0.6476	0.1797	-3.8143	-0.2409
19.3	-8.4700	-4.1492	-0.3212	-0.0440	-3.5536	-0.2964
27.8	-8.4700	-4.0748	-0.4224	-0.1746	-3.4554	-0.2937
43.2	-8.4600	-4.0792	-0.8092	-0.4182	-3.2451	-0.3034

Table 9 (continued)

Temperature °K	C_{111} $\times 10^{12}$ dyn/cm^2	C_{112} $\times 10^{12}$ dyn/cm^2	C_{123} $\times 10^{12}$ dyn/cm^2	C_{144} $\times 10^{12}$ dyn/cm^2	C_{166} $\times 10^{12}$ dyn/cm^2	C_{456} $\times 10^{12}$ dyn/cm^2
			Germanium (continued)			
56.7	-8.4600	-4.1952	-1.3276	-0.6549	-3.0294	-0.3242
68.6	-8.4600	-3.7144	-0.4672	-0.5130	-3.2230	-0.2709
77.4	-8.2200	-4.3992	-1.3600	-0.3987	-3.0884	-0.3399
100.5	-8.2900	-4.0052	-1.6089	-0.4371	-3.1546	-0.3009
124.3	-8.3400	-4.5440	-1.7428	-0.5741	-2.9857	-0.3599
148.4	-8.3800	-4.1568	-1.1708	-0.5550	-3.0822	-0.3195
160.5	-8.3600	-4.1048	-1.1980	-0.6532	-2.9532	-0.3414
184.5	-8.2800	-4.6400	-2.1712	-0.7448	-2.7978	-0.3769
220.5	-8.3000	-4.3256	-1.5800	-0.6422	-2.9437	-0.3412
245.1	-8.1700	-4.5524	-1.8332	-0.5566	-2.9144	-0.3636
270.2	-7.8800	-5.3032	-2.8648	-0.4559	-2.7342	-0.4409
Room temp.	-7.7820	-4.9852	-2.3652	-0.3639	-2.8052	-0.4055

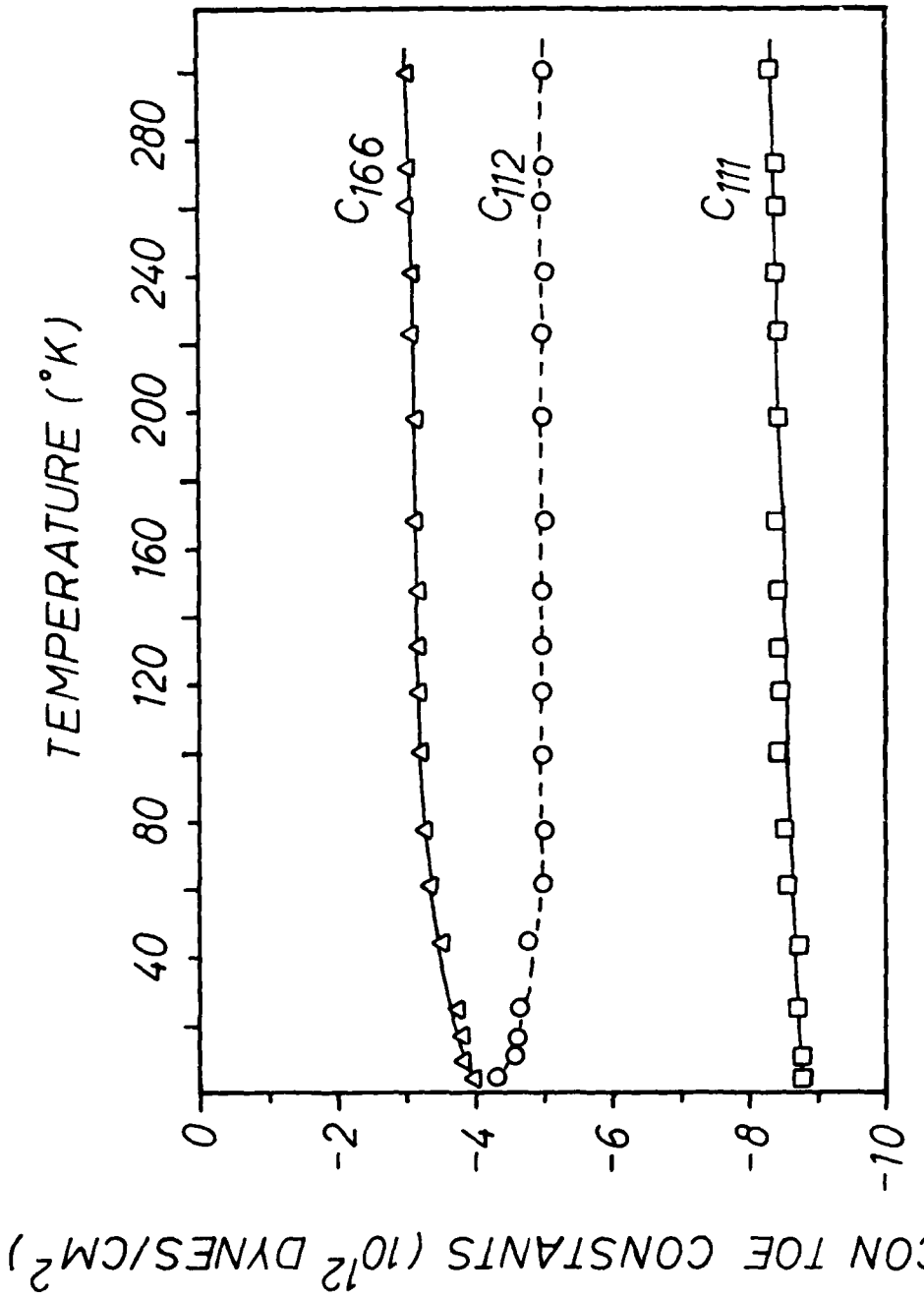

Figure 25. Temperature variation of the TOE constants C_{111}, C_{112} and C_{166} of silicon.

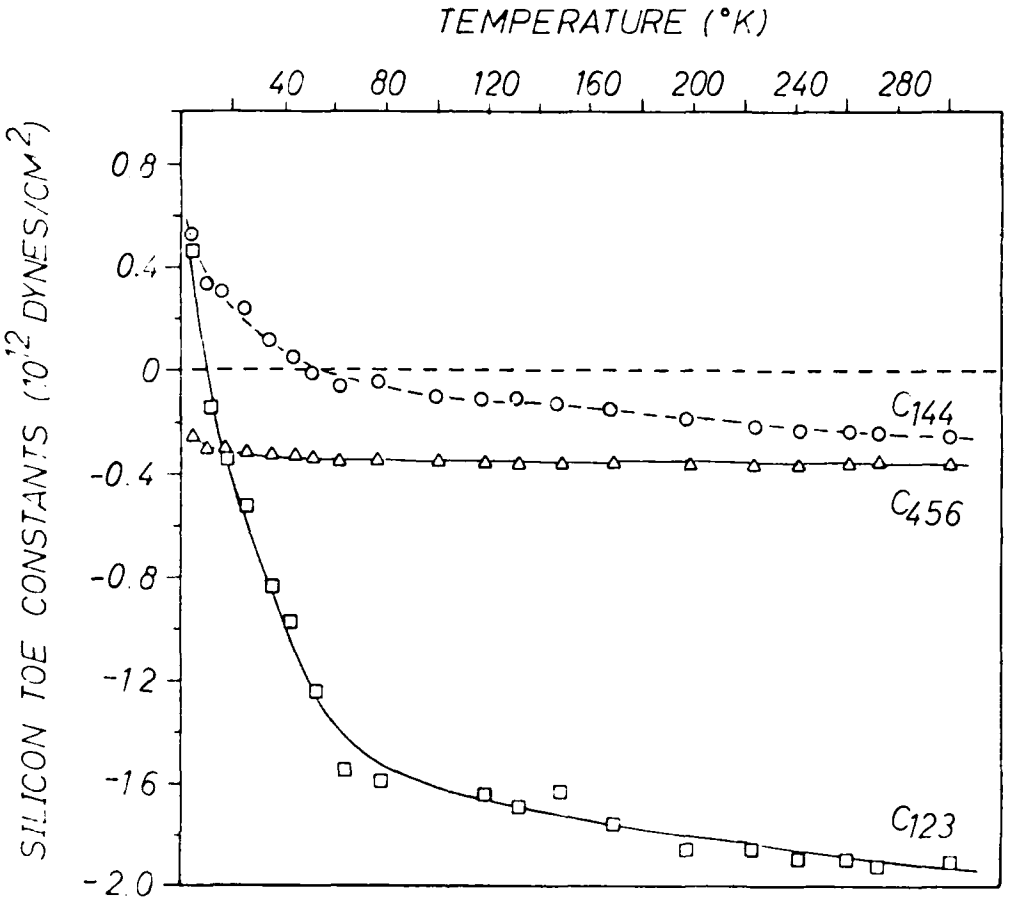

Figure 26. Temperature variation of the TOE constants C_{123}, C_{144} and C_{456} of silicon.

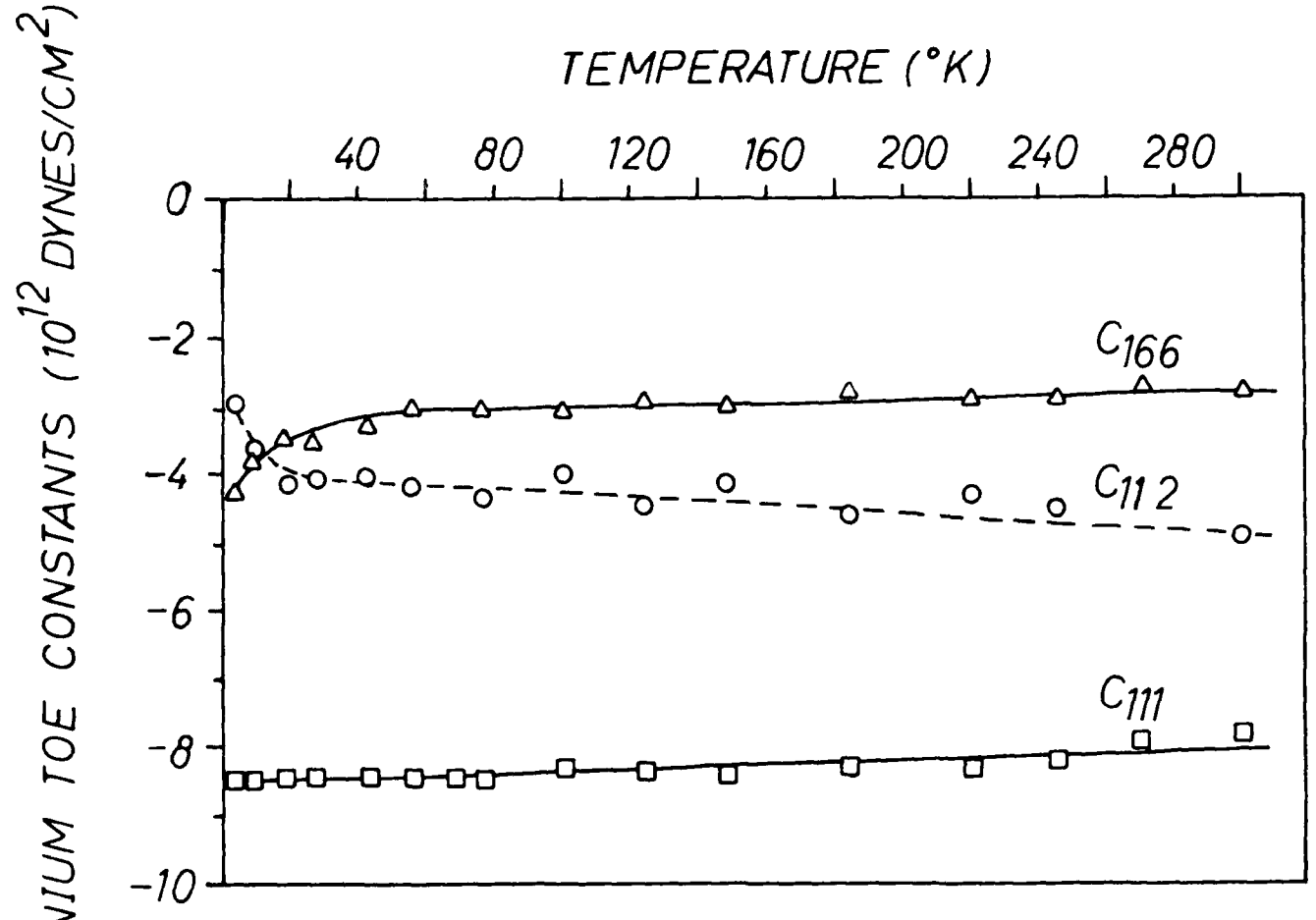

Figure 27. Temperature variation of the TOE constants C_{111}, C_{112} and C_{166} of germanium.

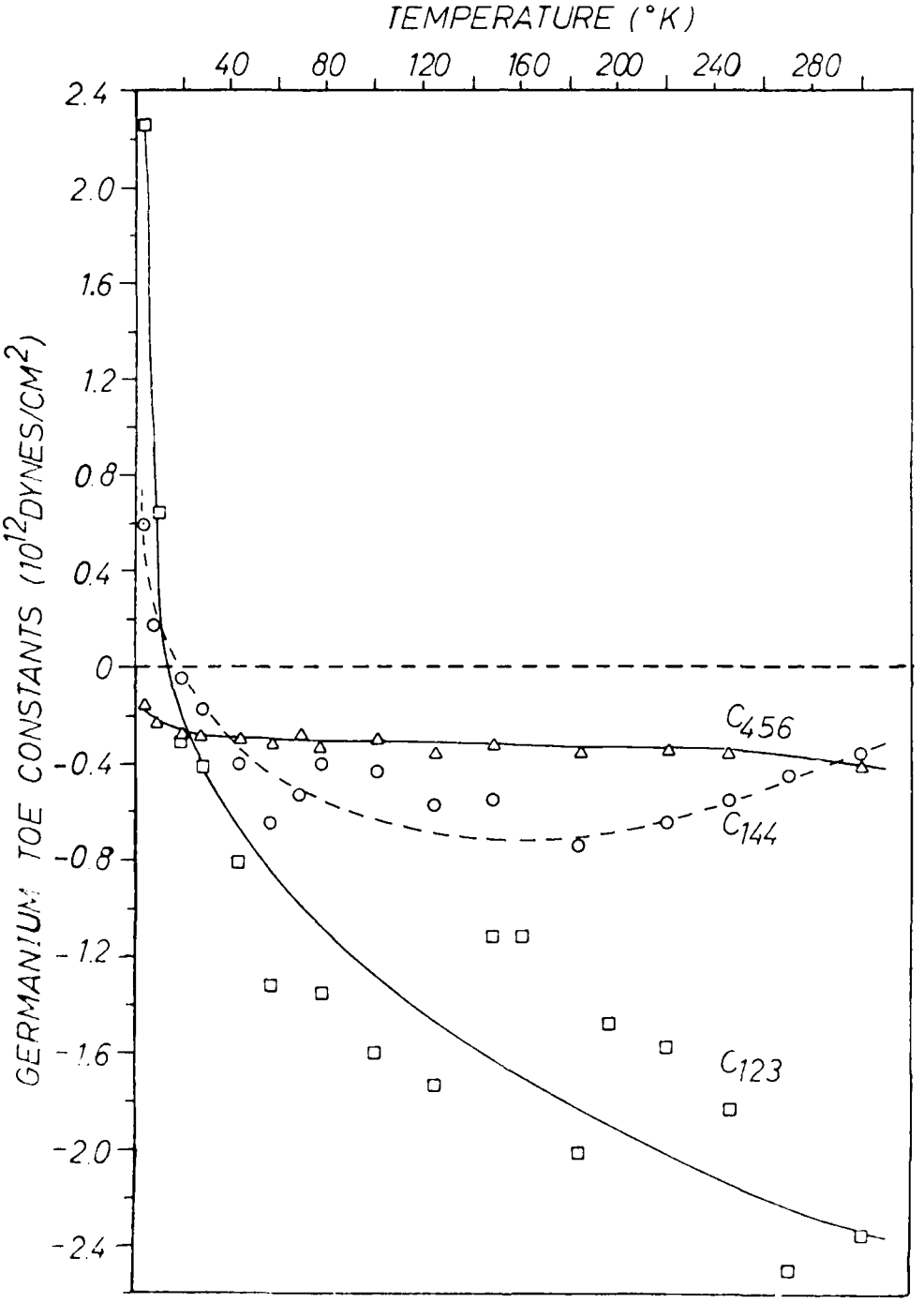

Figure 28. Temperature variation of the TOE constants C_{123}, C_{144} and C_{456} of germanium.

from the figures, the temperature variation of the TOE constants of silicon and germanium are similar, as can be expected. The room temperature values are in agreement with those obtained by McSkimin et al.[26] The greatest disagreement is found in C_{123}. The constants which show maximum sensitivity to temperature changes are C_{123} and C_{144}. They take on positive values at very low temperatures for both materials.

It should be mentioned that in the above calculations one obviously has to make the assumption that the thermal effects in elastic constants are solely due to changes in force constants. This assumption is open to question. Temperature dependent terms in the internal energy also might contribute to the elastic constants. Such effects, we believe, would be negligible compared to the variations occurring from changes in force constants.

d. Temperature Dependence of the Grüneisen Parameter, Thermal Expansion and Other Anharmonic Parameters of Silicon and Germanium

As is well known, the Grüneisen parameter represents the strain derivative of the lattice vibrational frequencies and is an important quantity in describing the anharmonic properties of solids. The method of evaluating the Grüneisen parameter using quasiharmonic theory is well established in literature.[71,72] The Grüneisen parameter γ is defined by

$$\gamma = \frac{\alpha}{K_T C_V} = \frac{\alpha}{K_S C_P} \tag{4.20}$$

where α is the thermal expansivity, K_T and K_S are the isothermal and

adiabatic compressibilities and C_p and C_V are the isochoric and isobaric heat capacities. Generalized γ's measure the strain dependence of the phonon frequencies and are no longer frequency dependent in the Debye model where the lattice vibrations are replaced by standing wave modes of a dispersionless elastic continuum. Their relationship with SOE and TOE coefficients have been derived earlier by Brugger[58] for arbitrary crystal symmetry and have been specialized to cubic point groups. In the quasiharmonic approximation, the Grüneisen γ can also be expressed as the weighted average of the generalized Grüneisen parameters γ_i by the relation

$$\gamma = \sum_i \gamma_i C_i / \sum_i C_i \tag{4.21}$$

where γ_i expresses the volume dependence of the lattice vibrational frequency for the ith mode and C_i is the Einstein heat capacity associated with that mode. If the sound speeds and their stress derivatives or the SOE and TOE constants are known, Eq. (4.21) can be evaluated in the continuum model even if the dispersion curves along many directions in the stressed and unstressed crystal are not known.

We follow the method due to Brugger and Fritz[72] to determine the Gruneisen γ's and thermal expansion of silicon and germanium. If p stands for the branch index and q for the wave vector, Eq. (4.21) can be written in the form

$$\gamma = \sum_{pq} \gamma(p,q)C(p,q) / \sum_{pq} C(p,q) \tag{4.22}$$

The continuum model has been introduced for the evaluation of γ with the following assumptions:

(i) The excitation of the optic modes may be neglected, so that the branch index p takes only the values 1, 2 and 3.

(ii) The acoustic modes obey the Debye distribution function (per unit volume) given by

$$g(p,q)dqd\Omega = (\frac{1}{3})q^2 dq d\Omega \quad . \tag{4.23}$$

(iii) The maximum value of the wave vector q along any direction is equal to the Debye radius

$$q_D = (\frac{6\pi^2}{V_0})^{1/3} \tag{4.24}$$

where V_0 is the volume of the primitive cell.

(iv) The acoustic modes are either nondispersive or they obey the sinusoidal dispersion relation

$$\frac{\omega}{\omega_{max}} = \sin(\frac{\pi}{2}\frac{q}{q_D}) \tag{4.25}$$

of the Born-von Karman model.

(v) The generalized Grüneisen parameter is independent of the wave number and is given by their long wave limits.

Applying the above assumptions, Eq. (4.22) takes the form

$$\gamma = \sum_p \oint d\Omega \gamma(P,N)C(P,N) / \sum_p \oint d\Omega C(P,N) \tag{4.26}$$

with

$$C(P,N) = (\frac{q_D}{2\pi})^3 \int_0^1 d\xi \frac{\xi^2 \Theta^2 e^\Theta}{(e^\Theta - 1)^2} \quad . \tag{4.27}$$

q_D is the Debye radius and in the Debye model the function Q is given by

$$Q(P,N,\varepsilon) = [\theta(P,N)/T]\varepsilon \tag{4.28}$$

where $\varepsilon(P,N)$ is the Debye characteristic temperature of the pth mode along the direction of q specified by the unit vector N. If S(P,N) is the elastic wave velocity of the pth mode, then[78]

$$\theta(P,N) = (\frac{hq_D}{k})S(P,N) \ . \tag{4.29}$$

For cubic crystals with a fourfold axis of symmetry, the expressions for $\gamma(P,N)$ have been derived earlier[72] and are given by

$$\gamma(P,N) = - \frac{1}{6W} [3B + 2W + K] \tag{4.30}$$

where

$$W(P,N) = C_{11}K_1 + C_{44}K_2 + C_{12}K_3 \tag{4.31}$$

and

$$K(P,N) = C_1K_1 + C_2K_2 + C_3K_3 \ . \tag{4.32}$$

The unknown quantities appearing in (4.31) and (4.32) are

$$\left.\begin{aligned} K_1(P,N) &= N_1^2U_1^2 + U_2^2U_2^2 + N_3^2U_3^2 \\ K_2(P,N) &= (N_2U_3 + N_3U_2)^2 + (N_3U_1 + N_1U_3)^2 + (N_1U_2 + N_2U_1)^2 \\ K_3(P,N) &= 2(N_2N_3U_2U_3 + N_1N_3U_1U_3 + N_1N_2U_1U_2 \end{aligned}\right\} \tag{4.33}$$

and

$$\left.\begin{aligned} C_1 &= C_{111} + 2C_{112} \\ C_2 &= C_{144} + 2C_{166} \\ C_3 &= C_{123} + 2C_{112} \end{aligned}\right\} \tag{4.34}$$

C_{ij}'s and C_{ijk}'s are the SOE and TOE constants of the solid. Also

$$B = \frac{1}{3}(C_{11} + 2C_{12}) \tag{4.35}$$

is the bulk modulus. The N's and U's appearing in Eqs. (4.33) are the direction cosines for the direction of propagation and direction of polarization characterized by the branch index P.

The thermal expansion is given by

$$\alpha = K \sum_{pq} \gamma(p,q)C(p,q) \tag{4.36}$$

where K is the isothermal compressibility. The thermal expansion of cubic crystals is isotropic and hence only the scalar γ of Eq. (4.26) need be evaluated for its determination.

Following the above procedure we have determined the Grüneisen parameter of silicon and germanium as a function of temperature from 300 to 3°K using the temperature dependent SOE and TOE constants that we have determined in the previous section. In Figures 29 and 30 we plot the Grüneisen parameter results obtained as a function of temperature for silicon and germanium respectively. The computations have been done with the help of a computer. Our curves are designated as "present work" in the figures. With the same computer program we have also evaluated the temperature variation of γ using room temperature values of TOE constants. This is the method adopted by Brugger and Fritz[72] who

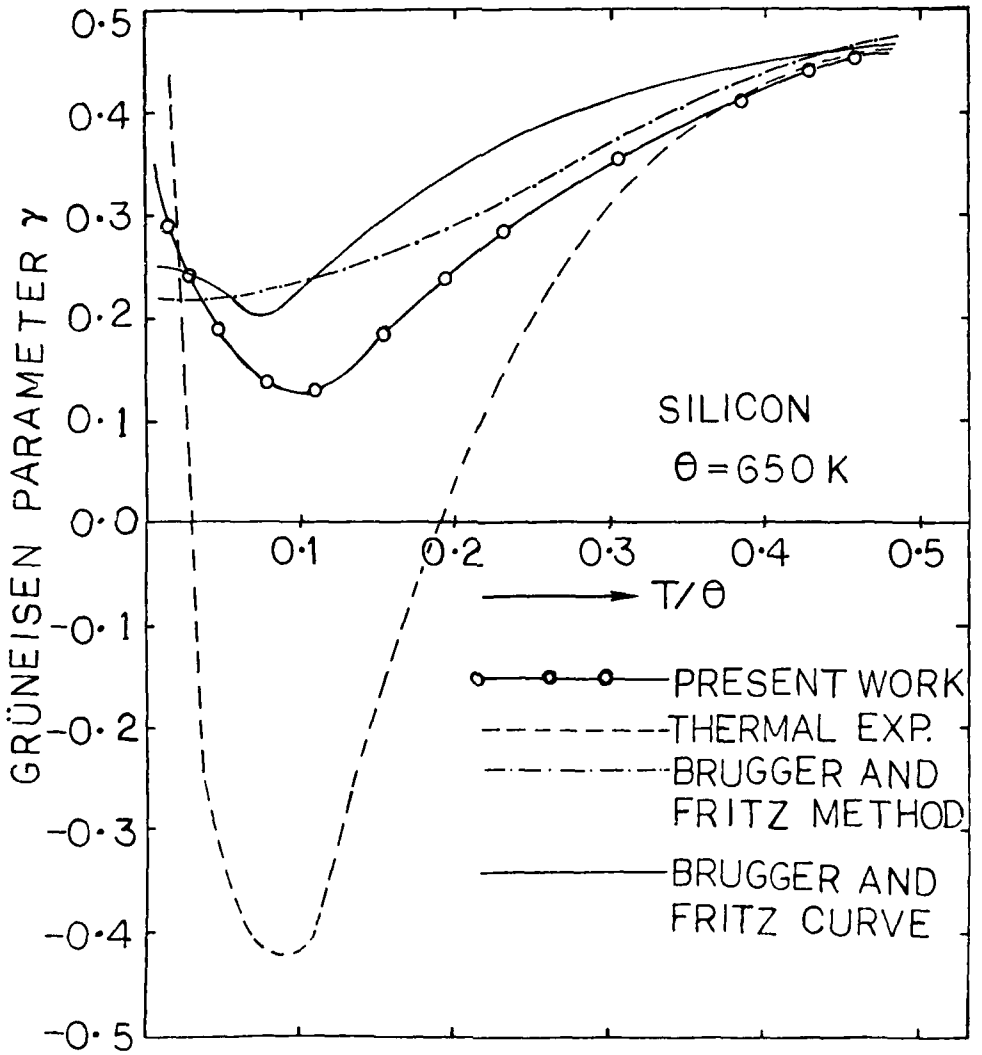

Figure 29. Grüneisen parameter of silicon plotted as a function of temperature.

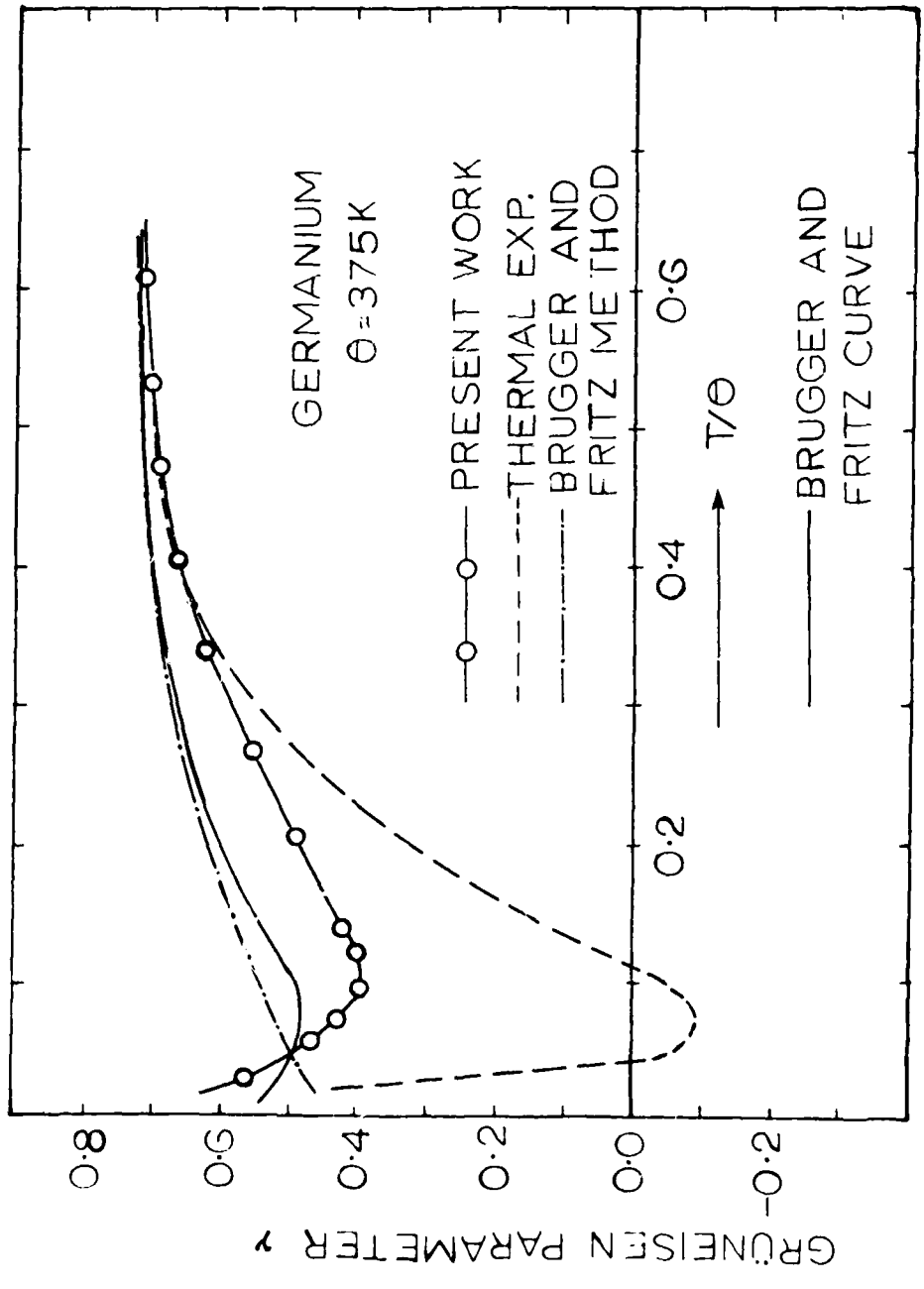

Figure 30. Grüneisen parameter of germanium plotted as a function of temperature.

have assumed that TOE constants are independent of temperature. These curves designated as "Brugger and Fritz Method" are also given in the figures along with the original curves drawn by Brugger and Fritz themselves for comparison. The curves drawn by Brugger and Fritz are denoted by "Brugger and Fritz Curves." The small difference between our curves drawn by the Brugger and Fritz method and the curves drawn by Brugger and Fritz are due to slight difference in the numerical values used. We have used the room temperature values of the TOE constants reported by McSkimin et al.[26] for both silicon and germanium, whereas Brugger and Fritz used the pressure derivatives of the SOE constants reported by McSkimin et al.[54] for silicon and McSkimin et al.[79] for germanium. In the figures we have also drawn the experimental curves of γ obtained from thermal expansion measurements.[69] These curves are denoted by "Thermal Exp" in the curves. It can be seen from the curves that our curves which take into account the temperature variation of the TOE constants are in better agreement with experimental curves, even though they also do not show any negative values for the Grüneisen parameter which has been calculated from thermal expansion data. A realistic physical reasoning for this disagreement is included in the discussion section.

In the quasiharmonic approximation, the thermal expansion is proportional to the Grüneisen parameter (Eq. 4.36) and so thermal expansion follows a similar temperature variation as the Grüneisen parameter. Since the thermal expansion curves are similar to the Grüneisen parameter curves, they are not reproduced. In the

high temperature limit the value of γ calculated from thermal expansion agrees well with measured values.

We have determined and drawn as a function of temperature the isothermal first pressure derivatives of the adiabatic SOE constants from the temperature dependent TOE constants. The relationships between pressure derivatives of the SOE constants and TOE constants are well known[80,81]

$$\left.\begin{aligned} \frac{dC_{11}}{dP} &= -\left(\frac{2C_{11} + 2C_{12} + C_{111} + 2C_{112}}{C_{11} + 2C_{12}}\right) \\ \frac{dC_{12}}{dP} &= -\left(\frac{-C_{11} - C_{12} + C_{123} + 2C_{112}}{C_{11} + 2C_{12}}\right) \\ \frac{dC_{44}}{dP} &= -\left(\frac{C_{11} + 2C_{12} + C_{44} + C_{144} + 2C_{166}}{C_{11} + 2C_{12}}\right) \\ \frac{dB}{dP} &= -\left(\frac{C_{111} + 6C_{112} + 2C_{123}}{3(C_{11} + 2C_{12})}\right) \end{aligned}\right\} \qquad (4.37)$$

where $B = \frac{1}{3}(C_{11} + 2C_{12})$ is the bulk modulus. The above pressure derivatives drawn as a function of temperature for silicon and germanium are reproduced in Figures 31 and 32 respectively.

Anderson[82] stated that the adiabatic bulk modulus of a material varies with temperature according to

$$B_S = B_0 - bT\, e^{T_0/T} \qquad (4.38)$$

where B_S is the bulk modulus at temperature T and B_0 is the bulk modulus at absolute zero. b and T_0 are empirical parameters characteristic of the solid. Anderson showed that the constant b is given by

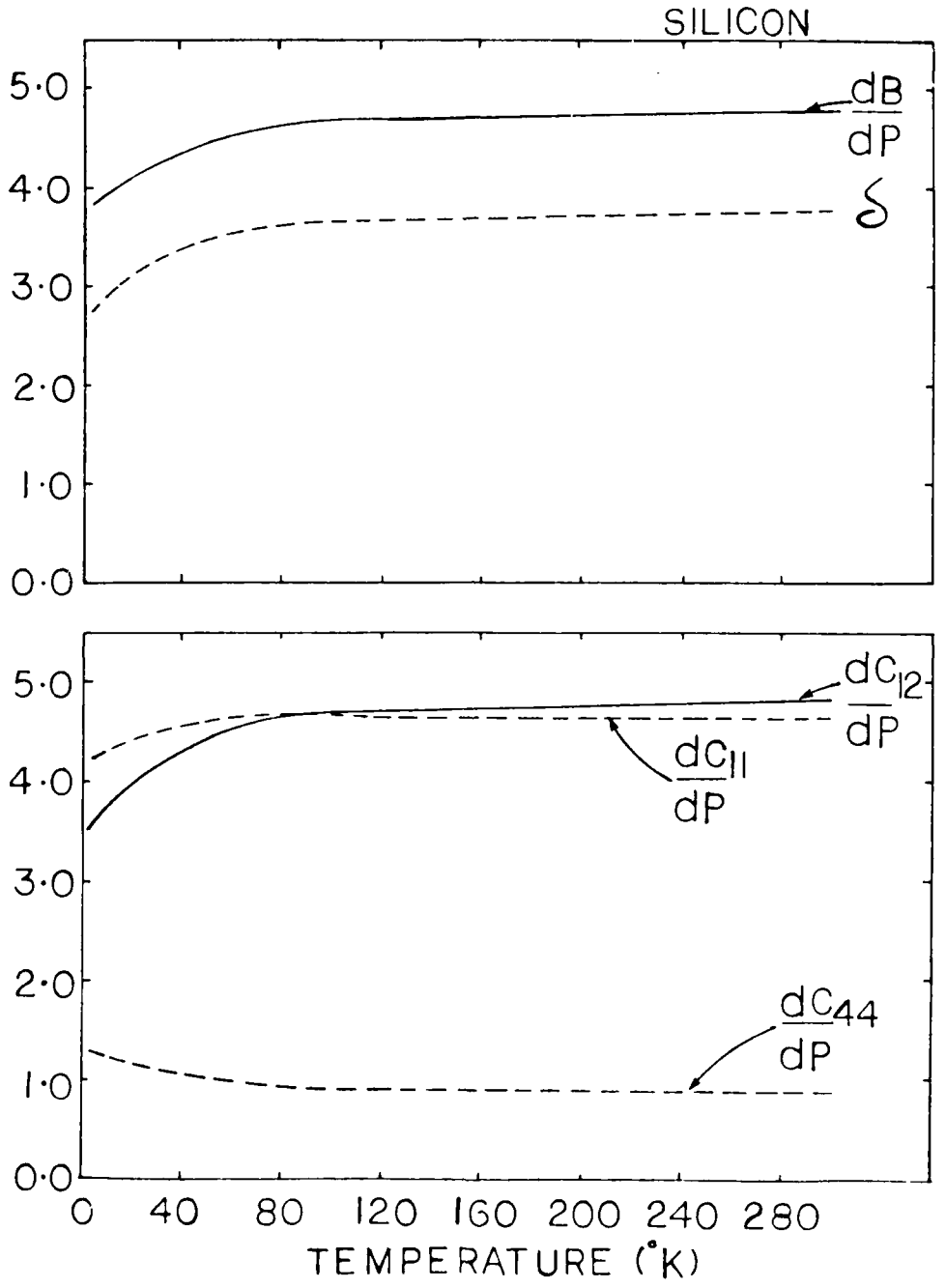

Figure 31. Temperature variation of $\frac{dB}{dP}$, $\frac{dC_{11}}{dP}$, $\frac{dC_{12}}{dP}$, $\frac{dC_{44}}{dP}$ and δ of silicon.

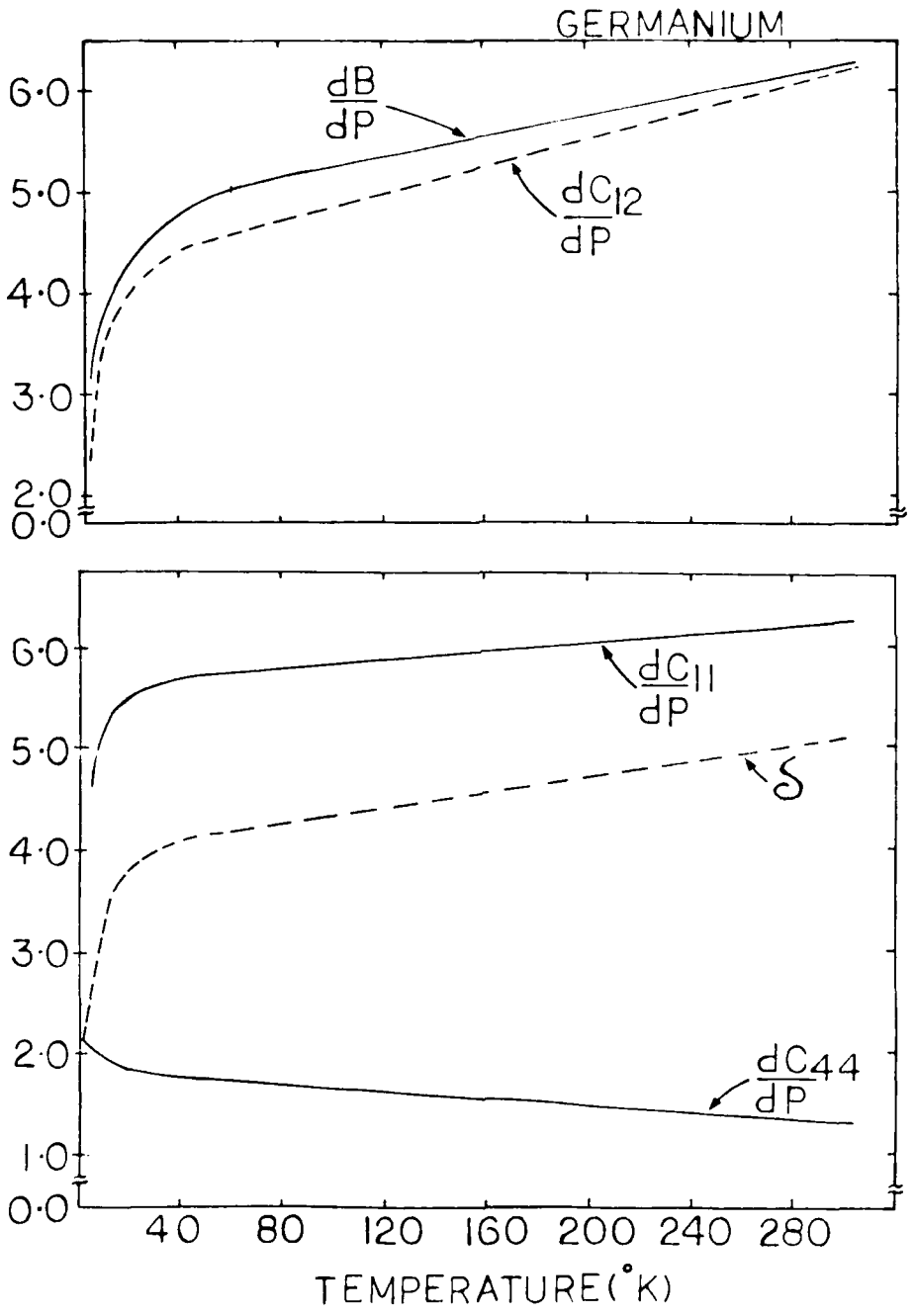

Figure 32. Temperature variation of $\frac{dB}{dP}$, $\frac{dC_{11}}{dP}$, $\frac{dC_{12}}{dP}$, $\frac{dC_{44}}{dP}$ and S of germanium.

$$b = 3R\gamma^2/V_0 \qquad (4.39)$$

where V_0 is the specific volume per atom at absolute zero, R is the gas constant, γ is the Grüneisen parameter and δ is a constant called the Anderson-Grüneisen parameter and it plays an important role in describing the temperature dependence of the bulk modulus and related anharmonic properties. Chang[83] showed that δ is related to the pressure derivative of the bulk modulus as

$$\delta = \left(\frac{\partial B_T}{\partial P} - 1\right) \text{ or } \left(\frac{\partial B_S}{\partial P} - 1\right) . \qquad (4.40)$$

Using this definition, the relationship between δ and TOE constants has been obtained by Rao[84] as

$$\delta = -\left(1 + \frac{C_{111} + 6C_{112} + 2C_{123}}{3(C_{11} + 2C_{12})}\right) . \qquad (4.41)$$

This expression has been used to determine the temperature variation of δ using temperature dependent TOE constants. δ as a function of temperature for silicon and germanium are also drawn in Figures 31 and 32.

e. Discussion and Conclusion

An elegant method of combining an experimental result and a successful theoretical model has enabled us to determine the temperature dependence of the TOE constants of silicon and germanium from liquid helium to room temperature for the first time. It is a remarkable step towards understanding the low temperature anharmonic properties of these solids even though the results do not fully account for some of the anomalous thermal properties exhibited by them at low temperatures.

Our assumption that the temperature variation of the elastic constants are due to thermal effects in the force constants is justifiable as we see that our Grüneisen parameter curves agree with the curves of others. As a matter of fact, our curves are in better agreement with curves derived from experimental thermal expansion curves than any previous results.

The Grüneisen parameter and thermal expansion of silicon and germanium are negative at certain temperatures in the low temperature region. This anomalous property has attracted a great amount of attention. But none of the calculations based on the anisotropic continuum model could predict or fully account for this anomalous behavior. Now it is more or less well established that the negative thermal properties are a result of some of the mode Grüneisen parameters going negative or the phonon frequencies decreasing with stress. A straightforward calculation based on anisotropic continuum model in the quasiharmonic approximation cannot account for these negative mode γ's. The overall temperature dependence of γ is explained as follows: At very low temperatures, the region in which γ is positive, the elastic portion of the lattice spectrum dominates giving positive γ. As the temperature is increased, the entire transverse acoustic modes (TA) contribute appreciably to γ. The mode γ's for the transverse modes decrease with temperature. In the negative γ temperature region, the contribution from TA modes dominates over the other modes making the net effect negative. As the temperature is increased further, the remainder of the acoustic branches coupled with the optic modes make γ positive again. In

the high temperature region all the theoretical calculations agree with experimental results. A complete understanding of the situation demands complete experimental data on the volume dependence of the frequencies of the individual branches in the dispersive region in the entire temperature region. Since such data are not available, Bienenstock[85] has done a calculation for germanium based on a modified shell model using the volume dependence of the elastic moduli and phonon frequencies reported by Brockhouse and Iyengar.[86] Bienenstock introduces an induced dipole term ω_D^2 which varies as V^{-n} where n is an adjustable parameter nearly equal to 1 and includes the optic modes in the Einstein approximation. He has calculated the Grüneisen parameters γ_j for a number of acoustic modes and has found that the transverse modes are rapidly varying functions of the wave vector q. They are assumed to be positive for small q and negative near the Brillouin zone surface. The calculated γ is in agreement with experiment at all temperatures when optical modes are included. Studies on phonon assisted tunnelling under pressure and measurements of the stress-induced shifts of the threshold energy for tunnelling in germanium and subsequent calculation of γ_i for TA modes near the the Brillouin zone boundary by Pyne[87] confirms the existence of negative γ_i for TA modes.

General Conclusion

The work presented in this technical report forms a nearly complete study of the temperature dependence of the third-order elastic constants of the typical diamond-like solids silicon and germanium.

The harmonic generation technique has found new application to the study of the anharmonic properties of these solids. Similar works applied to other groups of solids might lead to an understanding of the temperature variation of their third-order elastic constants and other anharmonic properties.

BIBLIOGRAPHY

BIBLIOGRAPHY

1. M. A. Breazeale and D. O. Thompson, Appl. Phys. Lett. 3, 77 (1963).

2. A. A. Gedroits and V. A. Krasilnikov, Sov. Phys. JETP 16, 1122 (1963).

3. D. C. Wallace, Thermodynamics of Crystals (John Wiley and Sons, Inc., New York, 1972).

4. A. A. Maradudin, E. W. Mantroll, G. H. Weiss, and I. P. Ipatova, "Theory of Lattice Dynamics in the Harmonic Approximation," in Solid State Physics (Academic Press, New York, 1971), Suppl. 3.

5. G. Leibfried and W. Ludwig, in Solid State Physics, edited by F. Seitz and D. Turnbull (Academic Press, New York, 1961), Vol. 12.

6. W. P. Mason, J. Acoust. Soc. Am. 32, 458 (1960).

7. J. Holder and A. V. Granato, in Physical Acoustics, edited by W. P. Mason and R. N. Thurston (Academic Press, New York, 1971), Vol. VIII.

8. A. Seeger and O. Buck, Z. Naturforschg. 15a, 1056 (1960).

9. R. A. Coldwell-Horsfall, Phys. Rev. 129, 22 (1963).

10. P. B. Ghate, Phys. Rev. 139, A1666 (1965).

11. Y. Hiki and A. V. Granato, Phys. Rev. 144, 411 (1966).

12. F. D. Murnaghan, Finite Deformation of an Elastic Solid (John Wiley and Sons, Inc., New York, 1951).

13. M. Born and K. Huang, Dynamical Theory of Crystal Lattices (Oxford University Press, London, 1954).

14. Brugger, K., Phys. Rev. 133, A1611 (1964).

15. K. Fuchs. Proc. Roy. Soc. (London) A153 , 622 (1936); A157, 447 (1936).

16. T. Suzuki, A. V. Granato, and J. F. Thomas, Jr., Phys. Rev. 175, 766 (1968).

17. E. R. Naimon, T. Suzuki, and A. V. Granato, Phys. Rev. B 4, 4297 (1971).

18. (a) F. Birch, Phys. Rev. 71, 809 (1947); (b) S. Bhagavantam and D. Suryanarayana, Nature (London) 160, 750 (1947).

19. H. J. McSkimin, J. Acoust. Soc. Am. 33, 12 (1961); 34, 609 (1962).

20. D. S. Hughes and J. L. Kelly, Phys. Rev. 92, 1145 (1953).

21. N. G. Einsprugh and R. J. Manning, J. Appl. Phys. 35, 560 (1964).

22. T. Bateman, W. P. Mason, and H. J. McSkimin, J. Appl. Phys. 32, 928 (1961).

23. R. N. Thurston and K. Brugger, Phys. Rev. 133, A1604 (1964).

24. G. R. Barsch and Z. P. Chang, J. Appl. Phys. 39, 3276 (1968).

25. K. Brugger, J. Appl. Phys. 36, 768 (1965).

26. H. J. McSkimin and P. Andreatch, Jr., J. Appl. Phys. 35, 3312 (1964)

27. Z. P. Chang, Phys. Rev. 140, A1788 (1965).

28. E. H. Bogardus, J. Appl. Phys. 36, 2504 (1965).

29. K. Salama and G. A. Alers, Phys. Rev. 161, 673 (1967).

30. R. A. Graham, J. Acoust. Soc. Am. 51, 1576 (1972).

31. J. Melngailis, A. A. Maradudin, and A. Seeger, Phys. Rev. 131, 1972 (1963).

32. J. H. Parker, Jr., F. Kelley, and D. I. Bolef, Appl. Phys. Lett. 5, 7 (1964).

33. G. L. Jones and D. R. Kobett, J. Acoust. Soc. Am. 35, 5 (1963).

34. L. H. Taylor and F. R. Rollins, Jr., Phys. Rev. 136, A591 (1964).

35. F. R. Rollins, Jr., Appl. Phys. Lett. 2, 147 (1963).

36. F. R. Rollins, Jr., L. H. Taylor, and P. H. Todd, Jr., Phys. Rev. 136, A597 (1964).

37. R. W. Dunham and H. B. Huntington, Phys. Rev. B 2, 1098 (1970).

38. I. L. Bajak and M. A. Breazeale, J. Acoust. Soc. Am. 68, 1245 (1980).

39. M. A. Breazeale and J. Ford, J. Appl. Phys. 36, 3486 (1965).

40. W. B. Gauster and M. A. Breazeale, Rev. Sci. Instrum. 37, 1544 (1966).

41. W. B. Gauster and M. A. Breazeale, Phys. Rev. 168, 655 (1968).

42. J. E. Mackey and R. T. Arnold, J. Appl. Phys. 40, 4806 (1969).

43. E. L. Meeks and R. T. Arnold, Phys. Rev. B 1, 982 (1972).

44. R. D. Peters, M. A. Breazeale, and V. K. Paré, Rev. Sci. Instrum. 39, 1505 (1968).

45. R. D. Peters, M. A. Breazeale, and V. K. Paré, Phys. Rev. B 1, 3245 (1970).

46. J. A. Bains, Jr., and M. A. Breazeale, Phys. Rev. B 13, 3623 (1976).

47. J. H, Cantrell, Jr., and M. A. Breazeale, Phys. Rev. B 17, 4864 (1978).

48. W. T. Yost, J. H. Cantrell, Jr., and M. A. Breazeale, J. Appl. Phys., scheduled for publication December 1980.

49. E. Borgnis, Phys. Rev. 98, 1000 (1955).

50. Z. A. Goldberg, Sov. Phys.-Acoust. 6, 306 (1961).

51. A. C. Holt and J. Ford, J. Appl. Phys. 38, 42 (1967).

52. R. E. Green, Jr., in Treatise on Materials Science and Technology (Academic Press, New York, 1973), Vol. 3.

53. H. J. McSkimin, J. Appl. Phys. 24, 988 (1953).

54. H. J. McSkimin and P. Andreatch, Jr., J. Appl. Phys. 35, 2161 (1964).

55. P. N. Keating, Phys. Rev. 149, 674 (1966).

56. R. N. Thurston, in Handbuch der Physik, edited by S. Flugge (Springer-Verlag, Berlin, 1974), Vol. VI a/4, p. 279.

57. J. H. Cantrell, Jr., Phys. Rev. B 21, 4191 (1980).

58. K. Brugger, Phys. Rev. 137, A1826 (1965).

59. J. A. Bains, Jr., Ph.D. dissertation (The University of Tennessee, 1974).

60. M. E. Fine, J. Appl. Phys. 26, 862 (1955).

61. R. F. S. Hearmon, in Landolt-Börnstein, edited by K. H. Hellwege (Springer-Verlag, Berlin, 1979), Vol. 11, Ch. 1 and 2 and references therein.

62. V. P. N. Sarma and P. J. Reddy, Phil. Mag. 27, 769 (1973).

63. P. N. Keating, Phys. Rev. 145, 637 (1966).

64. D. F. Gibbons, Phys. Rev. 112, 136 (1958).

65. S. I. Novikova and P. G. Strelkov, Sov. Phys. Solid State 1, 1687 (1960).

66. S. I. Novikova, Sov. Phys. Solid State 2, 37 (1960).

67. P. W. Sparks and C. A. Swenson, Phys. Rev. 163, 779 (1967).

68. R. D. McCammon and G. K. White, Phys. Rev. Lett. 10, 234 (1963).

69. R. H. Carr, R. D. McCammon, and G. K. White, Phil. Mag. 12, 157 (1965).

70. W. B. Daniels, Phys. Rev. Lett. 8, 3 (1962).

71. F. W. Sheard, Phil. Mag. 3, 1381 (1958).

72. K. Brugger and T. C. Fritz, Phys. Rev. 157, 524 (1967).

73. J. G. Collins, Phil. Mag. 8, 323 (1963).

74. K. C. Sharma and S. K. Joshi, Phil. Mag. 9, 507 (1964).

75. C. Kittel, Introduction to Solid State Physics (John Wiley and Sons, New York, 1956).

76. W. Cochran, Proc. Roy. Soc. (London) A258, 260 (1959).

77. M. Nandanpawar and S. Rajagopalan, Phys. Rev. B 19, 3130 (1979).

78. S. L. Quimby and P. M. Sutton, Phys. Rev. 91, 1122 (1953).

79. H. J. McSkimin and P. Andreatch, Jr., J. Appl. Phys. 34, 651 (1963).

80. G. R. Barsch and Z. P. Chang, J. Appl. Phys. 39, 3276 (1968).

81. J. F. Thomas, Jr., Phys. Rev. B 7, 2385 (1973).

82. O. L. Anderson, Phys. Rev. 144, 553 (1966).

83. Y. A. Chang, J. Phys. Chem. Solids 28, 697 (1967).

84. R. R. Rao, Phys. Rev. B 10, 4173 (1974).

85. A. Bienenstock, Phil. Mag. 9, 755 (1964).

86. B. N. Brockhouse and P. K. Iyengar, Phys. Rev. 111, 747 (1958).

87. R. T. Payne, Phys. Rev. Lett. 13, 53 (1964).

88. R. Truell, C. Elbaum, and B. B. Check, Ultrasonic Methods in Solid State Physics (Academic Press, New York, 1969).

APPENDIXES

APPENDIX A.1

THE DETECTOR EQUIVALENT CIRCUIT

Figure 33 shows the detector as it is connected for measurements of nonlinearity. It is assumed that the detector load is an ideal resistive load R. A large coupling capacitor C_b provides dc blocking for the amplifier. Its effect on the RF signals can be ignored. R_b is a large (≈ 1 to 10 mΩ) resistor used to prevent large current discharges in the event of arcing in the detector. It is very large compared to R so that no appreciable current flows through it and V_b. If one considers the sample end vibrating sinusoidally at frequency ω with amplitude 2A, where A is the acoustic wave amplitude in the sample, then the gap spacing changes with time according to

$$S = S_0 + 2A \sin \omega t \ . \qquad (A.1\text{-}1)$$

The factor 2 enters because the reflection of the wave at the stress-free surface leads to a vibration amplitude of the sample end which is twice the wave amplitude inside the sample. Thus the capacitance of the detector, considered as a parallel plate capacitor, is given by

$$1/C = 1/C_0(1 + \frac{2A}{S_0} \sin \omega t) \qquad (A.1\text{-}2)$$

where $C_0 = \frac{\varepsilon \alpha}{S_0}$ is the static capacitance of the detector, ε, α and S_0 being the dielectric constant of the medium (=1 for air), area of the electrode and static spacing of the detector, respectively. Summing

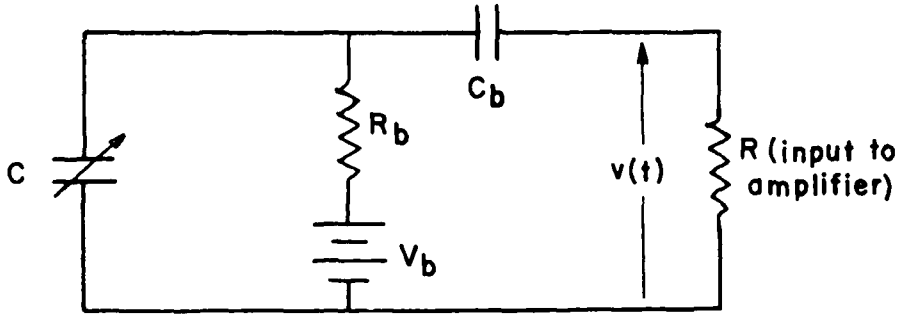

Figure 33. General detector circuit.

voltages around the outside loop of Figure 33, we get

$$\frac{q(t)}{c} - V_b = -R \frac{dq}{dt} = V(t) \ . \qquad \text{(A.1-3)}$$

Substituting (A.1-1)and (A.1-2) in (A.1-3) and assuming a steady-state solution of the form

$$q = q_0 + a \sin \omega t \qquad \text{(A.1-4)}$$

one obtains

$$V(t) = \frac{2AV_b}{S_0} R \omega C_0 \frac{1}{\sqrt{1 + R^2\omega^2 C_0^2}} \cos(\omega t + \phi) \qquad \text{(A.1-5)}$$

where

$$\phi = \tan^{-1}(R \omega C_0) \ . \qquad \text{(A.1-6)}$$

Consider a signal generator of amplitude $V = \frac{2AV_b}{S_0}$ feeding R through a capacitance of value C_0. The voltage across R can be shown to be precisely the same (in both amplitude and phase) as Eq. (A.1-5). A complex load of impedance Z, rather than R, can also be treated. One has simply $\frac{AV_b}{S_0} \sin \omega t$ feeding C_0 and Z in series. This situation more accurately represents the experimental case because of stray line capacitance shunting the input to the amplifier. For most experimental situations this stray capacitance is sufficiently large to require that during the calibration to determine V, one feeds through a substitutional capacitor of value C_0, even if R is chosen to be quite large.

APPENDIX A.2

RF GATE, MOSFET GATE AND FREQUENCY DOUBLER

To prevent overloading of the amplifiers due to the feedthrough signal, two gates have been built. An RF gate, shown in Figure 34, is used between the capacitive detector and the 30 MHz amplifier to pass only the echoes of interest. A slower MOSFET gate, shown in Figure 35, is used between the detected output of the 30 MHz or 60 MHz broadband amplifier and the boxcar integrator. The RF gate is able to handle the RF pulses, but the on-to-off ratio is not very great. However, if a x10 attenuator is placed between the gate and the 30 MHz amplifier, and the amplifier is operated at higher gain (to prevent overloading of the first stage, which has fixed gain), the attentuation of the feedthrough is sufficient to prevent overload of the 30 MHz amplifier.

The MOSFET gate is used to protect the more sensitive boxcar integrator from overload. The on-to-off ratio of the MOSFET gate is very high, but the gate is useful only for low frequency signals. Both gates are driven by a pair of complementary pulses from a GR1398-A pulse generator. A delayed trigger output from the boxcar integrator allows the gating pulse to be positioned in time.

The frequency doubler used in the calibration equipment during room temperature measurements is essentially a ring bridge modulator-phase sensitive detector followed by a tunable series resonant filter shown in Figure 36. It provides a signal which is precisely twice the

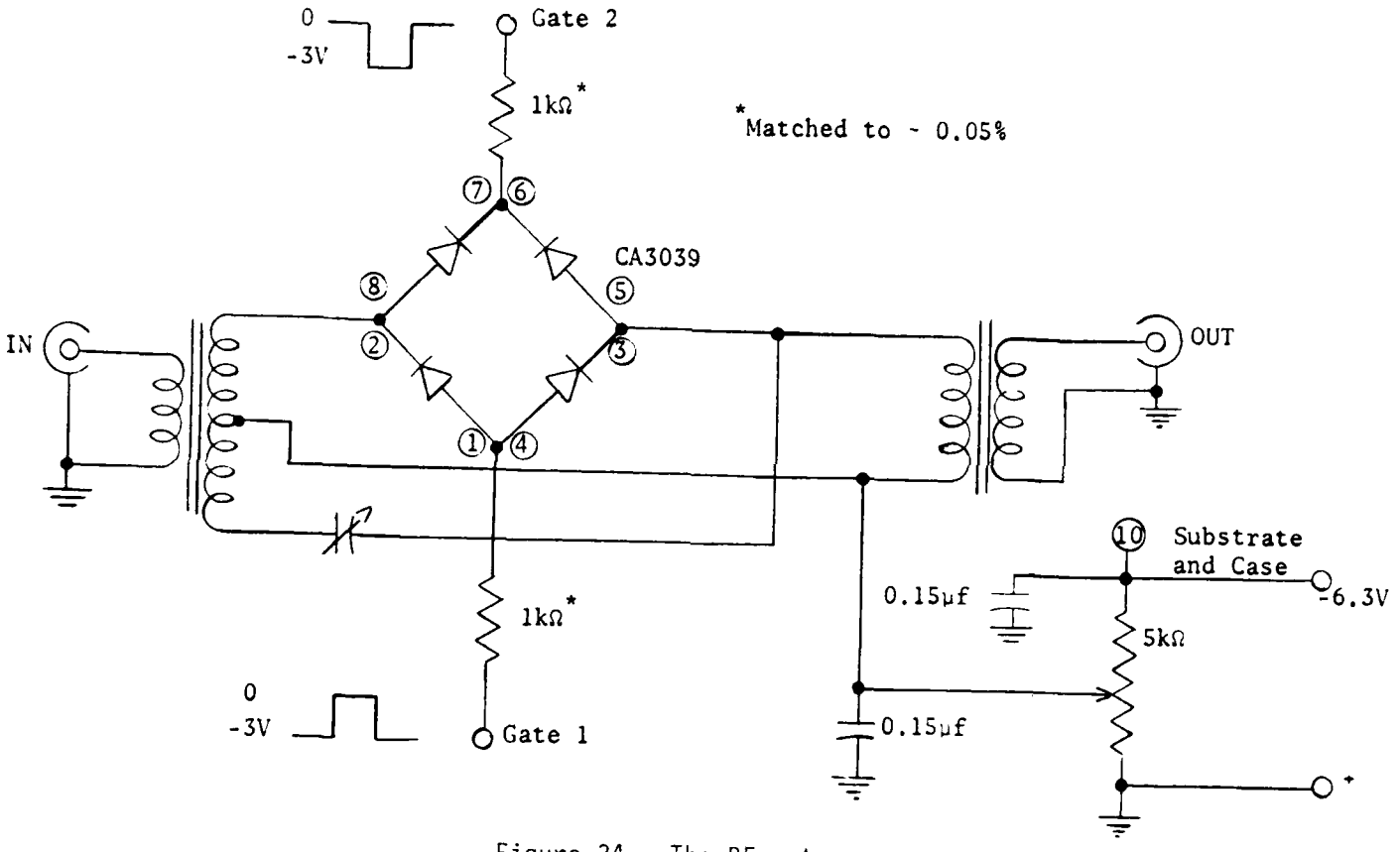

Figure 34. The RF gate.

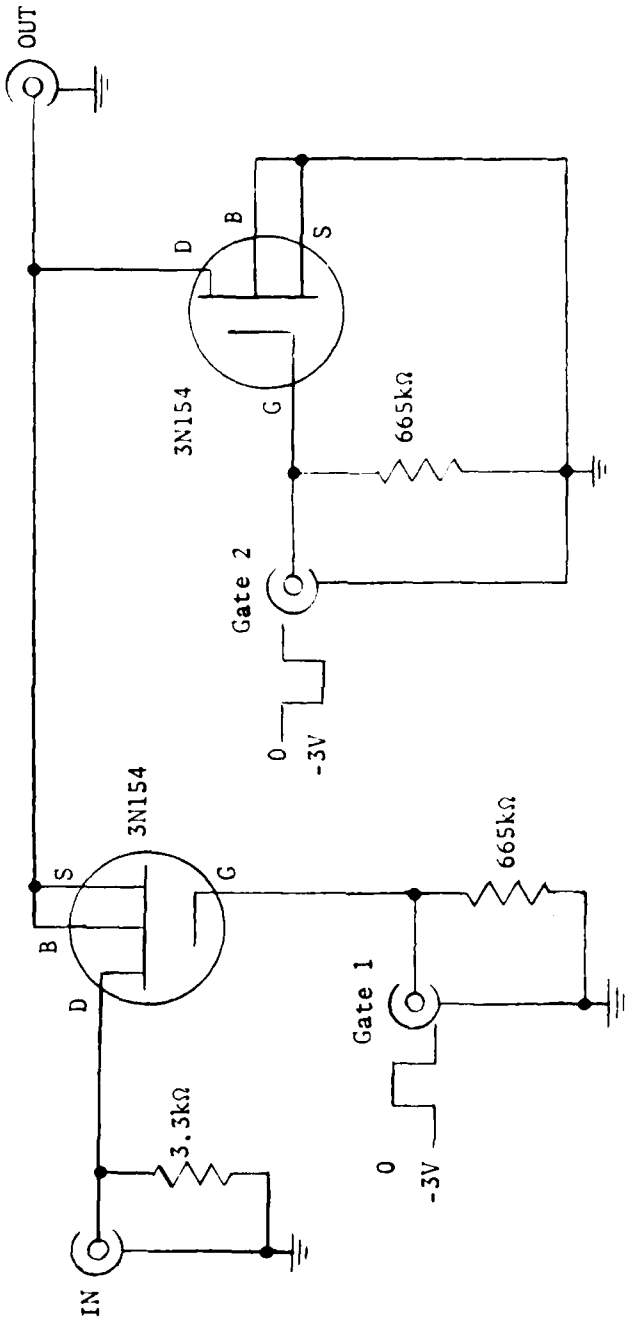

Figure 35. The MOSFET gate.

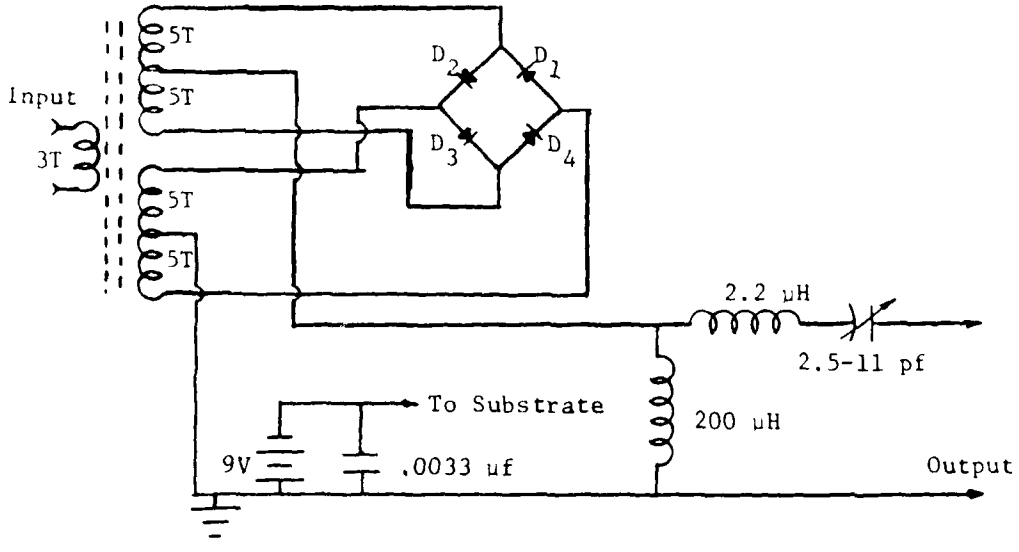

Figure 36. Schematic diagram of the frequency doubler.

frequency of the fundamental used in the study. The diodes D_1-D_4 shown in the figure are RCA type CA3039. The doubler has been tested for spectral purity with a spectrum analyzer.

APPENDIX A.3

ATTENUATION AND HARMONIC LOSS EFFECTS

As the ultrasonic wave propagates in the sample, the second harmonic amplitude A_2 changes as a function of distance. There is a growth of A_2 proportional to the square of the first harmonic amplitude A_1 and there is a decay of the wave due to attenuation of A_2. Therefore the amplitude of the second harmonic as a function of distance in the sample a is given by the differential equation

$$\frac{dA_2}{da} = -\alpha_2 A_2 + \frac{3}{8} k^2 \beta A_1^2 \qquad (A.3\text{-}1)$$

where α_2 is the attenuation coefficient of A_2. If one assumes that the change in A_1 as a function of a is due only to the attenuation of A_1 and the loss of power into the second harmonic, neglecting the power loss into third and higher harmonics, one obtains

$$\frac{dA_1}{da} = -\alpha_1 A_1 - \frac{3}{8} k^2 \beta A_2 A_1 \qquad (A.3\text{-}2)$$

where α_1 is the attenuation coefficient of A_1.

The simultaneous solution of Eqs. (A.3-1) and (A.3-2) has not been obtained, but two special cases can be solved. The first special case is the one for which we can neglect the term due to power loss from the fundamental into the second harmonic. Equation (A.3-2) then becomes

$$\frac{dA_1}{da} = -\alpha_1 A_1 \ . \qquad (A.3\text{-}3)$$

Equations (A.3-1) and (A.3-3) can be solved simultaneously to give

$$\frac{A_2}{A_1^2} = \frac{3}{8} k^2 \beta e^{2\alpha_1 a} \frac{e^{-2\alpha_1 a} - e^{-\alpha_2 a}}{\alpha_2 - \alpha_1} \tag{A.3-4}$$

The attenuation coefficients for silicon have been measured.[88] For a 30 MHz fundamental, the coefficients are of the order of $\alpha_1 \approx 0.09$ db/cm and $\alpha_2 \approx 0.27$ db/cm. For a 5 cm sample (which is longer than any of the samples used in the present measurements) A_2/A_1^2 gives a value for $(3/8)k^2\beta a$ which is approximately 2.6% low. Since this is much smaller than the other sources of error in the absolute measurements, no attenuation correction is necessary.

The second special case is that for which $\alpha_1 = \alpha_2 = 0$. Equations (A.3-1) and (A.3-2) then reduce to

$$\frac{dA_2}{da} = \frac{3}{8} k^2 \beta A_1^2 \tag{A.3-5}$$

and

$$\frac{dA_1}{da} = -\frac{3}{8} k^2 \beta A_2 A_1 \ . \tag{A.3-6}$$

Equations (A.3-5) and (A.3-6) have the simultaneous solution

$$\begin{aligned} \frac{3}{8} k^2 \beta a &= \frac{\sinh^{-1}(A_2/A_1)}{\sqrt{A_1^2 + A_2^2}} \\ &= \frac{\ln (A_2 + \sqrt{A_2^2 + A_1^2}) - \ln A_1}{\sqrt{A_1^2 + A_2^2}} \end{aligned} \tag{A.3-7}$$

This equation is the same as Eq. (3.2) of Chapter III. For the entire range of amplitudes used in the room temperature measurements of silicon, the difference between (A_2/A_1^2) and the quantity calculated from Eq. (A.3-7) is very small.

REPORTS DISTRIBUTION LIST FOR ONR PHYSICS PROGRAM OFFICE
UNCLASSIFIED CONTRACTS

Director Defense Advanced Research Projects Agency Attn: Technical Library 1400 Wilson Blvd. Arlington, Virginia 22209	3 copies
Office of Naval Research Physics Program Office (Code 421) 800 North Quincy Street Arlington, Virginia 22217	3 copies
Office of Naval Research Assistant Chief for Technology (Code 200) 800 North Quincy Street Arlington, Virginia 22217	1 copy
Naval Research Laboratory Department of the Navy Attn: Technical Library Washington, DC 20375	3 copies
Office of the Director of Defense Research and Engineering Information Office Library Branch The Pentagon Washington, DC 20301	3 copies
U.S. Army Research Office Box 12211 Research Triangle Park North Carolina 27709	2 copies
Defense Documentation Center Cameron Station (TC) Alexandria, Virginia 22314	12 copies
Director, National Bureau of Standards Attn: Technical Library Washington, DC 20234	1 copy
Commanding Officer Office of Naval Research Branch Office 536 South Clark Street Chicago, Illinois 60605	3 copies

Commanding Officer Office of Naval Research Branch Office 1030 East Green Street Pasadena, California 91101	3 copies
San Francisco Area Office Office of Naval Research One Hallidie Plaza Suite 601 San Francisco, California 94102	3 copies
Commanding Officer Office of Naval Research Branch Office 666 Summer Street Boston, Massachusetts 02210	3 copies
New York Area Office Office of Naval Research 715 Broadway, 5th Floor New York, New York 10003	1 copy
Director U.S. Army Engineering Research and Development Laboratories Attn: Technical Documents Center Fort Belvoir, Virginia 22060	1 copy
ODDR&E Advisory Group on Electron Devices 201 Varick Street New York, New York 10014	3 copies
Air Force Office of Scientific Research Department of the Air Force Bolling AFB, D.C. 22209	1 copy
Air Force Weapons Laboratory Technical Library Kirtland Air Force Base Albuquerque, New Mexico 87117	1 copy
Air Force Avionics Laboratory Air Force Systems Command Technical Library Wright-Patterson Air Force Base Dayton, Ohio 45433	1 copy
Lawrence Livermore Laboratory Attn: Dr. W. F. Krupke University of California P.O. Box 808 Livermore, California 94550	1 copy

Harry Diamond Laboratories — 1 copy
Technical Library
2800 Powder Mill Road
Adelphi, Maryland 20783

Naval Air Development Center — 1 copy
Attn: Technical Library
Johnsville
Warminster, Pennsylvania 18974

Naval Weapons Center — 1 copy
Technical Library (Code 753)
China Lake, California 93555

Naval Training Equipment Center — 1 copy
Technical Library
Orlando, Florida 32813

Naval Underwater Systems Center — 1 copy
Technical Library
New London, Connecticut 06320

Commandant of the Marine Corps — 1 copy
Scientific Advisor (Code RD-1)
Washington, DC 20380

Naval Ordnance Station — 1 copy
Technical Library
Indian Head, Maryland 20640

Naval Postgraduate School — 1 copy
Technical Library (Code 0212)
Monterey, California 93940

Naval Missile Center — 1 copy
Technical Library (Code 5632.2)
Point Mugu, California 93010

Naval Ordnance Station — 1 copy
Technical Library
Louisville, Kentucky 40214

Commanding Officer — 1 copy
Naval Ocean Research & Development Activity
Technical Library
NSTL Station, Mississippi 39529

Naval Explosive Ordnance Disposal Facility — 1 copy
Technical Library
Indian Head, Maryland 20640

Naval Ocean Systems Center — 1 copy
Technical Library
San Diego, California 92152

Naval Surface Weapons Center — 1 copy
Technical Library
Dahlgren, Virginia 22448

Naval Surface Weapons Center (White Oak) — 1 copy
Technical Library
Silver Springs, Maryland 20910

Naval Ship Research and Development Center — 1 copy
Central Library (Code L42 and L43)
Bethesda, Maryland 20084

Naval Avionics Facility — 1 copy
Technical Library
Indianapolis, Indiana 46218

Dr. Werner G. Neubauer — 1 copy
Code 8130
Physical Acoustics Branch
Naval Research Laboratory
Washington, DC 20375

Dr. Bill D. Cook — 1 copy
Dept. of Mechanical Engineering
University of Houston
Houston, Texas 77004

Dr. Floyd Dunn — 1 copy
Biophysical Research Laboratory
University of Illinois
Urbana, Illinois 61801

Dr. E. F. Carome — 1 copy
Department of Physics
John Carroll University
University Heights
Cleveland, Ohio 44017

Albert Goldstein, Ph.D. — 1 copy
Chief, Division of Medical Physics
Henry Ford Hospital
2799 West Grand Boulevard
Detroit, Michigan 48202

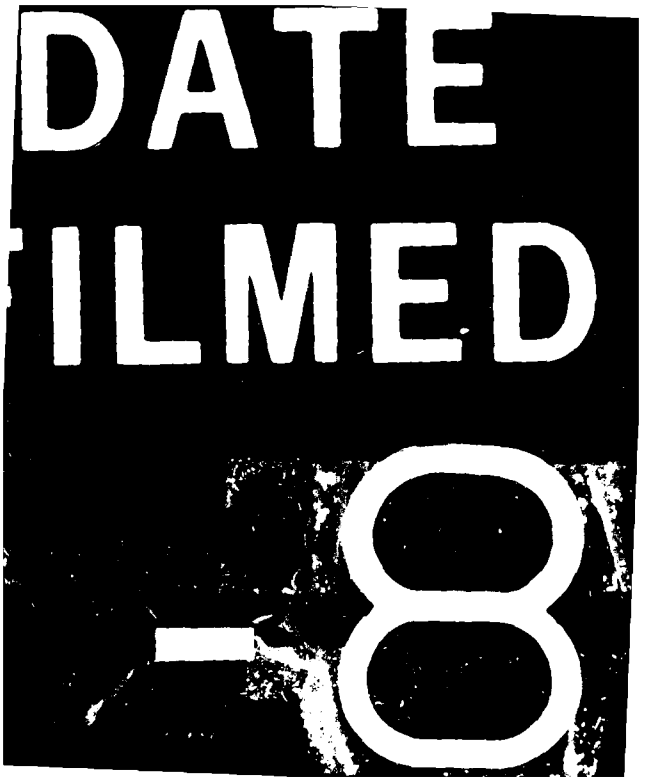
DATE
ILMED
-8